

# MASS TRANSFER DURING BARROVIAN METAMORPHISM OF PELITES, SOUTH-CENTRAL CONNECTICUT. II: CHANNELIZED FLUID FLOW AND THE GROWTH OF STAUROLITE AND KYANITE

JAY J. AGUE

Department of Geology and Geophysics,  
Yale University,  
P.O. Box 208109  
New Haven, Connecticut 06520-8109

**ABSTRACT.** Petrologic study of quartz veins and their wallrocks from the Wepawaug Schist, Connecticut, constrains the role of fracture flow in the chemical and mineralogical evolution of amphibolite facies (staurolite and kyanite zone) pelites during Barrovian metamorphism. Quartz veins may contain accessory calcite and pyrite in the chlorite and biotite zones and plagioclase, micas, kyanite, staurolite, apatite, and sulfides at higher metamorphic grades. Crack-seal textures are widespread. Measured vein densities increase from about 2 to 4 percent in the lowest grade rocks to about 20 to 30 percent in the kyanite zone. In the amphibolite facies, veins are commonly surrounded by a highly aluminous selvage rich in staurolite  $\pm$  kyanite and micas and poor in quartz and plagioclase. Staurolite and kyanite are typically absent from the less aluminous wallrocks located beyond the selvage margins. The selvage width increases as a function of vein width at a ratio of  $\sim 1.3$ . Most vein development occurred after garnet crystallization had begun but pre- to syn-staurolite  $\pm$  kyanite growth.

Four critical lines of evidence suggest that the quartz veins were major conduits for the regional scale movement of metamorphic fluids. (1) Mass balance analysis of two selvages and their protoliths indicates that major and trace elements were mobilized during selvage development by reactions that destroyed quartz, plagioclase, and micas and produced staurolite and kyanite. The reactions suggest significant hydrogen metasomatism. (2) Estimated  $f_{HCl}/f_{H_2O}$  is highest in the selvages directly adjacent to veins, which suggests that the most altered rocks were infiltrated by fluids with elevated  $f_{HCl}/f_{H_2O}$  and that the avenues for infiltration were quartz veins. (3) The amount of silica loss from local pelitic wallrocks can only account for about 70 percent of the total volume of quartz in the average amphibolite facies vein. The other 30 percent is inferred to have been externally-derived through widespread fluid infiltration down regional T and P gradients. (4) Because previously published stable isotopic studies have shown that quartz in amphibolite facies veins may be significantly out of oxygen isotopic equilibrium with wallrock quartz, the fluid that precipitated quartz was probably in part externally-derived.

Selvage formation resulted in significant decreases in Na/Al and, in some cases, K/Al which stabilized aluminous index minerals. The staurolite and kyanite isograds in Barrovian terranes therefore may reflect P, T, fluid composition, protolith lithology, and metasomatic shifts in bulk chemistry caused by fluid infiltration. Widespread amphibolite facies quartz vein development and associated staurolite

**and kyanite growth may mark regions of major fluid outflow and advective heat transport in orogenic belts.**

## INTRODUCTION

Exhumed syn-metamorphic vein systems provide unequivocal evidence for mass transfer of rock-forming elements during orogenesis and, in many cases, preserve a comprehensive petrologic record of fracture-controlled fluid flow events in the crust. Fractures may increase significantly the porosity and permeability of metamorphic rocks, resulting in the focusing of fluid flow into fracture networks. Focused fracture-controlled flow may have critical consequences for the physical and chemical evolution of the crust. For example, Chamberlain and Rumble (1988), Brady (1988), and Hoisch (1991) concluded that fracture-controlled fluid flow can produce major regional thermal anomalies in orogenic belts. Furthermore, fluid transport in fracture networks will lead to mass transfer of a diverse suite of rock-forming and trace elements. The fracturing will expose extensive areas of wallrock to chemically reactive infiltrating fluids and promote chemical and isotopic metasomatism (Vidale, 1974; Rye and others, 1976; Tracy and others, 1983; Rye and Bradbury, 1988; Bebout and Barton, 1989; Ferry and Dipple, 1991; Manning and Bird, 1991; Hanson and others, 1993). As shown by Schandl, Davis, and Krogh (1990), Philippot and Selverstone (1991), and Ayers and Watson (1993), among others, even high field strength elements such as Zr and Ti may be mobile.

Despite these advances in our understanding of channelized fluid flow in the deep crust, significant disagreement exists over the role that vein development plays in the hydrologic and petrologic evolution of Barrovian metamorphic terranes. For example, Walther and Orville (1982), Walther (1990), Ferry and Dipple (1991), and Ferry (1992), among others, have maintained that quartz veins represent major conduits for the regional scale movement of metamorphic fluids. On the other hand, Yardley (1975) and Yardley and Bottrell (1992) concluded that quartz veins are segregations produced only by local mass transfer. As a consequence of these contrasting views, the processes by which mineral mass is deposited in veins and the sources of the mass remain unclear. Is the mass transported out of local wallrocks by diffusion, or is it precipitated from fluids flowing through fractures, or both (compare Fisher and Brantley, 1992)?

If veins are the pathways for regional fluid transport during Barrovian metamorphism, then metasomatic alteration of pelitic wallrocks *must occur* (Ague, 1991, 1992, 1994; Yardley and Bottrell, 1992). Although metamorphic wallrock alteration has been the focus of a number of pioneering studies (Read, 1932; Chapman, 1950; Ramberg, 1952; Tracy and others, 1983; Yardley, 1975, 1986; Kerrick, 1988; Oliver, Valenta, and Wall, 1990), many fundamental questions remain. For example, what types of chemical reactions proceed when vein fluids interact with wallrocks? Could the development of index minerals such as

staurolite and kyanite be related to regional scale metasomatism associated with channelized fluid flow?


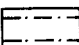
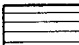


In an effort to address these issues, an investigation of syn-metamorphic veins in the Wepawaug Schist, south-central Connecticut, has been carried out (fig. 1). Mass balance analysis of the Wepawaug pelites strongly suggests that prograde Barrovian metamorphism was accompanied by significant chemical alteration involving transport of silica, phosphorous, and key alkali, alkaline earth, and transition metals (Ague, 1994). Attention is focused here on gaining a better understanding of how the chemical alteration of large volumes of pelitic rock was related to syn-metamorphic fracturing and hydrothermal flow events. Because metapelites are the most common type of metasedimentary rock worldwide, the conclusions reached herein should have broad applicability to other orogenic belts.

#### REVIEW: VEINS AND MASS TRANSFER

Four broad hydrologic regimes have been proposed for vein formation: (1) single-pass or one-way fluid flow toward the Earth's surface (Fyfe, Price, and Thompson, 1978; Walther and Orville, 1982; Walther, 1990; Ferry and Dipple, 1991), (2) local or regional scale fluid convection (Etheridge, Wall, and Vernon, 1983), (3) deformation-controlled advective recycling of fluids trapped beneath low permeability cap rocks (Yardley and Bottrell, 1992), and (4) static regimes (Yardley, 1975; Fisher and Brantley, 1992). The mechanics of rock failure that lead to vein formation have likewise received considerable attention (Sibson, Robert, and Poulsen, 1988; Ramsay, 1980; Walther and Orville, 1982; Vrolijk, 1987; Nishiyama, 1989; Nur and Walder, 1990; Oliver, Valenta, and Wall, 1990). Two modes of mass transport that may be involved in vein formation are relevant to this study.

First, fluid flow advects solutes through fractures. The solute load of the fluid is partially deposited in response to supersaturation caused by decreases in temperature, decreases in pressure, and/or changes in fluid composition along the flow path (Walther and Orville, 1982, 1983; Walther, 1990; Ferry and Dipple, 1991). The formation of quartz veins has been widely attributed to the movement of silica saturated fluids down regional temperature and pressure gradients (Walther and Orville, 1982; Walther, 1990; Ferry, 1992). Under typical metamorphic conditions, the time-integrated fluid fluxes necessary to form quartz veins in this manner are probably on the order of  $10^6$  to  $10^7$   $\text{m}^3 \text{m}^{-2}$  (Walther, 1990; Ferry and Dipple, 1991). These large fluxes are likely to be two to five orders of magnitude greater than those due to pervasive flow regimes (Ferry and Dipple, 1991) and are sufficient to cause significant chemical and isotopic metasomatism in wallrocks (Yardley and Bottrell, 1992).

The second mode involves transport of vein-forming components (for example, silica) from local wallrocks to fractures by diffusion down chemical potential gradients. Transport may occur regardless of whether

-  Mesozoic Volcanic and Sedimentary Rocks
-  Wepawaug Schist  
(Devonian or Silurian or Both)
-  Maltby Lakes Metavolcanics  
(Middle? Ordovician)
-  Allingtown Metavolcanics  
(Middle? Ordovician)
-  Oronoque Schist  
(Lower? Ordovician)

5 km

73° 7.5' W  
41° 15' N +

East Derby Fault

WS  
MF

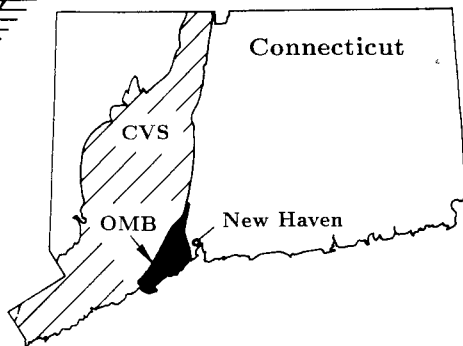


Fig. 1. Generalized geologic map of the Orange-Milford belt of south-central Connecticut, modified from Fritts (1962a,b, 1963, 1965a,b), Dieterich (ms), and Rodgers (1985). WS: axis of the Wepawaug syncline. MF: Mixville fault. Dip-slip displacements on this fault, quantified from observations of Mesozoic rocks to the north of the Wepawaug Schist, are small (~100 m; Fritts, 1965a). The position of the Orange-Milford belt (OMB) in the Connecticut Valley Synclinorium (CVS) is shown on the inset location map.

or not the fluid in the fractures is flowing. The chemical potential gradients may result from a number of phenomena, including gradients in: (1) fluid pressure (compare Fisher and Brantley, 1992), (2) quartz surface and strain free energy (Yardley, 1975), and (3) effective pressure ( $=P_{\text{solid}} - P_{\text{fluid}}$ ) (Elliot, 1973; Paterson, 1973; Rutter, 1983; Elias and Hajash, 1992). If vein mass is extracted from wallrocks by diffusional processes, then wallrocks at the margins of the veins must be depleted in the vein-forming components (Ramberg, 1952; Turekian and Wedepohl, 1961; Yardley, 1975; Ramsay, 1980).

There are two fundamental distinctions between the two modes. First, large time-integrated fluid fluxes will generally be required to form quartz veins if mass transport is by advection, whereas they are not required if mass transport is diffusion-controlled. Second, in the advective case, the mineral mass deposited in the veins may be derived either from within or outside the local rock, depending on the length scale of fluid flow (Walther, 1990; Yardley and Botrell, 1992). In contrast, diffusional processes redistribute mass only on the local scale. Thus, in order to obtain a quantitative understanding of fluid and mass fluxes through metamorphic terranes, it becomes critical to determine the source of the mineral mass deposited in veins and the mechanisms of vein formation.

#### METHODS OF INVESTIGATION

Macroscopic observations of pelitic schist and veins were made in the field and on over 300 cut rock slabs. One hundred seventeen thin sections cut from 84 rock samples were examined. Mineral compositions were determined using the JEOL JXA-8600 electron microprobe in the Department of Geology and Geophysics at Yale University and natural and synthetic standards. Off-peak background corrections were used for all elements. Data reduction used ZAF correction procedures for silicates and oxides and  $\phi(\rho z)$  procedures for carbonates. The microprobe was also used to obtain backscattered electron images of key fracture-controlled alteration features. Rock density was measured with a Micromeritics 1305 manual gas pycnometer. The density measurements are accurate to  $\pm 0.005 \text{ g cm}^{-3}$ , based on replicate analyses of a quartz standard. Bulk-rock XRF analyses were done by X-ray Assay Laboratories, Don Mills, Ontario. The accuracy and long-term reproducibility of results from this laboratory have been documented elsewhere (Ferry, 1992; Ague, 1994). Modal analyses were carried out using the line integration method (Brimhall, 1979) in conjunction with a semi-automated digitizing petrographic microscope. The density of quartz veins was estimated at 13 field localities using linear measurement traverses. Vein density was taken as the ratio (total vein length)/(total vein + rock length). When more than one site was measured at a given locality, average results were calculated using the measure of location discussed by Aitchison (1989). The localities were chosen on the basis of freshness and the absence of pervasive low-temperature metamorphic

recrystallization. The widths of veins and their associated aluminous selvages were measured perpendicular to vein-wallrock contacts on cut rock slabs using a millimeter scale. Care was taken to make the vein-selvage measurements on veins that were not intensely folded so as to minimize distortion due to deformation. Sample locations are shown in figure 2.

#### OVERVIEW: GEOCHRONOLOGY AND REGIONAL STRUCTURE

The Wepawaug Schist is part of the Orange-Milford belt of the Connecticut Valley Synclinorium (fig. 1; Rodgers, 1985). Metamorphic grade ranges from chlorite zone in the east to kyanite zone in the west (fig. 2). Mineral assemblages are discussed in detail by Hewitt (1973) and Ague (1994). The ages of deposition, metamorphism, and deformation in the Orange-Milford belt remain the focus of ongoing investigation. Fritts (1962b) assigned a Siluro-Devonian depositional age to the Wepawaug Schist and correlated it with the Waits River and Northfield Formations of Vermont. Although recent work has shown that the Waits River Formation is Silurian-Early Devonian in age, at least in part (Hueber and others, 1990), the correlation of the Waits River Formation with the Wepawaug Schist is not certain. Dieterich (ms) concluded, on the basis of structural and stratigraphic arguments, that prograde metamorphism occurred during the Acadian orogeny (~420-360 Ma; Gates, 1975; Osberg and others, 1989; Armstrong, Tracy, and Hames, 1992). Acadian metamorphism is supported by the preliminary geochronologic work of Palin and Seidemann (1990) and Lanzirotti and Hanson (1992). The significantly younger mica K-Ar ages generally obtained in the region (220-280 Ma; Clark, ms; Burger, Hewitt, and Vidale, 1968; Moecher and Cosca, 1992) are evidence that some reheating of the rocks took place during the Alleghanian orogeny. Radiometric age constraints indicate that prograde metamorphism was probably associated with the Acadian orogeny, although pre-Acadian metamorphism cannot be ruled out. Additional evidence, which supports the Acadian metamorphism hypothesis, includes: (1) the Taconic orogenic belt lies to the west of the Wepawaug Schist (Zen, 1991; Armstrong, Tracy, and Hames, 1992), and (2) the pressures and temperatures of metamorphism in the staurolite and kyanite zones of the Wepawaug (see below) are similar to those documented by other workers for Acadian amphibolite facies metamorphism in central-western Connecticut (Hames, Tracy, and Bodnar, 1989; Miller and Tracy, 1991; Armstrong, Tracy, and Hames, 1992).

The structural geology of the Orange-Milford belt is complex and may reflect the superposition of as many as three regional fold systems (Dieterich, ms). A penetrative schistosity, which strikes north-northeast, is present throughout the Wepawaug Schist. For convenience, this fabric is herein referred to as " $S_2$ ." Bedding in the Wepawaug has been deformed into tight to isoclinal folds (Fritts, 1963, 1965a, b; Dieterich, ms).  $S_2$  is approximately parallel to bedding on fold limbs and marks the axial planes of the folds in their hinges. In thin section, the crenulated remnants of an earlier fabric(s),  $S_1$ , are present between the  $S_2$  schistosity

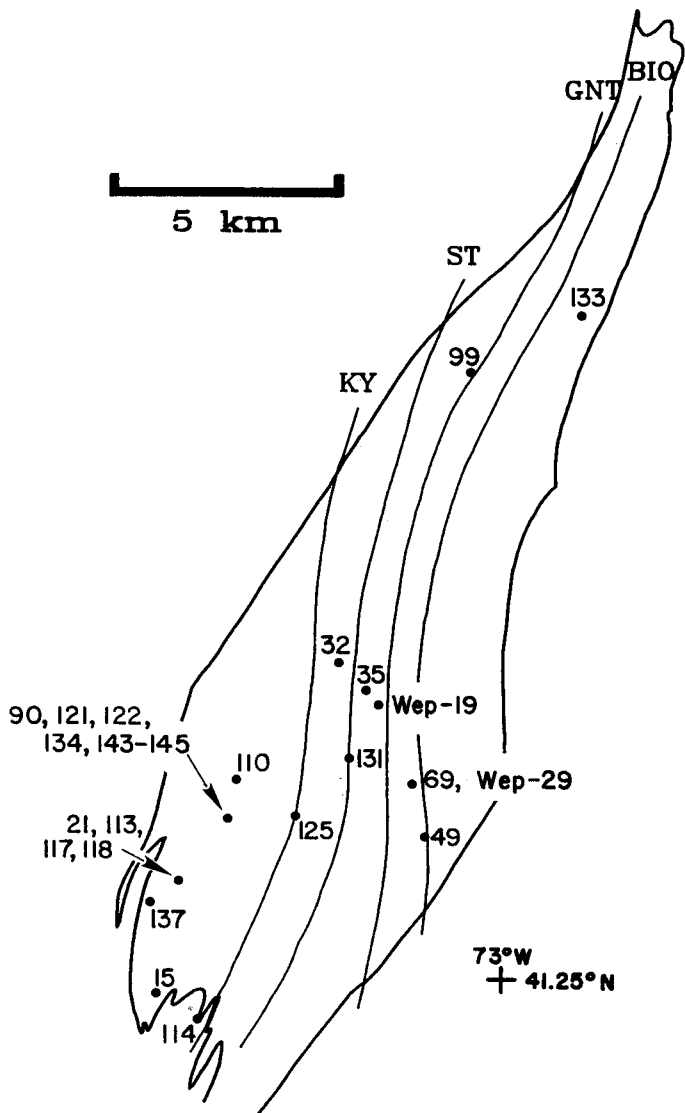


Fig. 2. Sample locations and metamorphic isograds. Isograd locations modified from Fritts (1963, 1965a,b) based on field mapping by Ague (5/90-1/93). Wep-19 and Wep-29 are sample localities of Hewitt (1973). All other samples belong to sample set JAW.

planes. Folds related to  $S_1$  development are extremely difficult to recognize in the field because later deformation has transposed and obscured them.  $S_2$  dips steeply to the west in the eastern part of the formation and steeply to the east in the western part. Fritts (1963, 1965a, b) proposed

that the major structure is a north-northeast plunging synformal syncline whose axis strikes through the center of the formation (fig. 1). The regional pattern of minor fold asymmetries as mapped by Dieterich (ms) is consistent with Fritts' hypothesis.

#### VEIN ASSEMBLAGES AND RELATIONS

##### *Mineral Assemblages and Petrography*

Vein mineral assemblages provide critical constraints on mass transfer processes. Vidale (1974) pointed out that vein mineralogy may be a consistent function of metamorphic grade in regional metamorphic belts. The predominant mineral in the Wepawaug veins is quartz. Accessory minerals, if present, generally constitute less than 5 volume percent of a given vein. Accessory mineral assemblages change as a function of metamorphic grade. Quartz veins in chlorite and biotite zone pelites may contain:

Calcite  $\pm$  pyrite  $\pm$  muscovite  $\pm$  chlorite  $\pm$  albite

(minerals are listed in the approximate order of decreasing abundance). In the garnet zone, accessory minerals include carbonate, plagioclase, micas, and sulfides. Staurolite zone vein minerals are similar to those in the garnet zone, but carbonates are absent. Quartz veins in kyanite zone pelites contain the most diverse suite of accessory minerals:

Plagioclase  $\pm$  muscovite  $\pm$  biotite  $\pm$  kyanite  $\pm$  staurolite

$\pm$  apatite  $\pm$  sulfides.

Aluminum-bearing accessory minerals (plagioclase, phyllosilicates, kyanite) tend to be concentrated at or near vein-wallrock contacts, regardless of metamorphic grade.

Vein quartz occurs as highly irregular anhedral crystals which are typically larger than the quartz grains in the adjacent wallrock. The largest optically continuous quartz grains observed are  $\sim 2$  cm in diameter. No systematic changes in quartz grain size as a function of metamorphic grade have been recognized. Fluid inclusions are widespread in vein quartz.

Accessory calcite occurs as twinned, anhedral to subhedral crystals. Grain size varies from the micron- to the millimeter-scale. In addition to quartz-calcite veins, some rocks contain small (millimeter-scale width) veinlets composed almost entirely of calcite  $\pm$  ankerite. These veinlets cross-cut the pervasive cleavage in the rocks and may be associated with the late-stage kink-folding described by Dieterich (ms).

Plagioclase (oligoclase-andesine) is the dominant accessory mineral in garnet, staurolite, and kyanite zone veins. It occurs as anhedral, subhedral, or euhedral crystals which range in length from a few microns to  $\sim 2$  cm. The veins typically contain about 0 to 5 percent plagioclase; the most plagioclase-rich vein observed ( $\sim 35$  volume percent plagioclase-



clase) was collected from schist adjacent to a syn-metamorphic tonalite dike. Reconnaissance microprobe analyses and optical determinations indicate that vein and wallrock plagioclase are similar in composition (within  $\sim \text{An}_5$ ). Sericitization and partial replacement of vein plagioclase by muscovite is common, but plagioclase in adjacent wallrocks appears fresh. In kyanite zone veins and adjacent wallrocks, plagioclase grain boundaries and microfractures within plagioclase may be lined with minute crystals of kyanite and, more rarely, staurolite.

Veins throughout the Wepawaug contain small amounts of chlorite, muscovite, and biotite. About 60 percent of the veins examined contain micron- to millimeter-scale phyllosilicate grains arranged in planes sub-parallel to vein-wallrock contacts (fig. 3; compare Silverman, ms; Breault, ms). The phyllosilicates are included within quartz grains. The spacing between the planes generally increases with the size of the phyllosilicate grains. Planes of micron-scale grains are spaced about 10 to 20 microns apart, while planes of millimeter-scale phyllosilicates are spaced  $\sim 1$  to 5 mm apart. In the chlorite and biotite zones, the phyllosilicates are muscovite and chlorite, whereas at higher metamorphic grades, only muscovite and biotite occur. The phyllosilicate inclusion planes are typically concentrated near vein-wallrock contacts. In some kyanite zone samples, quartz grains containing mica inclusions are truncated by areas of inclusion-free quartz. The above textures are similar in many respects



Fig. 3. Crystal of vein quartz (at extinction) containing abundant sub-parallel planes of mica (muscovite and biotite) inclusions (compare Ramsay, 1980). The inclusion planes are sub-parallel to the vein-wallrock contact, which lies just outside the field of view below the lower edge of the photo. JAW-113B5, kyanite zone. Field of view is 2.2 mm wide.

to those described by Ramsay (1980) in the context of the “crack-seal” mechanism of vein formation. Phyllosilicates can also occur more randomly arranged at contacts between quartz crystals or as inclusions within individual quartz and plagioclase grains.

Other vein accessory minerals include sulfides, kyanite, and apatite. In the veins cutting low-grade rocks, pyrite occurs either as euhedral cubes or irregular masses of xenoblastic crystals. Sulfides are markedly less abundant as metamorphic grade increases; small amounts of pyrite or pyrrhotite have been noted in several thin sections of amphibolite facies veins. Although microscopic kyanite occurs in association with plagioclase in veins, macroscopic kyanite is rare. Macroscopic kyanite crystals (2–8 cm long) were found in veins at two localities in the southern portion of the kyanite zone. Most veins do not contain apatite. When present, apatite typically occurs in miniscule amounts (1 or 2 ~ 5 micron long grains per thin section), although several vein samples contain isolated grains as much as ~0.5 mm in diameter.

#### . *Wallrock Inclusions*

Macroscopic (~1 to ~10 cm scale) inclusions of rock material are widespread in the Wepawaug veins. The inclusions are generally composed of the same minerals as the wallrock and appear to have been removed from vein-wallrock contacts (fig. 4). On this basis, it is concluded that the inclusions are “xenoliths” derived from the local wallrock via deformational processes associated with vein development.

#### *Regional Variations in Vein Density*

Mapping the regional distribution of the veins is critical in order to assess the intensity of metamorphic mass transfer and relate chemical alteration in wallrocks to vein-related fluid flow. The proportion of quartz veins increases as a function of increasing metamorphic grade in the Wepawaug Schist (fig. 5). Because vein abundances were measured predominantly at road cuts, railroad grades, and new building developments, the results in figure 5 are not due to differential weathering effects. The vein percentages include veins in all the lithologic units at the measurement sites. However, the veins are, by far, most abundant in the pelitic rocks (compare fig. 2 in Ague, 1994). In contrast, quartzites, metasiltstones, and quartzose pelites contain 0 to, at most, ~5 percent veins. In some cases, the veins are localized where pelites are in contact with other lithologic units. In a number of chlorite zone exposures, the veins appear to be concentrated along small (<0.5 m wide) fault zones.

In order to assess the local variability of vein density in heavily veined high-grade exposures, four sites along a 140 m long railroad cut in the kyanite zone were investigated (loc. A in fig. 5). The total exposure lengths measured at the sites were 4.5, 3.2, 3.0, and 9.1 m, and the corresponding vein proportions were 23, 30, 26, and 24 percent. The proportions are all significantly higher than values in the chlorite, biotite, and garnet zones. Based on the vein density measurements done else-

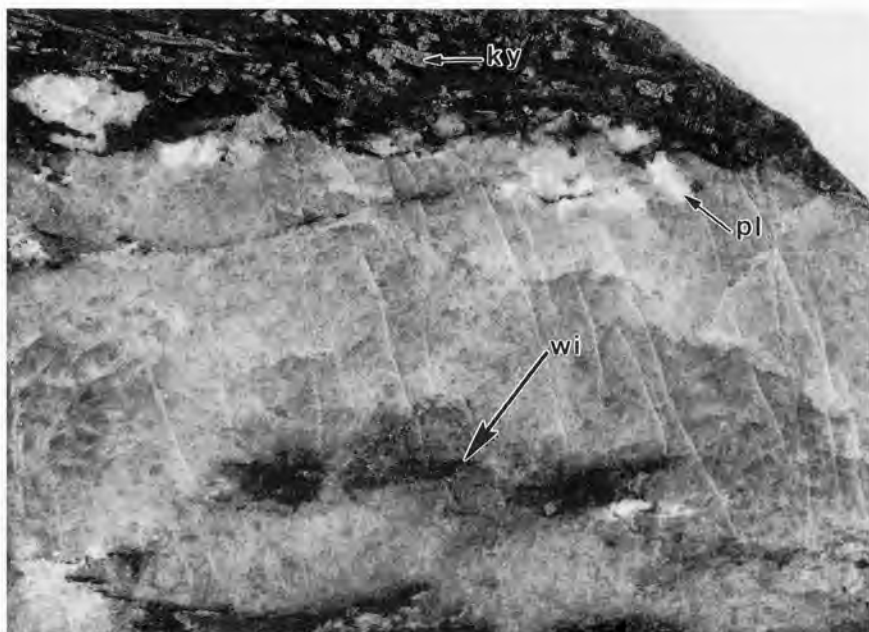


Fig. 4. Photograph of cut rock slab illustrating a quartz vein that contains a wallrock inclusion (wi). The inclusion appears to have been dislodged from the lower vein-wallrock contact. White crystals at upper vein-wallrock contact are plagioclase (pl). Note abundant kyanite (ky) in aluminous selvage adjacent to vein. Sample JAW-134B, kyanite zone. Field of view is 10.7 cm wide.

where in the Formation and visual inspection of exposures, the level of variability documented at locality A is typical for the Wepawaug Schist.

Systematic regional variations in vein width have not been recognized. Vein width ranges from the millimeter to the meter scale regardless of the metamorphic grade of the rocks; the maximum width observed was  $\sim 1.5$  m. The average vein width is in the range of 2 to 3 cm.

#### *Aluminous Selvages Adjacent to Veins*

Although severe deformation may obscure vein-wallrock relations, many veins in staurolite and kyanite grade pelitic units are clearly surrounded by aluminous mica-rich selvages (figs. 6 and 7), similar in many ways to those described by Yardley (1975). Aluminous selvages are also evident in several garnet zone exposures. The selvages "wrap around" fold hinges in the quartz veins to which they are adjacent. In addition, selvages are often cut by small (millimeter-centimeter scale) veinlets of quartz (fig. 7A and C).

There are several important distinctions between the selvages and the less aluminous wallrocks. First, micas, Fe-Ti oxides, graphite, tourmaline, and the index minerals staurolite and kyanite are concentrated in

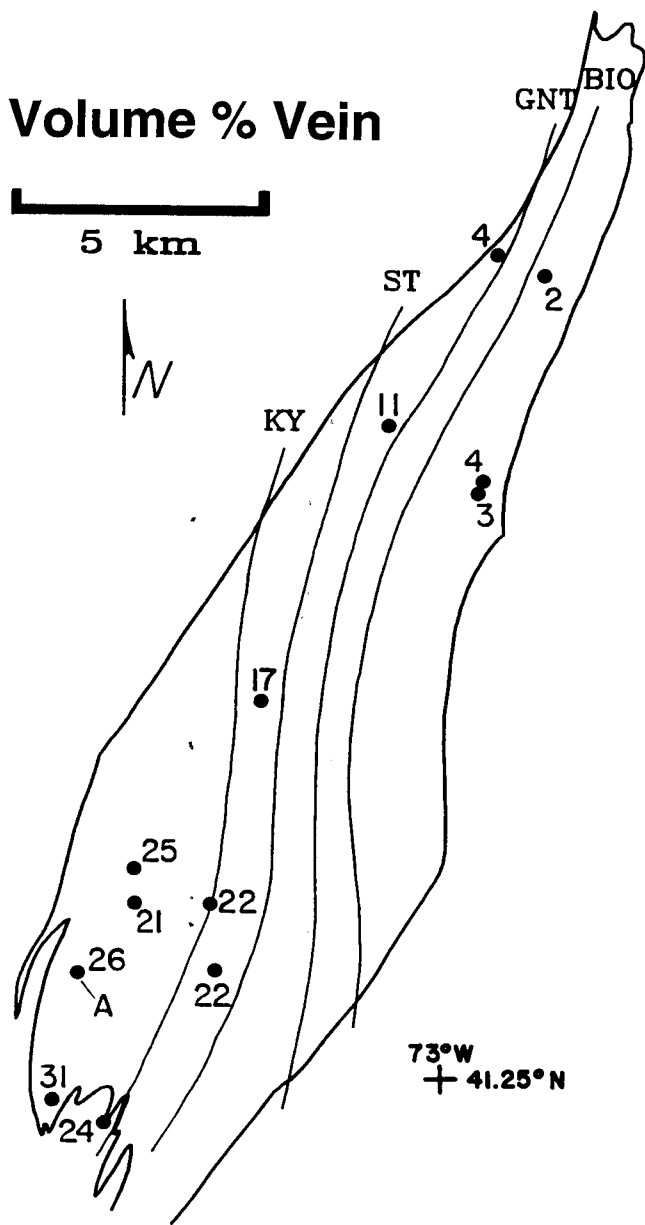


Fig. 5. Regional variations in vein density (volume percent). Note progressive increase in quartz vein abundance with metamorphic grade. Locality A is discussed further in the text.



Fig. 6. Typical field appearance of selvages (arrows) adjacent to veins. The "rough" texture in the selvage areas is due to weathering, which has exposed abundant garnet, staurolite, and kyanite porphyroblasts. The less aluminous wallrock outside the selvages is quartzofeldspathic garnet-biotite schist. Sample JAW-51, kyanite zone. Field of view is 16 cm wide.

the selvages (fig. 7A, B, and C). Second, the selvages contain very little quartz. Third, the micas, particularly biotite, tend to be larger (by a factor of  $\sim 2$  to  $\sim 100$ ) in the selvages. Finally, staurolite and kyanite are typically absent from the wallrock located beyond the selvage margins. Spatial zonation of mineral assemblages is sometimes observed in the selvages. When present, the primary features of the selvage zoning are: (1) the proportions of mica increase dramatically within 0.5 to 2 cm of vein-wallrock contacts (fig. 7A), and/or (2) the proportions of staurolite and kyanite increase either gradually or abruptly as vein-pelite contacts are approached (fig. 7B).

The widths of the selvages on either side of a given vein are generally about equal, but markedly asymmetrical selvages also occur (fig. 7). The total width of the selvage (the sum of the selvage widths on either side of the vein) increases with increasing vein width (fig. 8). The ratio of (total selvage width)/(vein width) varies between about 1:1 and 2:1 (fig. 8); the average (geometric mean) value is  $1.3_{-0.19}^{+0.22}$  ( $\pm 2\sigma$ ). In regions that contain a high density (30-40 percent) of quartz veins, distinct vein margin zones are not readily distinguishable. In such cases, the wallrock is a highly micaceous aluminous schist that is typically rich in staurolite and, at appropriate metamorphic grade, kyanite.

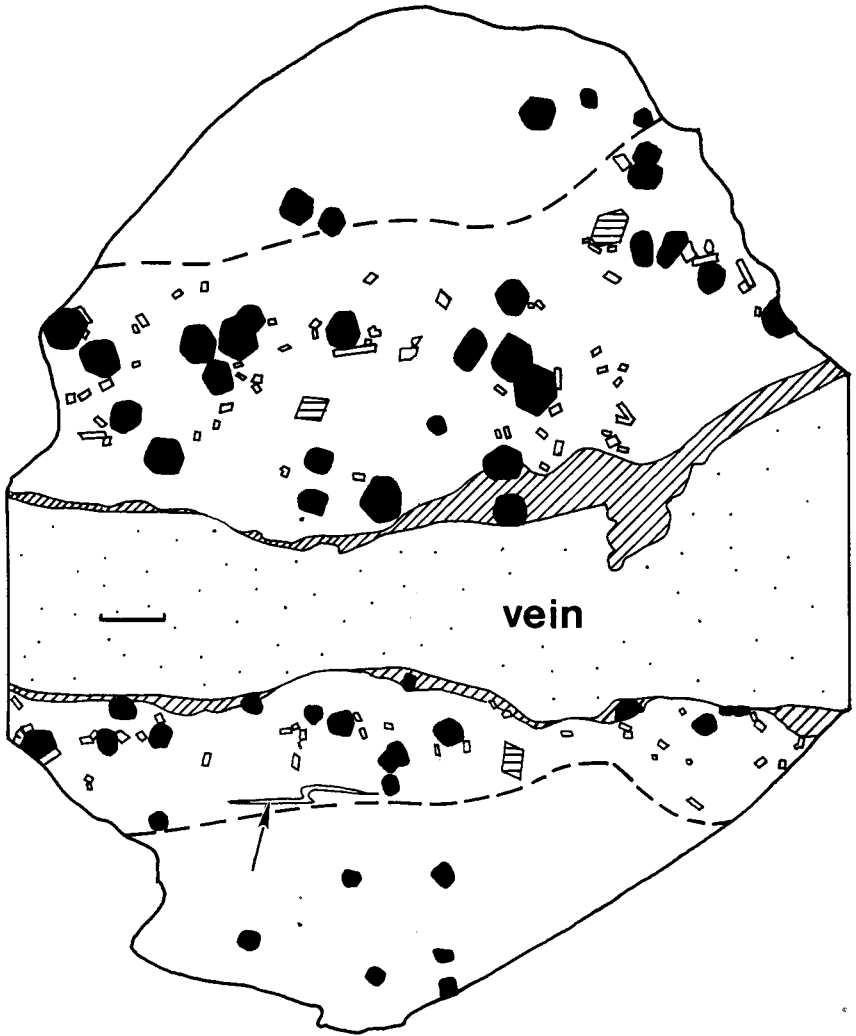


Fig. 7. Selvage-vein relations. Black: garnet; horizontal rule: staurolite; open: kyanite. (A) Asymmetrical selvages adjacent to vein in sample JAW-144. Limits of macroscopically observable selvages indicated by dashed lines. Diagonal ruled pattern denotes areas composed almost entirely of coarse-grained (mm-cm scale) biotite crystals at vein-wallrock contacts. Arrow points to small quartz veinlet. Scale bar = 1 cm.

The consistent relation between vein width and selvage width strongly suggests that the veins and their selvages are genetically related. The simplest explanation of the vein-selvage relations is that the selvages are regions where the wallrock has been chemically altered by vein-forming processes.

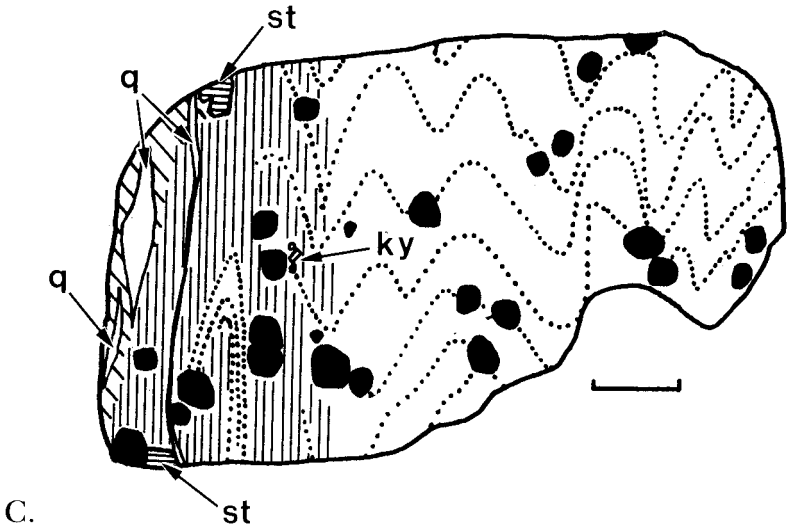
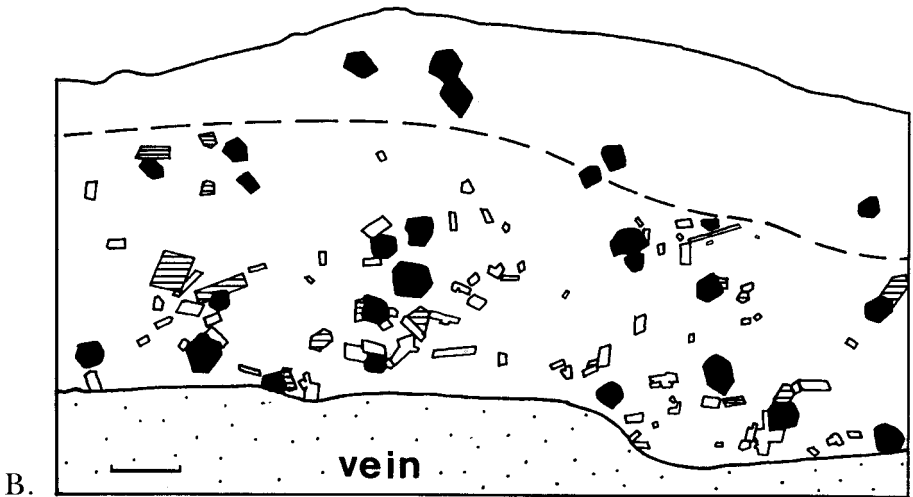


Fig. 7(B) Detail of selvage in sample JAW-134A. Dashed line indicates limit of macroscopically observable selvage. Note subtle increase in the proportions of staurolite and kyanite as the vein-wallrock contact is approached. Scale bar = 1 cm.

(C) Sketch of thin section illustrating selvage relations in sample JAW-125A. The vein-wallrock contact is at the left edge of the drawing (the vein is not shown). st: staurolite; ky: kyanite. Pattern of folded relict sedimentary layering is indicated by dotted lines. The aluminous selvage zone is denoted by the vertical lines. Note that the relict sedimentary layering can be traced into the selvage. Small quartz veinlets (q) cut the selvage. Diagonal ruled pattern at vein contact denotes region where biotite becomes noticeably coarser grained. The tightening of folds within the selvage is interpreted to be the result of metasomatic volume loss. See text for further discussion. Scale bar = 0.5 cm.

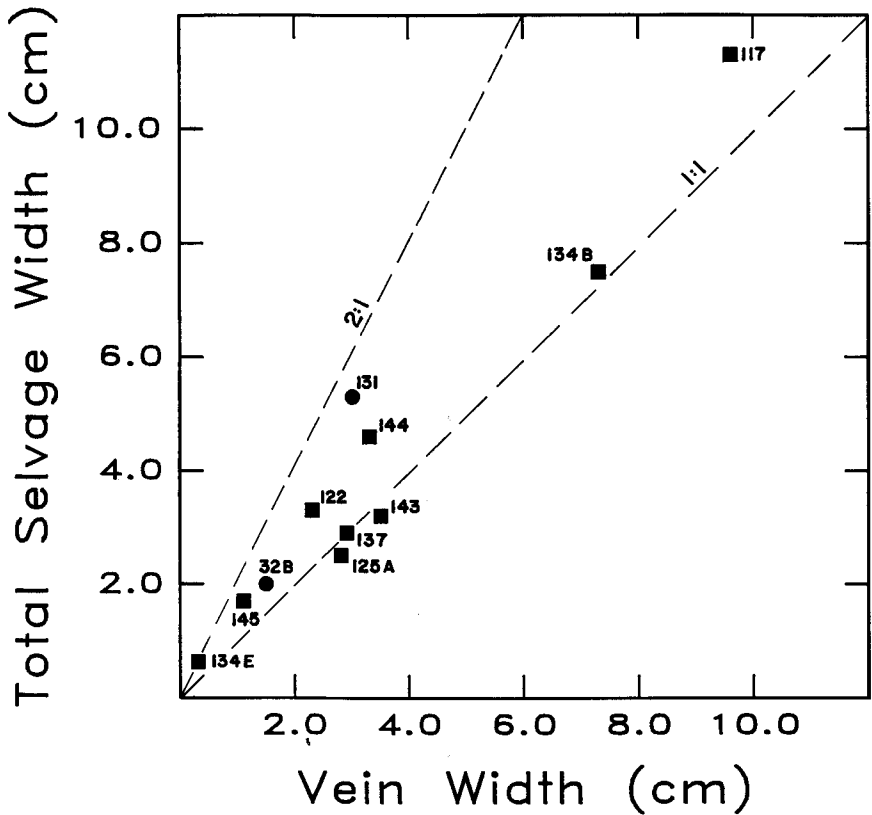


Fig. 8. Total selvage width (the sum of the selvage widths on either side of a vein) versus vein width. Filled circles: staurolite zone; filled squares: kyanite zone.

#### RELATIVE TIMING OF METAMORPHIC, DEFORMATIONAL, METASOMATIC, AND IGNEOUS EVENTS

Although the absolute timing of orogenic events in the Orange-Milford belt is still a matter of debate, the relative timing of porphyroblast growth, schistosity development, veining, and metasomatism in the Wepawaug Schist can be ascertained through field and petrographic observations. It is necessary to constrain the mineral paragenesis so that a temporal framework relating metamorphism, deformation, and mass transfer can be established. Furthermore, because the intrusion of magmas may cause hydrothermal fluid circulation and mass transfer in metamorphic terranes (compare Ferry, 1992), the relative timing of igneous activity in the Wepawaug must also be discussed.

#### *Relative Timing of Porphyroblast Growth and Deformation*

A full discussion of porphyroblast and matrix textures is beyond the scope of this paper; only a brief summary, based on the work of Dieterich



(ms), Breault (ms), and Ague (unpublished), is given. Inclusions in garnet, staurolite, and kyanite are principally quartz, graphite, rutile, and ilmenite. Although quartz inclusions are widespread in garnets, they are considerably less common in staurolite and kyanite. Inclusion trails in garnets in most of the samples indicate post- $S_1$  but pre- to syn- $S_2$  garnet crystallization. A small proportion (5-10 percent) of the rocks contain helicitic garnets (Spry, 1969) which are inferred to have crystallized post- $S_2$ . Staurolite and kyanite growth was largely syn- to post- $S_2$ , although some samples contain textures indicative of pre- $S_2$  crystallization.

#### *Relative Timing of Vein Development in Pelitic Schist*

The textural relations between matrix porphyroblasts and veins provide essential constraints for determining the relative timing of veining in relation to metamorphism. Throughout the garnet, staurolite, and kyanite zones, garnet porphyroblasts are cut and broken into two or more pieces by the veins (fig. 9). A common example is garnet split in two such that the two halves of the garnet are now across from each other in wallrock on opposite sides of the vein. In some samples, garnet fragments were incorporated directly into the veins. Post-fracturing garnet growth took place commonly along the contacts between fractured garnets and

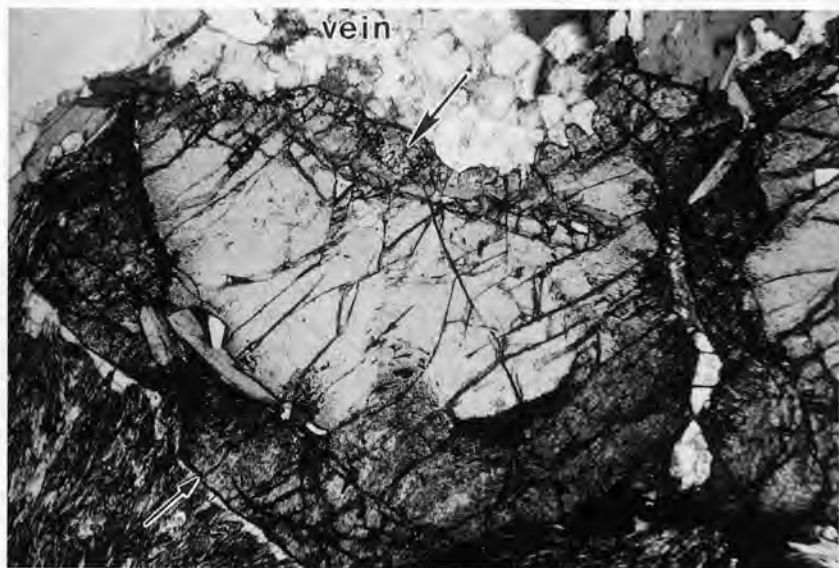


Fig. 9. Photomicrograph (plane polarized light) of garnet porphyroblasts cut by a quartz vein. Note post-fracturing garnet growth (upper arrow) that took place along the vein-garnet contact. The post-fracturing garnet contains micron scale inclusions of euhedral quartz crystals and abundant fluid inclusions. Graphite inclusions are rare in the garnet core, but they are extremely abundant in the garnet rim and the surrounding muscovite-rich matrix. Lower arrow highlights garnet-matrix contact. See text for further discussion. JAW-113B5, kyanite zone. Field of view is 4.4 mm wide.

veins (fig. 9). The composition of the post-fracturing overgrowth is similar to the rim composition of the fractured porphyroblast but contrasts markedly with the porphyroblast's core composition (fig. 10). In contrast to the garnet-vein relationships, no clear examples of veins that cut staurolite or kyanite porphyroblasts have been observed. However, staurolite and kyanite occur preferentially in wallrock directly adjacent to veins (fig. 7), and primary kyanite is observed in veins both as micron-scale grains, which formed from alteration of plagioclase (see below), and large (2-8 cm) euhedral blades. Thus, most veins started to develop after garnet growth began and continued to develop under amphibolite facies conditions during staurolite and kyanite growth.

Most quartz veins in the Wepawaug Schist are deformed (see fig. 2 in Ague, 1994). Folds in the veins are generally tight to isoclinal, and many of the fold limbs are extended and boudinaged. Because the axial planes of the folds are sub-parallel to the regional  $S_2$  fabric (Dieterich, ms), the veins were folded during deformation associated with  $S_2$  development. Petrographic examination indicates that undulose extinction, deformation bands, and subgrains are common in vein quartz, regardless of metamorphic grade. Mortar texture, defined by large, old, strained grains or grain aggregates surrounded by fine, recrystallized grains (Spry, 1969), has been observed in veins in low-grade pelites (Silverman, ms). Quartz grains in some amphibolite facies veins have a shape preferred orientation, especially near vein-wallrock contacts. Although isolated cross-cutting relationships between different vein generations have been observed, the intensity of deformation prohibits the construction of a detailed paragenetic sequence of veining events on the basis of field criteria alone.

Vein-matrix mineral relationships in chlorite and biotite zone rocks are not diagnostic of the metamorphic conditions attending vein formation.

#### *Relative Timing of Mass Transfer in Pelitic Schist*

Ague (1994) concluded that considerable losses of silica and Na, relative to the low-grade chlorite + biotite zone protoliths, took place during progressive metamorphism of pelites to amphibolite facies conditions. Furthermore, on average, staurolite zone pelites gained K and Ba, kyanite zone rocks lost P, and amphibolite facies pelites gained Mn and Zn. Some Ca and Sr may also have been lost from amphibolite facies rocks. In order to understand the role of mass transfer processes in the Barrovian metamorphism of the Wepawaug pelites, constraints must be placed on the relative timing of metasomatic activity. This task is difficult, because deformation and recrystallization attending orogenesis tend to obscure diagnostic textural relations. Nonetheless, the rocks contain critical evidence bearing on the relative timing of Si, Na, and K transport.

*Silica transport.*—In ~30 percent of the pelites studied by Ague (1994), quartz-rich inclusion trails in garnet that preserve a pre-existing quartzose fabric not now evident in the surrounding matrix are present (fig. 11A). For example, in sample JAW-114A, quartz-rich inclusion trails

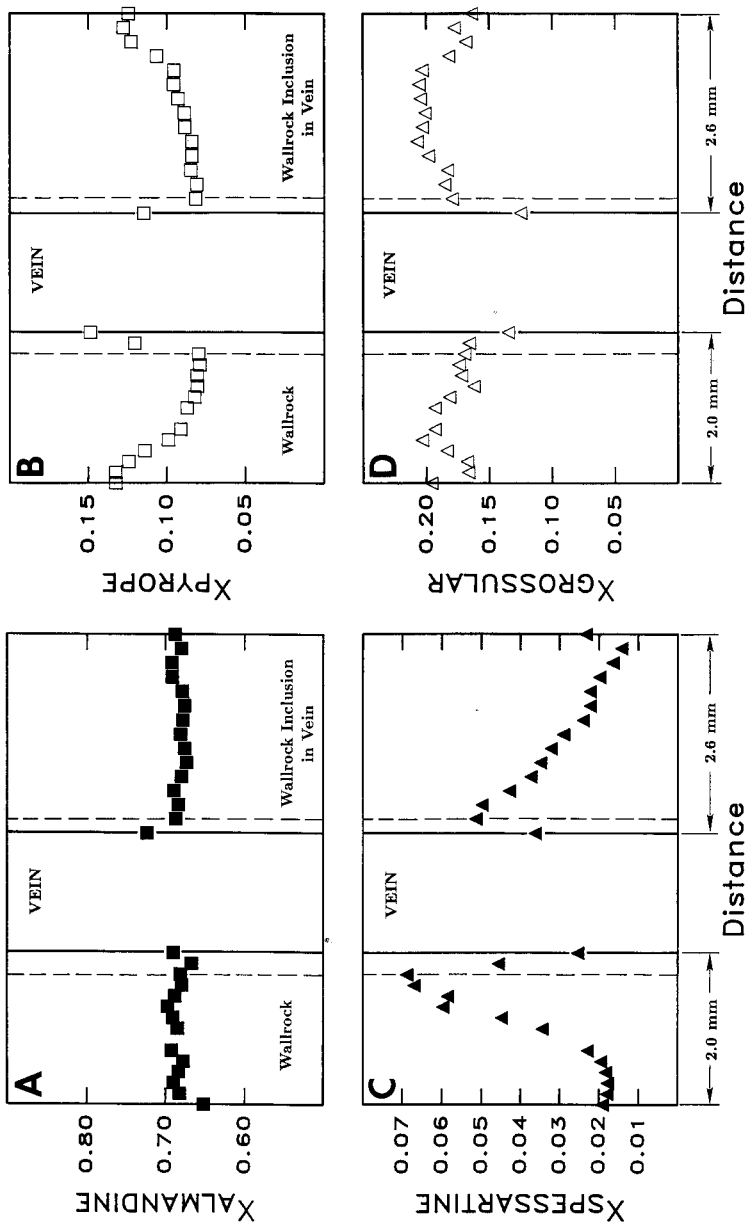


Fig. 10. Compositional profiles across a garnet porphyroblast cut by a vein, sample JAW-125D, kyanite zone. The left half of the garnet is contained in wallrock adjacent to the vein; the right half is contained in a wallrock inclusion within the vein (compare fig. 4). Vein-garnet contacts are denoted by the solid vertical lines; vertical dashed lines indicate where post-fracturing garnet overgrowth (compare fig. 9) begins. The distance between the two halves of the porphyroblast is 0.75 cm (not shown to scale for clarity). The composition of the overgrowths are similar to the garnet's rim composition but contrast markedly with the composition of the garnet core.

(A) Mole fraction almandine. (B) Mole fraction pyrope. (C) Mole fraction spessartine. Note that the bell-shaped growth zoning profile is truncated by the vein. (D) Mole fraction grossular.



Fig. 11. Textures bearing on the relative timing of mass transfer.

(A) Relict schistosity preserved in garnet (arrow). This fabric has been completely destroyed in the surrounding matrix. Quartz inclusions (arrow) are abundant in the garnet cores, but quartz is present in only trace amounts in the matrix. Matrix minerals are coarsely crystalline kyanite, biotite, and staurolite. JAW-114A, kyanite zone. Plane polarized light. Field of view is 4.4 mm wide. (B) Growth of kyanite porphyroblast at the expense of plagioclase. The plagioclase is preserved as inclusions (arrows) within the kyanite grain. Because the inclusions are optically continuous, they were probably originally part of a single plagioclase crystal. JAW-113B1, kyanite zone. Plane polarized light. Field of view is 4.4 mm wide.

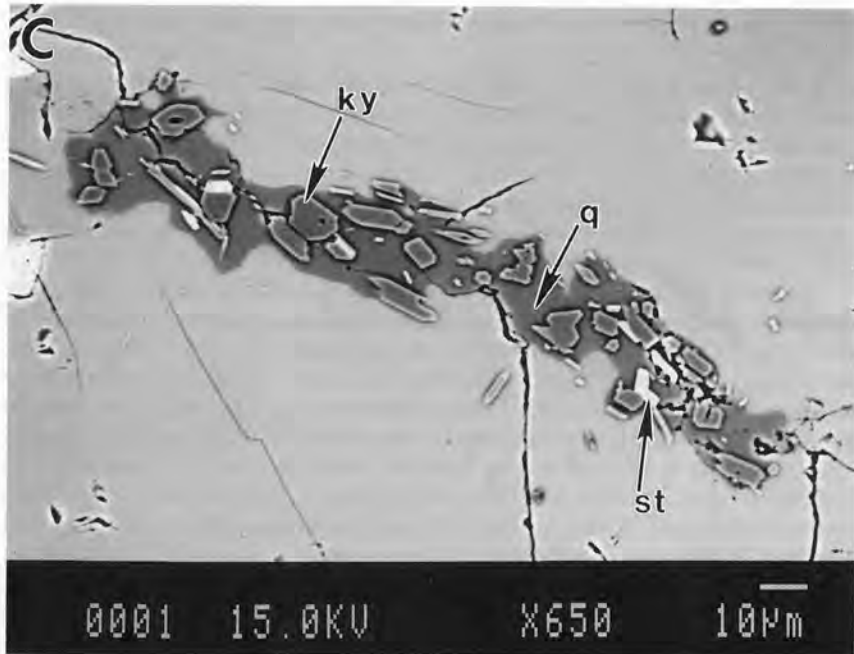
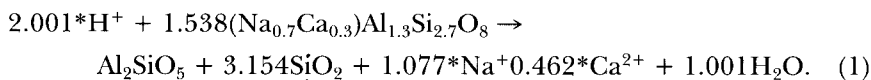


Fig. 11(C) Backscattered electron image of a fracture in a plagioclase crystal filled with microcrystalline quartz (q), kyanite (ky), and staurolite (st). The plagioclase is located at a vein-wallrock contact in sample JAW-122. (D) Intergrowth of kyanite (two cleavages, high relief) and quartz. Quartz (arrow) contains inclusions of graphite which mark the positions of pre-existing muscovite-rich zones. The kyanite and quartz are inferred to have formed from muscovite breakdown (see text for further discussion). Vein-wallrock contact is just visible along the upper edge of the photo. JAW-134E, kyanite zone. Plane polarized light. Field of view is 4.4 mm wide.

are widespread in garnets, especially in their cores, but the surrounding matrix is composed almost entirely of coarsely crystalline biotite, kyanite, staurolite, and rutile (fig. 11A). Quartz comprises only about 1 percent of the matrix mode, but ~17 percent of the volume of the garnet porphyroblasts is made up of quartz inclusions. These textural relations strongly suggest that a dramatic reduction in the amount of matrix quartz took place at some time after garnet growth began.

Garnets in amphibolite facies pelites generally have graphite-poor cores and graphite-rich rims (fig. 9). In contrast, graphite inclusions in staurolite and kyanite tend to be more evenly distributed. The graphite-rich garnet rims crystallized over the micaceous, graphitic matrix now evident in the schists (fig. 9). These relations suggest that an increase in graphite concentration in the matrix took place during garnet growth. One possibility is that as quartz was lost from the matrix, graphite was concentrated in a residual fashion. Alternatively, the graphite could have been precipitated from infiltrating fluids (Frost, 1979; Rumble and Hoering, 1986).

*Sodium transport.*—Metamorphic reactions involving plagioclase almost certainly produced the marked Na loss in the amphibolite facies pelites (Ague, 1994). About 40 percent of the thin sections of amphibolite facies rocks and veins contain staurolite and/or kyanite in an apparent reaction relationship with plagioclase (fig. 11B and C). Micron-scale kyanite and staurolite crystals occur along microfractures and grain boundaries in plagioclase, a relationship best developed in plagioclase grains in veins or wallrocks directly adjacent to veins (fig. 11C). The plagioclase in figure 11C is An<sub>30</sub> and is unzoned. If we assume an Al reference frame (Al immobile) and ignore the traces of staurolite present, a possible reaction that describes the fracture-controlled alteration is:



Throughout this paper, asterisks are used to indicate that speciation in the aqueous phase has not been determined. For this reaction, the volumetric quartz/kyanite ratio should be 1.62, if all the silica liberated from plagioclase breakdown is fixed in quartz (molar volume data from Berman, 1988, 1991). Based on a modal analysis of the image in figure 11C, the observed ratio is 2.31. Thus, for an Al reference frame, silica was added to the fracture zone such that ~30 volume percent of the quartz was externally derived. Regardless of the reference frame chosen, Na and Ca were quantitatively removed. Mass transport, either by fluid motion or diffusion, occurred preferentially in grain boundaries and cracks (Brantley, 1992; Hames and Menard, 1993). The mass transfer must have taken place under amphibolite facies conditions because the alteration products are kyanite and staurolite.

*Potassium transport.*—Observed growth of kyanite + quartz or staurolite + quartz at the expense of muscovite is evidence for possible K<sup>+</sup>

transport directly adjacent to some of the kyanite zone veins (fig. 11D). The positions of the original muscovite layers are marked by graphite inclusions in the quartz grains. For an Al reference frame, a possible reaction is:



The predicted volumetric quartz/kyanite ratio for this reaction is 0.515. The observed ratio for the rock pictured in figure 11D, based on modal analysis, is 0.524. Thus, K has probably been transported out of the regions now occupied by the quartz + kyanite intergrowths. The problem of whether or not K can be transported out of kyanite zone wallrocks entirely is addressed below. As was the case for Na, the K mass transfer took place under amphibolite facies conditions, because the products of the muscovite breakdown are kyanite or staurolite.

#### *Relative Timing of Igneous Activity*

Leucocratic igneous rocks of broadly tonalitic composition crop out sporadically in the staurolite and kyanite zones. Fritts (1965a) mapped the rocks as "Woodbridge granite" and "Devonian Pegmatite." The rocks are composed primarily of oligoclase (sometimes antiperthitic), quartz, muscovite, microcline, and garnet. Tonalitic rocks predominate, but granodiorites and granites are also present. Xenoliths of pelitic schist, many of which contain quartz veins, are commonly observed. In some of the pegmatitic/aplitic dikes that cut kyanite zone schists, garnet xenocrysts occur which contain quartz, graphite, and rutile inclusion trails identical to those found in the garnets in the adjacent wallrock. Furthermore, the garnet xenocrysts have the same size and shape as the wallrock garnets. One sample contains a magmatic dike which clearly cuts quartz veins and garnet and staurolite crystals. Field observations indicate that in the northwestern part of the Wepawaug, pelites in contact with Woodbridge granite are enriched in plagioclase feldspar and/or mica relative to "typical" pelite. Field and petrographic evidence of post-crystallization deformation and recrystallization of the igneous rocks is widespread (Bahr, ms).  $S_2$  marks the axial planes of folds in intrusive dikes. In addition, small ( $\sim 0.5$  mm) crystals of undeformed kyanite and staurolite may overgrow igneous textures, especially near contacts with pelites. Quartz veins ranging in width from a few millimeters to  $\sim 1.5$  m commonly cut the intrusions.

The garnet xenocrysts in magmatic dikes indicate that some or all the intrusive activity took place after metamorphic grade reached garnet zone conditions. In addition, magma intrusion occurred after a considerable volume of quartz veins had developed in the schists. However, the  $S_2$ -related folds and the growth of metamorphic staurolite and kyanite in the intrusions demonstrate that some of the magmas had crystallized prior to the cessation of high-grade metamorphism.

The lower-grade portions of the Wepawaug contain small amounts of deformed and metamorphosed igneous rocks of intermediate compo-

sition, which Bahr (ms) concluded were originally volcanic or shallowly emplaced intrusions. Although Fritts (1963, 1965a, b) mapped the rocks as "Woodbridge granite," it is unclear if they are genetically related to the intrusive tonalites exposed in the higher-grade portions of the Wepawaug.

### *Synthesis*

The field and textural evidence preserved in the rocks allows a relative chronology of events to be constructed. Attention is focused on rocks metamorphosed under amphibolite facies conditions, because they underwent the most extensive metasomatic alteration (Ague, 1994), and they contain the most complete textural record of deformation, metamorphism, and metasomatism. The sequence of events begins after the formation of the early fabric(s),  $S_1$ . Widespread fracturing took place, and quartz vein development was initiated (fig. 12A). Garnet crystals were cut and fractured, fragments of wallrock were dislodged from vein-wallrock contacts, and crack-seal textures evolved during vein growth. As the veins continued to develop, aluminous wallrock alteration zones developed around them (fig. 12B). Significant silica and alkali metal transport probably commenced at this stage. Staurolite (and kyanite?) began to crystallize preferentially in the aluminous vein margin regions over  $S_1$ . As deformation proceeded,  $S_2$  began to form in the rock at the expense of  $S_1$ . Staurolite and/or kyanite continued to crystallize in the wallrock alteration zones. Some buckling and folding of the quartz veins began (fig. 12C). Next, peraluminous magmas intruded the sequence (fig. 12D). Quartz veins which cut the intrusions and the surrounding schist developed. Deformation associated with the evolution of  $S_2$  continued, and the schistosity was "compressed" around earlier porphyroblasts. Staurolite and/or kyanite continued to crystallize. Finally, during the end-stages of metamorphism and deformation, some intrusive rocks underwent metamorphism leading to the growth of subsolidus staurolite and kyanite. Folds in the quartz veins continued to evolve, and fold limbs were extended and boudinaged (fig. 12E).  $S_1$  remained only as crenulated remnants between  $S_2$  cleavage planes and as inclusion trails within porphyroblasts. Whether or not the deformation that produced  $S_1$  and  $S_2$  was one continuous event or two or more separate ones is not known. What is important to emphasize, however, is that intense deformation, metamorphism, mass transfer, and magma intrusion proceeded synchronously during orogenesis and  $S_2$  development.

The geologic history of the greenschist facies portion of the Wepawaug is not as well constrained. However, on the basis of field and petrographic observations, the sequence of events in the garnet zone rocks appears to be comparable to that given above. The primary differences are that quartz vein development was not nearly as widespread, and intrusive activity was much more limited. Because the deformation that produced  $S_2$  appears to have affected the entirety of the Wepawaug Schist (Dieterich, ms), cleavage formation and  $S_2$ -related



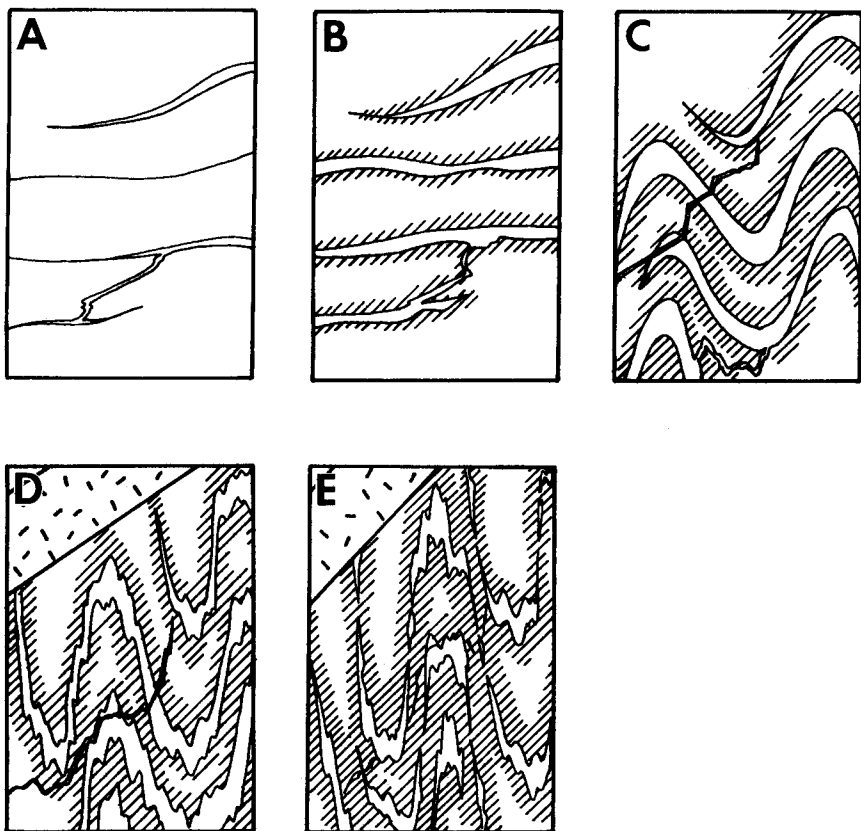


Fig. 12. Highly schematic diagrams illustrating the general structural evolution of veins and selvages during amphibolite facies metamorphism. (A) Quartz vein initiation. A substantial amount of garnet growth has already taken place in the rocks. The principal direction of extension is roughly parallel to the long edge of the drawing. (B) As deformation continues and the veins grow, aluminous selvages (diagonal ruled pattern) develop around them. (C) With continued deformation, the veins and their selvages begin to buckle.  $S_2$  begins to develop sub-parallel to the axial planes of the folds. Some new veins begin to grow. (D) Pods, sills, and dikes of tonalitic rock intrude the schists (upper left). (E) In some areas, extreme deformation resulted in nearly isoclinal folding of veins, boudinage of fold limbs, and recrystallization of igneous intrusions.

folding probably took place penecontemporaneously throughout the Formation.

#### PRESSURE, TEMPERATURE, AND FLUID COMPOSITION

The field and textural evidences presented above establish that mass transfer of rock-forming constituents in the Wepawaug pelites occurred during regional metamorphism and deformation. The next task is to quantify the pressures, temperatures, and depth regimes of metamor-

phism. Furthermore, the compositions of the metasomatic fluids must be ascertained. In this regard, particular attention is focused on the fugacity systematics of HF and HCl, because the halogens may play a crucial role in transporting metals in metamorphic hydrothermal systems. Mineral assemblages in a wide range of pelitic bulk compositions were investigated in order to elucidate genetic links between metasomatic shifts in bulk chemistry (Ague, 1994), the chemical systematics of infiltrating fluids, and the development of quartz veins.

### *Methods*

Rims of phases in mutual contact that were, on textural grounds, inferred to represent metamorphic parageneses were analyzed. Five to 16 "spot" analyses of 1 to 4 crystals of each phase were performed for each of the thin sections. At least 9 spot analyses were done for biotites to constrain better their average F and Cl contents. Average mineral compositions computed using the standard arithmetic mean and the statistical measure of location advocated by Aitchison (1989) are nearly identical, because there is little variability in the compositions of the mineral rims (see Ague, 1994 for additional discussion). Therefore, standard arithmetic means are given in the mineral composition tables. Appreciable chemical zoning was found only in garnet (fig. 10). In addition, plagioclase grains in some samples contain irregular domains of varying composition. The overall amount of variability in a given crystal, however, is small ( $\pm \sim \text{An}_3$ ). Mineral analyses are presented in tables 1 through 7.

The pressure (P) and temperature (T) of equilibration were estimated in most samples with the multi-equilibrium method of Berman (1991). P, T,  $f_{\text{HCl}}/f_{\text{H}_2\text{O}}$ ,  $f_{\text{HF}}/f_{\text{H}_2\text{O}}$ , and  $a_{\text{H}_2\text{O}}$  estimation procedures are discussed in detail in app. A.

### *Samples*

Mineral assemblages that are at least 2 cm away from the nearest quartz vein were examined in the following pelites: JAW-15B (-15B2), -21, -35B, -49, -69, -90A, -99A, -113B (-113B1), -113D, -114A, -125A (-125Ai), and -137B (-137Bi). More than one thin section was made from samples JAW-15B, -113B, -125A, and -137B; the numbers in parentheses denote the specific thin sections investigated. As noted by Ague (1994), small (< 2 mm) Mn-rich garnets occur in a few chlorite and biotite zone pelites (compare Fritts, 1963). JAW-49 is an example of a garnet-bearing pelite from the biotite zone.

Mineral assemblages in close proximity to quartz veins were examined in one sample from the staurolite zone (JAW-131A) and in three samples from the kyanite zone (JAW-125A, -113B, and -137B). Thin sections JAW-125Aii, -131A, and -137Bii were cut from clearly defined aluminous selvages in contact with quartz veins. The mineral assemblages analyzed in these three sections are no more than 1 cm away from vein-wallrock contacts. Kyanite occurs in selvages in a few staurolite zone pelites (Ague, 1994); JAW-131A is an example of a kyanite-bearing

TABLE I  
Muscovite analyses

Zone	49 (BIO)	35B (GNT)	99A (GNT)	131A (ST)	90A (KY)	113B1 (KY)	113B5 (KY)	113D (KY)	125Aii (KY)	137Bii (KY)
SiO <sub>2</sub>	46.84	46.64	48.07	47.33	46.88	46.83	46.96	46.95	47.75	47.30
TiO <sub>2</sub>	0.36	0.40	0.36	0.43	0.47	0.50	0.54	0.55	0.46	0.47
Al <sub>2</sub> O <sub>3</sub>	33.67	35.28	34.17	35.85	35.55	35.93	36.13	35.57	35.63	36.19
FeO	1.78	0.82	1.69	0.86	0.81	0.90	0.82	0.82	0.89	0.85
MnO	0.03	0.03	0.01	0.01	0.02	0.01	0.02	b.d.	0.02	b.d.
MgO	1.23	0.77	1.08	0.78	0.78	0.65	0.58	0.65	0.81	0.55
BaO	0.19	0.28	0.25	0.42	0.33	0.26	0.34	0.27	0.23	0.21
Na <sub>2</sub> O	0.52	1.38	0.85	1.27	1.15	1.39	1.39	1.34	1.45	1.64
K <sub>2</sub> O	9.80	8.88	9.74	9.10	9.08	8.98	8.86	8.99	8.94	8.68
F	0.01	0.05	0.06	0.03	0.04	0.03	0.04	0.04	0.03	0.02
Cl	b.d.	b.d.	b.d.	b.d.	b.d.	b.d.	0.01	b.d.	b.d.	b.d.
Total	94.43	94.53	96.28	96.08	95.11	95.48	95.69	95.18	96.21	95.91
Structural Formula (11 Oxygens)										
Si	3.143	3.105	3.161	3.103	3.103	3.088	3.088	3.103	3.120	3.096
Al <sup>iv</sup>	0.857	0.895	0.839	0.897	0.897	0.912	0.912	0.897	0.880	0.904
Al <sup>vi</sup>	1.805	1.873	1.809	1.873	1.876	1.880	1.888	1.874	1.863	1.888
Ti	0.018	0.020	0.018	0.021	0.023	0.025	0.027	0.028	0.022	0.023
Fe	0.100	0.045	0.093	0.047	0.045	0.049	0.045	0.045	0.049	0.046
Mn	0.002	0.002	0.001	0.001	0.001	0.001	0.001	—	0.001	—
Mg	0.123	0.076	0.106	0.076	0.077	0.063	0.057	0.064	0.079	0.054
Σ <sup>vi</sup>	2.048	2.016	2.027	2.018	2.022	2.018	2.018	2.011	2.014	2.011
Ba	0.005	0.007	0.006	0.011	0.009	0.007	0.009	0.007	0.006	0.005
Na	0.067	0.179	0.108	0.161	0.148	0.178	0.177	0.172	0.183	0.208
K	0.839	0.755	0.817	0.761	0.766	0.755	0.743	0.758	0.746	0.725
Σ <sup>xii</sup>	0.911	0.941	0.931	0.933	0.923	0.940	0.929	0.937	0.935	0.933
F	0.002	0.011	0.011	0.005	0.008	0.007	0.009	0.009	0.007	0.004
Cl	—	—	—	—	—	—	0.001	—	—	—

Notes: All Fe as FeO. b.d.: below detection.

assemblage from the staurolite zone. In thin section JAW-113B5, minerals directly at a vein-wallrock contact were analyzed (fig. 9). Muscovite, biotite, plagioclase, and kyanite in the vein are in contact with garnets in the wallrock that were fractured during vein formation. Small amounts of post-fracturing garnet grew along the contacts between the fractured

TABLE 2: Biotite analyses

Zone	49 (BIO)	69 (BIO)	35B (GNT)	99A (GNT)	131A (ST)	15B2 (KY)	21 (KY)	90A (KY)	113B1 (KY)	113B5 (KY)	113D (KY)	114A (KY)	125A1 (KY)	125A11 (KY)	137B1 (KY)	137B11 (KY)	
SiO <sub>2</sub>	37.20	37.13	37.37	36.88	37.85	36.28	36.32	37.24	35.98	36.34	36.14	36.94	36.25	35.95	36.99	36.92	
TiO <sub>2</sub>	1.59	1.64	1.66	1.59	1.31	1.31	1.27	1.27	1.48	1.40	1.52	1.56	1.51	1.50	1.30	1.44	
Al <sub>2</sub> O <sub>3</sub>	18.27	17.70	19.08	18.14	19.39	19.56	19.81	19.67	18.90	19.03	19.28	18.87	18.63	18.81	19.11	18.73	
FeO	18.42	17.74	15.22	20.18	14.74	17.76	16.98	16.24	17.87	18.00	17.20	16.05	15.61	15.65	18.52	18.66	
MnO	0.14	0.12	0.02	0.13	0.09	0.09	0.06	0.04	0.05	0.04	0.04	0.16	0.03	0.05	0.02	0.03	
MgO	10.61	11.65	12.53	9.67	12.96	11.43	11.77	11.33	11.00	10.65	11.42	11.92	12.64	12.67	10.79	10.56	
BaO	0.02	0.01	0.11	0.05	0.09	0.05	0.07	0.11	0.14	0.06	0.01	0.12	0.06	0.07	0.07	0.01	
Na <sub>2</sub> O	0.05	0.04	0.16	0.03	0.13	0.08	0.12	0.16	0.15	0.18	0.16	0.12	0.07	0.13	0.18	0.17	
K <sub>2</sub> O	9.16	8.54	8.87	8.85	9.13	9.12	9.08	9.18	8.79	8.86	8.89	9.36	9.22	9.07	9.12	9.02	
F	0.29	0.55	0.24	0.32	0.21	0.14	0.18	0.23	0.20	0.16	0.17	0.18	0.18	0.18	0.31	0.20	
Cl×10*	0.05	0.09	0.09	0.19	0.16	0.09	0.23	0.11	0.07	0.20	0.15	0.08	0.08	0.10	0.11	0.24	
Total	95.76	95.13	95.27	95.86	95.92	95.83	95.68	95.48	94.57	94.74	94.85	95.29	94.21	94.09	96.42	95.76	
Structural Formula (11 Oxygens)																	
Si	2.796	2.801	2.773	2.792	2.782	2.715	2.712	2.773	2.733	2.752	2.724	2.763	2.738	2.720	2.762	2.774	
Al <sup>iv</sup>	1.204	1.199	1.227	1.208	1.218	1.285	1.288	1.227	1.267	1.248	1.276	1.237	1.262	1.280	1.238	1.226	
Al <sup>vi</sup>	0.415	0.375	0.441	0.410	0.461	0.441	0.456	0.499	0.425	0.451	0.438	0.427	0.397	0.398	0.444	0.432	
Ti	0.090	0.093	0.093	0.090	0.072	0.074	0.071	0.071	0.084	0.080	0.086	0.088	0.086	0.086	0.073	0.081	
Fe	1.158	1.119	0.945	1.278	0.906	1.112	1.060	1.011	1.136	1.140	1.084	1.094	0.987	0.990	1.157	1.173	
Mn	0.009	0.008	0.001	0.008	0.006	0.006	0.004	0.003	0.003	0.003	0.003	0.010	0.002	0.003	0.001	0.002	
Mg	1.189	1.310	1.386	1.091	1.420	1.275	1.310	1.258	1.246	1.203	1.283	1.328	1.423	1.429	1.208	1.182	
Σ <sup>vi</sup>	2.861	2.905	2.866	2.877	2.865	2.908	2.901	2.842	2.894	2.877	2.894	2.857	2.895	2.906	2.883	2.870	
Ba	0.001	—	0.003	0.002	0.003	0.002	0.002	0.003	0.004	0.002	—	0.003	0.002	0.002	0.002	—	
Na	0.008	0.006	0.024	0.004	0.018	0.012	0.017	0.023	0.022	0.026	0.023	0.018	0.010	0.019	0.026	0.024	
K	0.878	0.822	0.839	0.854	0.856	0.871	0.865	0.872	0.852	0.855	0.855	0.893	0.889	0.876	0.869	0.864	
Σ <sup>xii</sup>	0.887	0.828	0.866	0.860	0.877	0.885	0.884	0.898	0.878	0.883	0.879	0.914	0.901	0.897	0.897	0.888	
F	0.068	0.131	0.055	0.077	0.049	0.033	0.043	0.053	0.048	0.038	0.041	0.043	0.043	0.042	0.073	0.047	
Cl×10**	0.006	0.012	0.011	0.024	0.020	0.011	0.029	0.014	0.010	0.026	0.019	0.010	0.010	0.013	0.014	0.031	

garnets and the vein (fig. 9). The compositions of the post-fracturing garnet and the vein muscovite, biotite, plagioclase, and kyanite were used for thermobarometry.

Calcite-dolomite thermometry was done using samples JAW-133 (chlorite zone), Wep-19 (garnet zone), and Wep-29c (biotite zone). Wep-19 and -29c were originally studied by Hewitt (1973). The carbonate analyses for these two samples published by Hewitt (1973) were used for temperature estimation.

### *Pressure and Temperature*

Estimated pressures and temperatures of equilibration are listed in table 8. For those samples that could be analyzed using Berman's (1991) multi-equilibrium approach, the calculated equilibria intersect over a small region of P-T space (table 8). Thus, the mineral assemblages in the pelites appear to be quite "well equilibrated" (see app. A). Systematic variations in the P-T estimates as a function of proximity to quartz veins are not evident.

Estimated temperatures range from  $\sim 400^\circ\text{C}$  in the chlorite zone to  $\sim 650^\circ\text{C}$  in the kyanite zone. The temperature estimates were plotted as a function of distance, measured perpendicular to the staurolite isograd, in order to illuminate the regional temperature regime (fig. 13A). The staurolite isograd was chosen as a frame of reference, because it is the most precisely located isograd in the field area. The metamorphic field temperature gradient (MFTG) is strikingly steep in the eastern portion of the Wepawaug Schist (fig. 13A). A least-squares fit yields a MFTG of  $55 \pm 14.4^\circ\text{C km}^{-1}$  ( $\pm 2\sigma$ ) from east-to-west across the eastern portion of the field area. The steep MFTG is consistent with the close spacing of the isograds (fig. 2). Calculated temperatures in the western kyanite zone are not consistent with the MFTG determined for the eastern part of the Wepawaug and cover a wide range from  $\sim 510^\circ$  to  $\sim 610^\circ\text{C}$ .

Spatial variations in equilibration pressures are shown in figure 13B and are mostly between about 0.7 and 0.9 GPa. The relatively high temperatures of the Barrovian isograd reactions (fig. 13A) were probably the consequence of metamorphism at high pressures. Pressures of 0.7 to 0.9 GPa are considerably higher than those inferred previously for the Orange-Milford belt ( $\sim 0.6$  GPa; Tracy and others, 1983). However, some samples in the western kyanite zone preserve equilibration pressures much lower than 0.7 to 0.9 GPa (fig. 13B).

The kyanite zone samples define a linear trend in which P and T are positively correlated (fig. 14). The ranges in estimated P and T for the entire kyanite zone (0.4 GPa and  $150^\circ\text{C}$ ) are greater than the uncertain-

---

Table 2 footnote: All Fe as FeO.

\*10 times the measured Cl wt percent. Based on replicate biotite analyses for each sample, the minimum and maximum Cl uncertainties ( $\pm 2\sigma$ ) are  $\pm 9.21 \times 10^{-4}$  wt percent (JAW-21) and  $\pm 6.39 \times 10^{-3}$  wt percent (JAW-113D), respectively; the average uncertainty for all samples is  $\pm 3.25 \times 10^{-3}$  wt percent.

\*\*10 times the calculated Cl atoms per formula unit.

TABLE 3: *Garnet analyses*

Zone	49 (BIO)	35B (GNT)	99A (GNT)	131A (ST)	15B2 (KY)	90A (KY)	113B1 (KY)	113B5 (KY)	113D (KY)	114A (KY)	125Aii (KY)	125A* (KY)	137Bii (KY)	137B* (KY)
SiO <sub>2</sub>	36.85	37.33	36.68	38.07	37.40	37.38	37.10	37.40	37.24	37.56	37.35	37.11	37.01	36.83
TiO <sub>2</sub>	0.05	0.09	0.05	0.06	0.02	0.12	0.01	b.d.	0.02	0.02	0.04	0.10	0.01	0.03
Al <sub>2</sub> O <sub>3</sub>	21.16	21.37	21.25	21.58	21.20	21.14	21.35	21.40	21.68	21.25	21.37	21.13	21.22	21.21
FeO	29.07	30.71	31.09	30.18	32.79	32.78	34.33	34.55	33.93	30.19	31.67	30.93	35.49	33.47
MnO	7.18	1.26	3.72	1.63	2.99	2.46	1.66	2.18	0.78	1.78	0.47	2.01	1.90	2.04
MgO	1.72	3.13	1.78	3.43	3.29	2.70	3.02	2.71	3.72	3.81	3.42	2.50	2.50	2.36
CaO	4.00	6.21	5.40	5.93	2.68	3.74	2.84	2.85	3.50	5.51	5.81	6.12	2.20	4.18
Total	100.03	100.10	99.97	100.88	100.36	100.29	100.31	101.09	100.87	100.12	100.13	99.90	100.33	100.12
	Structural Formula (12 Oxygens)													
Si	2.979	2.973	2.962	2.996	2.991	2.994	2.975	2.982	2.956	2.984	2.973	2.977	2.982	2.968
Al <sup>iv</sup>	0.021	0.027	0.038	0.004	0.009	0.006	0.025	0.018	0.044	0.016	0.027	0.023	0.018	0.032
Al <sup>vi</sup>	1.995	1.979	1.985	1.997	1.990	1.990	1.993	1.993	1.985	1.974	1.978	1.975	1.997	1.982
Ti	0.003	0.005	0.003	0.004	0.001	0.008	0.001	—	0.001	0.001	0.002	0.006	0.001	0.002
Σ <sup>vi</sup>	1.998	1.984	1.988	2.001	1.991	1.998	1.994	1.993	1.986	1.975	1.980	1.981	1.998	1.984
Fe	1.965	2.046	2.100	1.986	2.193	2.200	2.303	2.300	2.252	2.006	2.108	2.075	2.392	2.256
Mn	0.492	0.085	0.255	0.108	0.203	0.166	0.113	0.147	0.052	0.120	0.032	0.137	0.130	0.139
Mg	0.208	0.372	0.214	0.403	0.392	0.322	0.361	0.323	0.440	0.451	0.406	0.299	0.300	0.283
Ca	0.346	0.530	0.467	0.500	0.230	0.318	0.244	0.243	0.298	0.469	0.495	0.526	0.190	0.361
X <sub>Alm</sub>	0.653	0.675	0.692	0.663	0.727	0.732	0.762	0.763	0.740	0.659	0.693	0.683	0.794	0.742
X <sub>Sp</sub>	0.163	0.028	0.084	0.036	0.067	0.055	0.037	0.049	0.017	0.039	0.011	0.045	0.043	0.046
X <sub>Py</sub>	0.069	0.123	0.071	0.134	0.130	0.107	0.119	0.107	0.145	0.148	0.134	0.098	0.100	0.093
X <sub>Gr</sub>	0.115	0.175	0.154	0.167	0.076	0.106	0.081	0.081	0.098	0.154	0.163	0.173	0.063	0.119

*Notes:* All Fe as FeO. b.d.: below detection. \*Bulk average garnet compositions used in computing overall heterogeneous reactions (see text and app. B). Averages were computed from random "spot" analyses of garnets; 29 and 17 spot analyses were done for samples 125A and 137B, respectively.

TABLE 4  
Plagioclase analyses

Zone	49 (BIO)	35B (GNT)	99A (GNT)	131A (ST)	15B2 (KY)	90A (KY)	113B1 (KY)	113B5 (KY)	113D (KY)	114A (KY)	125Aii (KY)	137Bii (KY)
SiO <sub>2</sub>	64.78	60.71	62.70	59.10	62.34	59.24	60.98	61.38	60.20	58.27	59.93	63.28
Al <sub>2</sub> O <sub>3</sub>	21.86	24.68	22.67	25.59	23.89	25.40	24.47	23.72	25.27	26.26	24.69	23.01
FeO	0.30	0.05	0.16	0.05	0.15	0.13	0.10	0.08	0.32	0.28	0.16	0.02
CaO	2.49	5.87	3.80	6.68	4.84	6.12	5.24	4.66	5.91	8.11	5.95	3.63
Na <sub>2</sub> O	10.27	8.33	9.57	7.90	8.89	8.20	8.76	9.13	8.36	6.98	8.25	9.75
K <sub>2</sub> O	0.15	0.05	0.08	0.08	0.06	0.05	0.05	0.05	0.05	0.08	0.06	0.07
Total	99.85	99.69	98.98	99.40	100.17	99.14	99.60	99.02	100.11	99.98	99.04	99.76
Structural Formula (8 Oxygens)												
Si	2.860	2.706	2.802	2.651	2.757	2.662	2.718	2.749	2.678	2.608	2.692	2.802
Al	1.138	1.296	1.194	1.353	1.246	1.346	1.286	1.252	1.325	1.386	1.307	1.201
Fe	0.011	0.002	0.006	0.002	0.006	0.005	0.004	0.003	0.012	0.010	0.006	0.001
Ca	0.118	0.280	0.182	0.321	0.229	0.295	0.250	0.223	0.282	0.389	0.287	0.172
Na	0.879	0.720	0.829	0.687	0.762	0.714	0.757	0.792	0.721	0.606	0.718	0.838
K	0.008	0.003	0.005	0.005	0.003	0.003	0.003	0.003	0.003	0.005	0.004	0.004
X <sub>An</sub>	0.117	0.279	0.179	0.317	0.231	0.291	0.248	0.219	0.280	0.389	0.284	0.170
X <sub>Ab</sub>	0.874	0.718	0.816	0.678	0.766	0.706	0.749	0.778	0.717	0.606	0.712	0.826
X <sub>Or</sub>	0.008	0.003	0.005	0.005	0.003	0.003	0.003	0.003	0.003	0.005	0.004	0.004

Note: All Fe as FeO.

ties for the individual P-T determinations calculated using the multi-equilibrium approach (fig. 14; app. A). The kyanite zone P-T trajectory (fig. 14) is broadly similar to that documented other workers for cooling and decompression following "peak" Acadian metamorphism in western Connecticut (Hames, Tracy, and Bodnar, 1989; Armstrong, Tracy, and Hames, 1992). Therefore, it is suggested that the variation in kyanite zone P-T estimates reflects equilibration of the rocks at different times during exhumation (Hodges and Royden, 1984). For reasons as yet unknown, the lowest pressures and temperatures of equilibration are restricted to the western kyanite zone.

#### $f_{\text{HCl}}/f_{\text{H}_2\text{O}}$ and $f_{\text{HF}}/f_{\text{H}_2\text{O}}$ of Infiltrating Fluids

The  $f_{\text{HCl}}/f_{\text{H}_2\text{O}}$  and  $f_{\text{HF}}/f_{\text{H}_2\text{O}}$  ratios attending metamorphism have been investigated as a function of metamorphic grade, proximity to quartz veins, and alteration intensity (table 9). The bulk-rock TiO<sub>2</sub>/SiO<sub>2</sub> ratio is used as a general indicator of alteration intensity, in view of the major silica mass loss and consequent residual enrichment of Ti, that took place during progressive metamorphism of the Wepawaug (fig. 15; Ague, 1994).  $f_{\text{HCl}}/f_{\text{H}_2\text{O}}$  tends to increase as alteration intensity increases, regard-

TABLE 5  
Staurolite analyses

Zone	125Aii (KY)	137Bii (KY)
SiO <sub>2</sub>	28.45	28.68
TiO <sub>2</sub>	0.60	0.63
Al <sub>2</sub> O <sub>3</sub>	53.64	54.27
FeO	11.82	13.00
MnO	0.14	0.13
MgO	1.56	1.27
ZnO	0.86	0.17
Total	97.07	98.15
Structural Formula (47 Oxygens)		
Si	8.075	8.059
Ti	0.129	0.134
Al	17.942	17.972
Fe	2.805	3.054
Mn	0.033	0.031
Mg	0.658	0.533
Zn	0.180	0.035

Note: All Fe as FeO.

TABLE 6  
Carbonate analyses; JAW-133  
Chlorite Zone

	Calcite	Ankerite
CaO	53.35	29.34
MgO	0.77	15.83
FeO	1.14	8.43
MnO	0.47	0.78
CO <sub>2</sub> *	44.02	45.75
Total	99.75	100.14
Structural Formula (6 Oxygens)		
Ca	1.911	1.001
Mg	0.039	0.752
Fe	0.032	0.225
Mn	0.013	0.021
C	2.003	2.001

\*Computed during  $\phi(\rho z)$  matrix correction iterations using stoichiometry constraints.

less of metamorphic grade (fig. 15). The average  $\log(f_{HCl}/f_{H_2O})$  signature preserved in the least altered rocks ( $\log(TiO_2/SiO_2) < -1.68$ ) is  $-4.64 \pm 0.13$ , whereas that preserved in the more altered ones ( $\log(TiO_2/SiO_2) > -1.68$ ) is  $-4.40 \pm 0.11 (\pm 2\sigma)$ . The two averages are different at the 98.3 percent confidence level. Moreover, average  $\log(f_{HCl}/f_{H_2O})$  was highest in the rocks directly adjacent to the veins ( $-4.33 \pm 0.12; \pm 2\sigma$ ). Therefore,  $f_{HCl}/f_{H_2O}$  in the vein margin areas was, on average, about a factor of two greater than in the least altered rocks. Because the activity of water does not appear to have been a function of alteration intensity (see below), the variations in  $f_{HCl}/f_{H_2O}$  are interpreted to be the result of variations in  $f_{HCl}$  during metamorphism. The  $f_{HCl}/f_{H_2O}$  relations strongly suggest that the most altered rocks were infiltrated by reactive fluids with



TABLE 7  
Ilmenite analyses

Zone	49 (BIO)	99A (GNT)	15B2 (KY)	90A (KY)	113B1 (KY)
TiO <sub>2</sub>	52.21	52.76	53.17	53.25	52.89
FeO	43.75	44.57	44.49	46.47	45.93
MnO	3.33	2.50	1.75	0.96	0.85
MgO	n.d.	n.d.	0.03	n.d.	0.04
Total	99.29	99.83	99.44	100.68	99.71
Structural Formula (3 Oxygens)					
Ti	0.999	1.002	1.016	1.003	1.005
Fe	0.931	0.942	0.945	0.974	0.971
Mn	0.072	0.053	0.038	0.020	0.018
Mg	—	—	0.001	—	0.002
X <sub>Ilm</sub>	0.928	0.947	0.960	0.979	0.980

Notes: X<sub>Ilm</sub> = Fe/(Fe + Mn + Mg). n.d.: not determined.

elevated  $f_{HCl}$ . Because the vein margin areas are characterized by the highest average  $f_{HCl}/f_{H_2O}$ , the elevated  $f_{HCl}$  fluids were probably introduced via flow through fractures.

$f_{HF}/f_{H_2O}$  systematics are different from those of  $f_{HCl}/f_{H_2O}$  (table 9). The average log ( $f_{HF}/f_{H_2O}$ ) for the least altered rocks is  $-5.57 \pm 0.12$ , whereas that for the more altered ones is  $-5.57 \pm 0.10$  ( $\pm 2\sigma$ ). The two averages are statistically indistinguishable from one another. Thus, at the level of resolution,  $f_{HF}/f_{H_2O}$  is not a function of alteration intensity.

#### Activity of H<sub>2</sub>O

There does not appear to be any systematic variation in estimated water activity ( $a_{H_2O}$ ) as a function of proximity to quartz veins or alteration intensity (table 9). Moreover, there is no correlation between estimates of  $f_{HCl}/f_{H_2O}$  and  $a_{H_2O}$  (table 9). Thus, although uncertainties on the  $a_{H_2O}$  estimates are large (app. A), the increase in  $f_{HCl}/f_{H_2O}$  with

TABLE 8  
*Temperature and pressure*

Sample	Zone	Assemblage*	T °C ( $\pm 1\sigma$ )	P GPa ( $\pm 1\sigma$ )
133	CHL	G	385	
Wep-29c**	BIO	G	505	
49	BIO	B	479 (15)	0.75 (0.03)
Wep-19**	GNT	G	536	
35B	GNT	A	561 (—)	0.84 (—)
99A	GNT	B	533 (11)	0.80 (0.02)
131A	ST	C	563 (2)	0.80 (0.02)
15B2§	KY	F	563 (10)	0.65 (0.04)
90A	KY	D	507 (34)	0.56 (0.04)
113B1	KY	D	556 (34)	0.63 (0.01)
113B5	KY	C	528 (1)	0.61 (0.01)
113D	KY	C	612 (2)	0.77 (0.01)
114A§	KY	E	645 (—)	0.89 (—)
125Aii	KY	C	570 (9)	0.84 (0.07)
137Bii	KY	C	510 (3)	0.59 (0.02)

Notes: Uncertainties derived from multiequilibrium calculations (Berman, 1991). A dash (—) indicates that uncertainties could not be calculated because only two independent equilibria were available for P-T estimation.

\*Mineral assemblages used for thermobarometry. **A:** muscovite + biotite + garnet + plagioclase + quartz; **B:** assemblage **A** + ilmenite + rutile; **C:** assemblage **A** + kyanite; **D:** assemblage **A** + ilmenite + rutile + kyanite; **E:** biotite + garnet + plagioclase + quartz + kyanite; **F:** assemblage **E** + ilmenite + rutile. **G:** calcite + dolomite.

\*\*Temperatures computed from carbonate analyses of Hewitt (1973).

§Sample JAW-114A does not contain prograde muscovite; sample JAW-15B2 contains muscovite, but it was not analyzed.

increasing alteration intensity (fig. 15) is probably not the result of variations in  $a_{H_2O}$ .

#### CHEMICAL ALTERATION OF PELITIC ROCKS ADJACENT TO VEINS

In order to ascertain how the chemical and mineralogic evolution of the pelites was influenced by the growth of metamorphic vein systems, the mass changes, volume changes, and overall metasomatic reactions that occurred adjacent to veins were evaluated at two localities in the kyanite zone. At both localities, the schists outside the selvage areas contain the mineral assemblage: Quartz–muscovite–biotite–plagioclase–

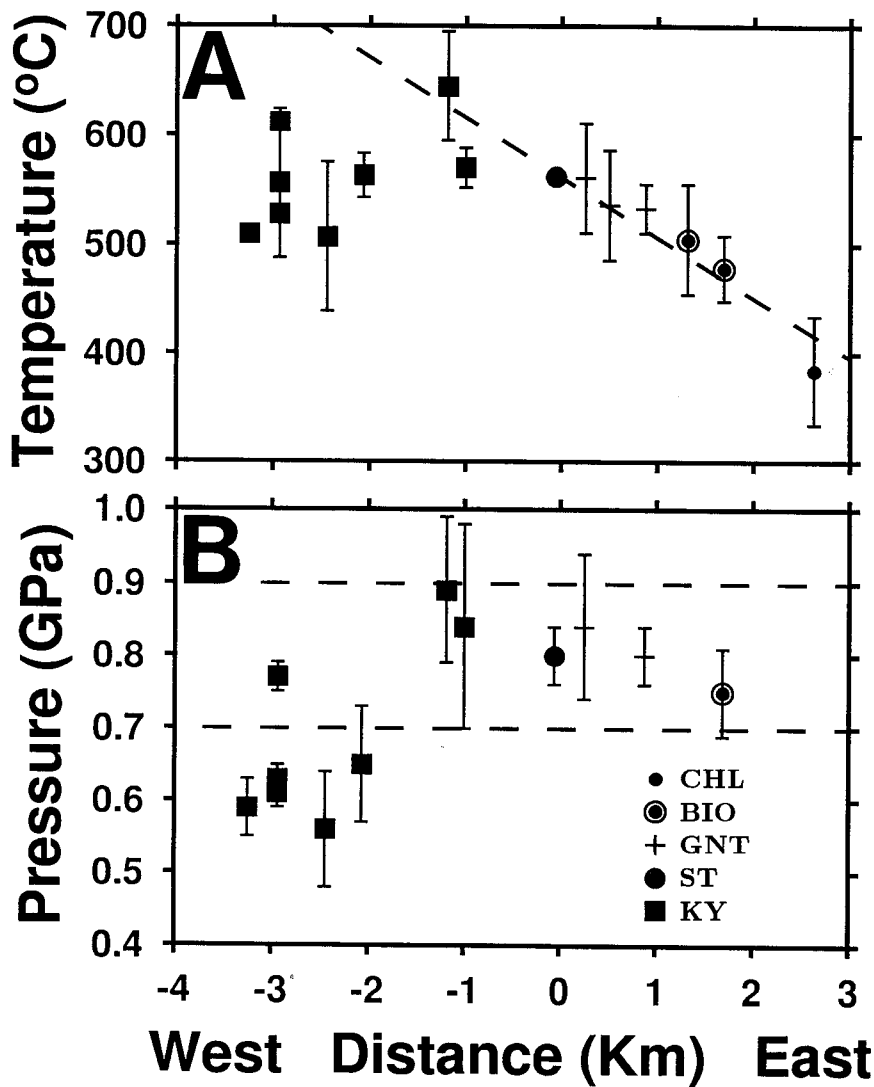


Fig. 13. Metamorphic temperature and pressure estimates plotted relative to the staurolite isograd ( $x = 0$ ). Metamorphic zones: CHL: chlorite; BIO: biotite; GNT: garnet; ST: staurolite; KY: kyanite. Error bars for most samples represent multi-equilibrium (TWEEQU) uncertainties ( $\pm 2\sigma$ ) for the P-T estimates (table 8; see Berman, 1991). Representative uncertainties of  $\pm 50^\circ\text{C}$  and  $\pm 0.1$  GPa were assigned in those cases where the multi-equilibrium method could not be used (see table 8).

(A) Temperature estimates. Note steep metamorphic field temperature gradient of  $55 \pm 14.4^\circ\text{C km}^{-1}$  (dashed line) leading into the amphibolite facies. (B) Pressure estimates. See text for further discussion.

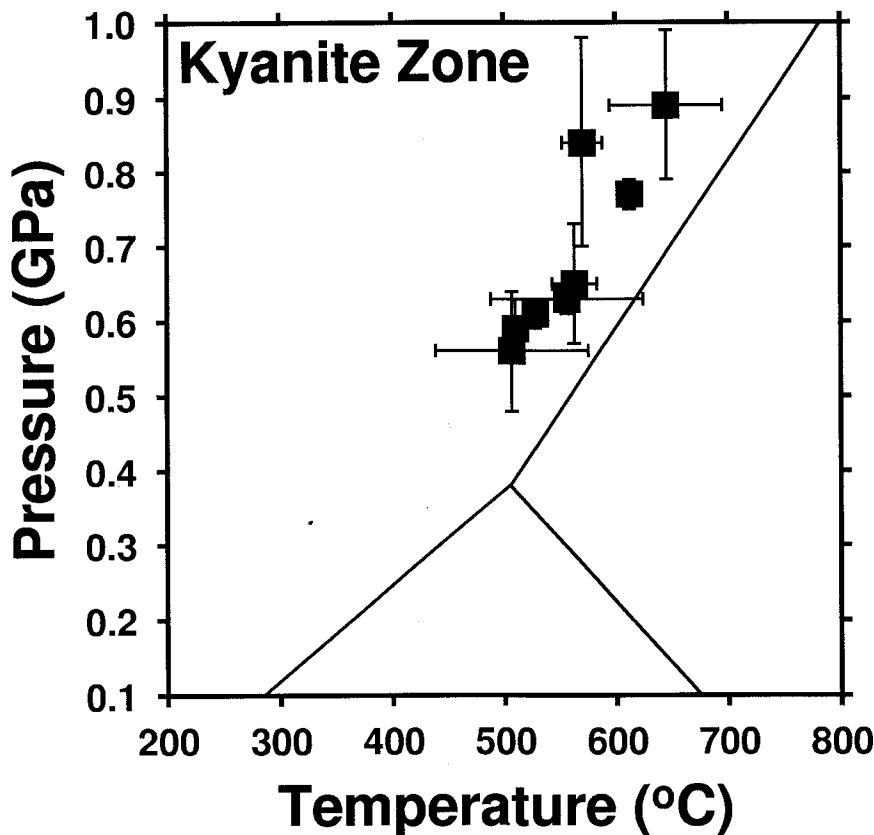


Fig. 14. Pressures and temperatures of equilibration for kyanite zone schists. Note positive correlation between P and T. Error bars for most samples represent multi-equilibrium (TWEEQU) uncertainties ( $\pm 2\sigma$ ) for the P-T estimates (table 8; see Berman, 1991). Representative uncertainties of  $\pm 50^\circ\text{C}$  and  $\pm 0.1$  GPa were assigned to the one sample (JAW-114A; table 8) which could not be analyzed using the multi-equilibrium method. Aluminosilicate phase diagram computed using thermodynamic data of Berman (1988).

garnet–rutile–graphite. In contrast, the aluminous selvages contain: Muscovite–biotite–plagioclase–garnet–quartz–staurolite–kyanite–rutile–graphite. Of basic importance here is determining why the index minerals staurolite and kyanite grew only in the selvages.

The first example (referred to as “example I”) is from a heavily veined exposure that crops out along the western shore of the Housatonic River (JAW-137 loc.; fig. 2). The P-T conditions preserved in the rocks are 0.59 GPa and  $510^\circ\text{C}$  (table 8). The veins are composed predominantly of quartz, but they may also contain isolated crystals of plagioclase at vein-wall-rock contacts. The vein studied in detail here is 2.9 cm wide and is surrounded on both sides by aluminous selvages 1.4 cm wide. Two

TABLE 9  
Fluid compositions

Sample	Zone	$\log(f_{HCl}/f_{H_2O})$	$\log(f_{HF}/f_{H_2O})$	$\log a_{H_2O}$
49	BIO	-4.936	-5.717	-0.55
69	BIO	-4.565	-5.329	—
35B	GNT	-4.504	-5.537	-0.19
99A	GNT	-4.274	-5.384	-0.24
131A	ST	-4.267	-5.610	-0.18
15B2	KY	-4.644	-5.692	—
21	KY	-4.214	-5.597	—
90A	KY	-4.641	-5.693	-0.29
113B1	KY	-4.687	-5.515	-0.16
113B5	KY	-4.338	-5.725	-0.26
113D	KY	-4.306	-5.409	-0.04
114A	KY	-4.467	-5.286	—
125Ai	KY	-4.545	-5.628	—
125Aii	KY	-4.422	-5.635	-0.19
137Bi	KY	-4.621	-5.529	—
137Bii	KY	-4.286	-5.713	-0.33

samples of pelitic wallrock outside the selvages (JAW-137Bi, -137Biii) and two samples of the selvages (JAW-137Bii, -137Biv) were investigated. The chemical compositions and grain densities ( $\rho_g$ ; rock density on a porosity-free basis) of the rocks are given in table 10, and mineral abundances are summarized in table 11.

Wallrock alteration example II is located on the kyanite isograd in the central part of the Wepawaug Schist (JAW-125 loc.; fig. 2). The estimated equilibration conditions for the rocks are 0.84 GPa and 570°C (table 8). The outcrop contains 22 percent quartz veins by volume (fig. 5). The vein studied here cuts a feldspathic metagraywacke unit and is surrounded by highly aluminous selvages (fig. 7C). Average vein and selvaige widths are 2.8 and 1.3 cm, respectively. Two samples of metagraywacke (JAW-125Ai and -125Aiii) and two samples of selvaige (JAW-125Aii and -125Aiii) were investigated (tables 11, 12).

Garnet porphyroblasts provide key constraints on the relative timing of vein growth and selvaige formation. One of the most striking differ-

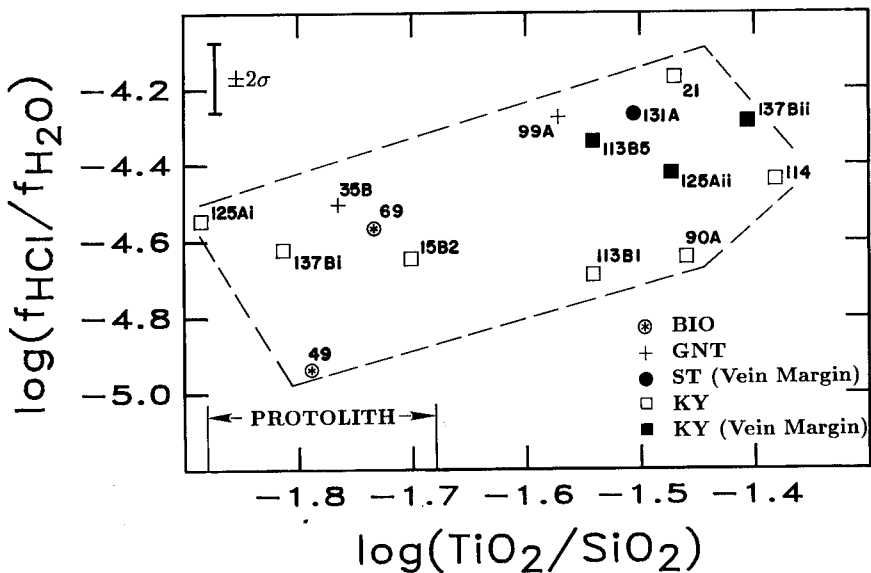


Fig. 15.  $\log(f_{HCl}/f_{H_2O})$  versus bulk-rock  $\log(TiO_2/SiO_2)$  (base 10 logarithms). Ague (1994) concluded that the presently exposed chlorite and biotite zone rocks are representative of the protolith for the higher grade schists. This protolith has low values of  $\log(TiO_2/SiO_2)$  ( $< -1.68$ ). Ague (1994) concluded that rock alteration intensity increases in a general way as  $TiO_2/SiO_2$  increases. As shown in the figure,  $\log(f_{HCl}/f_{H_2O})$  increases with increasing  $\log(TiO_2/SiO_2)$ , regardless of metamorphic grade. Note the high  $\log(f_{HCl}/f_{H_2O})$  values for assemblages directly adjacent to veins (filled symbols). Error bar represents  $2\sigma$  uncertainty in mean  $\log(f_{HCl}/f_{H_2O})$ , calculated by propagating the average analytical uncertainty for  $\log(X_{Cl}/X_{OH})$  through the expressions used to compute the fugacity ratio. Whole-rock chemistry is given in this paper (tables 10 and 12) and Ague (1994). Sample JAW-113D is not plotted because its bulk chemistry has not been determined.

ences between the selvages and the protolith wallrocks far removed from veins is that the selvages contain far less quartz than the protolith does. However, garnets in the example I selvages contain abundant quartz inclusions. These relations strongly suggest that major decreases in bulk-rock silica content associated with selvage formation occurred at some time after the garnets grew (compare fig. 11A). Garnets in the example II selvages are cut by the vein (compare fig. 9), and post-fracturing garnet growth took place along contacts between fractured garnets and the vein (see compositional profiles for sample JAW-125D in fig. 10). Thus, vein formation started after they garnets began to grow but before they had finished growing.

#### Mass Changes

The mass and volume changes resulting from metasomatism can be quantified using petrologic mass balance methods (Ague, 1991, 1994). The mass balance equations and statistical methods used in this study are

TABLE 10  
JAW-137B (example I) bulk chemical analyses

	137Bi (Protolith)	137Bii (Selvage)	137Biii (Protolith)	137Biv (Selvage)	Average* Protolith	Average* Selvage
SiO <sub>2</sub>	65.00	44.10	63.70	51.50	64.53	47.99
TiO <sub>2</sub>	1.00	1.73	1.02	1.41	1.01	1.57
Al <sub>2</sub> O <sub>3</sub>	16.00	27.70	16.50	25.40	16.29	26.71
Fe <sub>2</sub> O <sub>3</sub>	7.39	12.20	8.14	10.00	7.78	11.12
MnO	0.15	0.27	0.14	0.18	0.15	0.22
MgO	2.27	3.48	2.51	2.80	2.39	3.14
CaO	0.79	0.86	0.92	0.68	0.85	0.77
Na <sub>2</sub> O	1.26	1.30	1.35	1.09	1.31	1.20
K <sub>2</sub> O	3.25	4.21	3.27	3.22	3.27	3.71
P <sub>2</sub> O <sub>5</sub>	0.11	0.10	0.11	0.11	0.11	0.11
LOI	1.98	3.63	2.25	2.80	2.12	3.21
Total	99.20	99.58	99.91	99.19	100.00	100.00
Trace Elements (ppm)						
Cr	102	173	100	148	101	161
Zr	361	484	310	374	336	428
Nb	20	36	27	29	23	33
Rb	143	183	161	155	152	170
Sr	177	178	194	159	186	169
Ba	530	685	537	483	535	579
Cu	23	56	b.d.	26	<17	38
Zn	54	176	41	281	47	224
Grain Density (g cm <sup>-3</sup> )						
	2.82	3.04	2.84	2.99	2.83	3.02

Notes: All Fe as Fe<sub>2</sub>O<sub>3</sub>. LOI: loss on ignition. b.d.: below detection limit (10 ppm). Grain density is rock density on a porosity-free basis.

\*Averages computed using the method of Aitchison (1989). Total wt percent includes trace elements summed as oxides.

TABLE 11  
*Mineral abundances (moles kg<sup>-1</sup>)*

	125A Protolith*	125Aii Selvage	125Aiv Selvage	137B Protolith*	137Bii Selvage	137Biv Selvage
Quartz	6.329	0.402	2.247	6.074	1.380	3.147
Rutile	0.051	0.106	0.076	0.079	0.144	0.115
Garnet	0.147	0.503	0.307	0.209	0.241	0.209
Plagioclase	0.754	0.492	0.885	0.398	0.363	0.319
Biotite	0.525	0.619	0.558	0.413	0.613	0.457
Muscovite	0.255	0.576	0.379	0.577	0.502	0.601
Kyanite	—	0.128	0.049	—	0.328	0.184
Staurolite	—	0.030	0.024	—	0.080	0.074

Note: See text and app. B for discussion.

\*Computed for average protolith compositions given in tables 10 and 13.

discussed in detail by Ague (1994). For the mass balance approach to be successful, two conditions must be met: (1) the pre-alteration starting material or "protolith" must be characterized, and (2) a geochemical reference frame must be established. For example I, the first condition is satisfied by making the reasonable assumption that the aluminous selvages were derived from wallrocks compositionally equivalent to those now exposed outside the selvage areas. For example II, original sedimentary bedding, defined by alternating quartz-rich and quartz + plagioclase-rich layers, can be traced from the metagraywacke into the selvage (fig. 7C). This relationship establishes that the selvage was derived from the metagraywacke.

Si-Ti-Al-Zr relations prove useful for establishing the geochemical reference frame. The bulk-rock SiO<sub>2</sub> contents of the protolith and the selvages are shown relative to the more residual components Al<sub>2</sub>O<sub>3</sub> and TiO<sub>2</sub> in figure 16. Logratio diagrams are used to take full account of the closure problem and the multivariate nature of compositional data (Aitchison, 1986; Ague, 1994). In (SiO<sub>2</sub>/Al<sub>2</sub>O<sub>3</sub>) and ln (SiO<sub>2</sub>/TiO<sub>2</sub>) decrease dramatically in the selvage areas. The most straightforward interpretation of the Si-Ti-Al relations is that silica was lost from the selvages, relative to the more residual components Ti and Al. Major mass loss of mobile constituents causes the *concentrations* of the residual (or "immobile") components to increase because of closure (all components in a composition must sum to 1; Aitchison, 1986), but their *masses* do not change during alteration. This phenomenon is investigated further in figure 16C, D, E, and F. Within the limits of resolution, ln (Al<sub>2</sub>O<sub>3</sub>/TiO<sub>2</sub>) and ln (Zr/Ti) are invariant as a function of ln (SiO<sub>2</sub>/TiO<sub>2</sub>). Thus, Al, Zr,



TABLE 12  
*JAW-125A (example II) bulk chemical analyses*

	125Ai (Protolith)	125Aii (Selvage)	125Aiii (Protolith)	125Aiv (Selvage)	Average* Protolith	Average* Selvage
SiO <sub>2</sub>	64.50	42.50	67.90	51.00	66.23	46.90
TiO <sub>2</sub>	0.84	1.43	0.79	1.10	0.82	1.26
Al <sub>2</sub> O <sub>3</sub>	15.10	25.70	14.00	21.70	14.55	23.79
Fe <sub>2</sub> O <sub>3</sub>	6.79	14.10	6.58	10.20	6.69	12.08
MnO	0.08	0.34	0.08	0.21	0.08	0.27
MgO	3.51	4.42	3.09	3.74	3.30	4.10
CaO	1.85	2.35	1.36	2.32	1.59	2.35
Na <sub>2</sub> O	2.19	1.39	1.43	2.25	1.77	1.78
K <sub>2</sub> O	2.80	4.68	2.77	3.80	2.79	4.25
P <sub>2</sub> O <sub>5</sub>	0.22	0.34	0.22	0.26	0.22	0.30
LOI	1.70	2.70	1.85	2.54	1.77	2.64
Total	99.58	99.95	100.07	99.12	100.00	100.00
Trace Elements (ppm)						
Cr	92	162	87	118	90	139
Zr	355	527	332	400	344	463
Nb	28	60	25	51	27	56
Rb	156	202	132	185	144	195
Sr	184	137	117	201	147	167
Ba	499	911	569	756	533	836
Cu	25	68	17	37	21	51
Zn	94	302	81	164	87	224
Grain Density (g cm <sup>-3</sup> )						
	2.76	3.04	2.76	2.89	2.76	2.97

Notes: All Fe as Fe<sub>2</sub>O<sub>3</sub>. LOI: loss on ignition. b.d.: below detection limit (10 ppm). Grain density is rock density on a porosity-free basis.

\*Averages computed using the method of Aitchison (1989). Total wt percent includes trace elements summed as oxides.

and Ti behaved similarly during selvage formation. As demonstrated by Ague (1994), these elements provide an effective geochemical reference frame for the Wepawaug pelites within which mass and volume changes can be quantified. However, Al must have been mobile to some degree directly adjacent to veins, because plagioclase occurs at some vein-wallrock contacts. In addition, the analytical uncertainty for Zr is higher than that for either Al or Ti (fig. 16E and F). Therefore, Ti is used as the reference species for the calculations presented here.

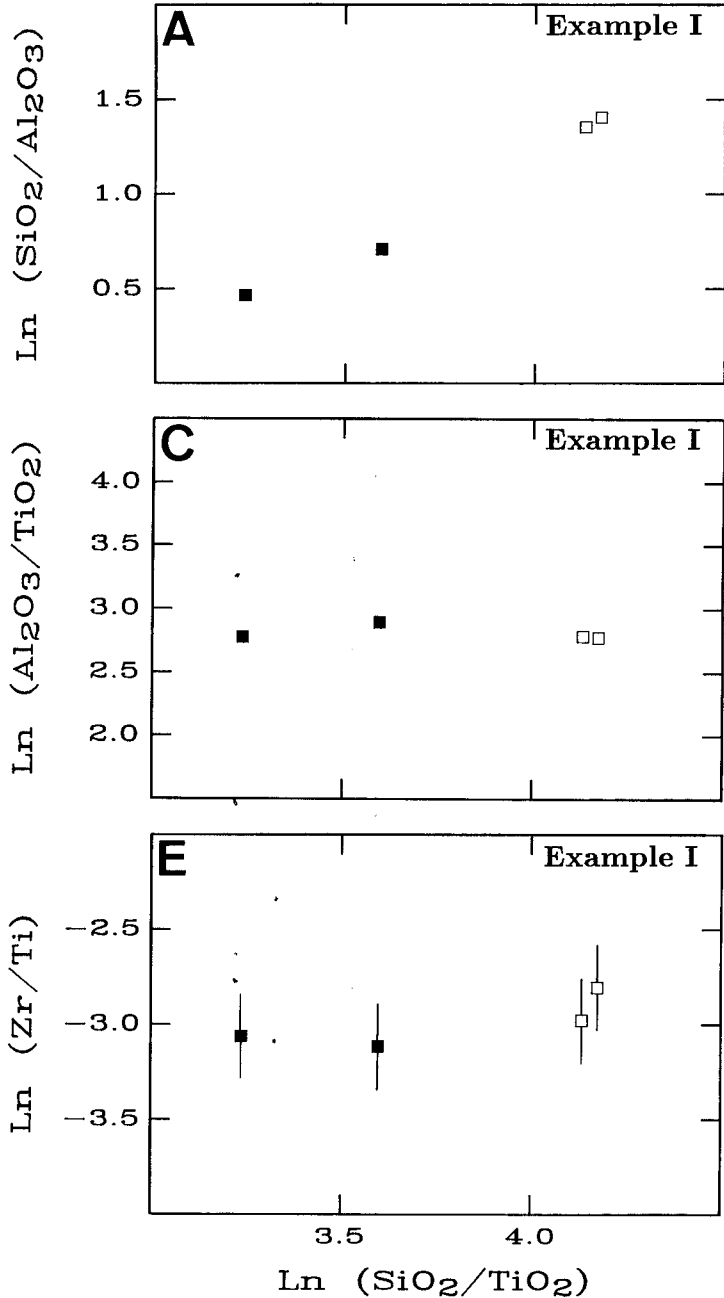


Fig. 16. Bulk chemical systematics for wallrock alteration examples I and II plotted in terms of base  $e$  logratios. Open squares: inferred protolith; filled squares: selvages. Error bars represent  $2\sigma$  expected variation for an individual chemical analysis due to analytical uncertainty, as determined by Ague (1994). Error bars for  $\ln (\text{SiO}_2/\text{TiO}_2)$ ,  $\ln (\text{Al}_2\text{O}_3/\text{TiO}_2)$ , and  $\ln (\text{SiO}_2/\text{Al}_2\text{O}_3)$  are comparable to the size of the data points and are omitted. (A), (B)  $\ln (\text{SiO}_2/\text{Al}_2\text{O}_3)$  versus  $\ln (\text{SiO}_2/\text{TiO}_2)$ .

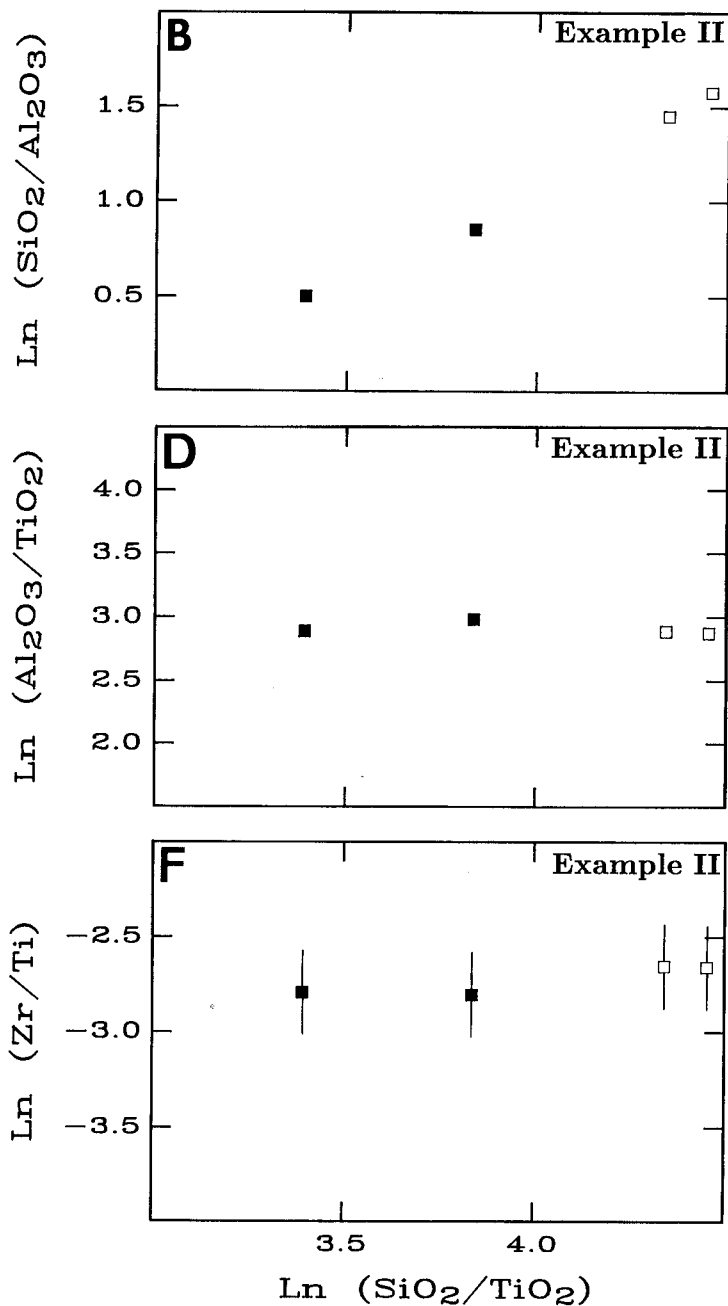


Fig. 16(C), (D)  $\ln (\text{Al}_2\text{O}_3/\text{TiO}_2)$  versus  $\ln (\text{SiO}_2/\text{TiO}_2)$ .  $\text{Al}_2\text{O}_3/\text{TiO}_2$  appears to have remained constant during selvage formation. (E), (F)  $\ln (\text{Zr}/\text{Ti})$  versus  $\ln (\text{SiO}_2/\text{TiO}_2)$ .  $\text{Zr}/\text{Ti}$  appears to have remained constant during selvage formation.

Mass balance analysis indicates that a diverse suite of major, minor, and trace elements were mobile during metamorphism (fig. 17). For alteration example I, the selvages lost Si, Na, K, Ca, P, Rb, Sr, and Ba and gained Cu and Zn, relative to the protolith wallrocks (fig. 17A). Some mass loss of Mg and Fe may also have occurred, but  $Mg/(Mg + Fe)$  remained virtually unchanged by the alteration (fig. 17A and 18A). The example II selvages lost Si, Na, Mg, Ca, and Sr and gained Fe, Mn, Zn, and Cu (fig. 17B). Inspection of figure 17 reveals that the chemical signatures of metasomatism recorded by examples I and II are similar.

Mass transfer involving the various mobile constituents led to substantial overall mass loss in the example I and II selvages. Estimates of the total mass loss for selvage samples JAW-137Bii and -137Biv are 41 and 28 percent, respectively. Mass loss estimates for JAW-125Aii and -125Aiv are 43 and 26 percent, respectively. Thus, the degree of chemical alteration was variable within the selvages.

#### *Volume Changes*

Both rock chemical and physical properties must be considered when assessing metasomatic volume changes (Brimhall and others, 1988; Ague, 1991, 1994). Grain density increases as a function of alteration intensity for both examples I and II (tables 10 and 12). The increases are the result of mass loss of low-density constituents, such as quartz, and the crystallization of new high-density aluminous porphyroblasts (Ague, 1994). Simultaneous consideration of metasomatic rock mass loss and grain density increases leads to the conclusion that JAW-137Bii, -137Biv, -125Aii, and -125Aiv lost 45, 32, 48, and 29 percent of their volume, respectively, relative to their protoliths. The volume loss is interpreted to have resulted in the tightening of folds directly adjacent to the example II vein (fig. 7C).

#### *Bulk-Chemical Shifts in the Selvages and the Average Kyanite Zone Pelite*

The geochemical evidence presented in the regional scale study of Ague (1994) strongly suggests that the metamorphism of the Wepawaug Schist was not an isochemical process. Furthermore, the selvage mass balance studies presented here indicate that extensive chemical alteration proceeded adjacent to quartz veins in the schists. The next question becomes: were the regional scale metasomatic changes in rock composition discussed by Ague (1994) caused by the development of metamorphic vein systems? This question can be addressed by comparing the bulk chemical shifts for the "average" kyanite zone pelite, as determined by Ague (1994), with the chemical alteration that caused selvage formation.

A key similarity between the average kyanite zone rock and the selvages is that they both have lost significant amounts of silica, relative to their respective protoliths. The  $\ln(SiO_2/Al_2O_3) - \ln(SiO_2/TiO_2)$  relations of the selvages (fig. 16A and B) are perfectly consistent with those of the medium and high-grade Wepawaug pelites (Ague, 1994). Another important similarity is that Na was transported out of the average kyanite zone\*

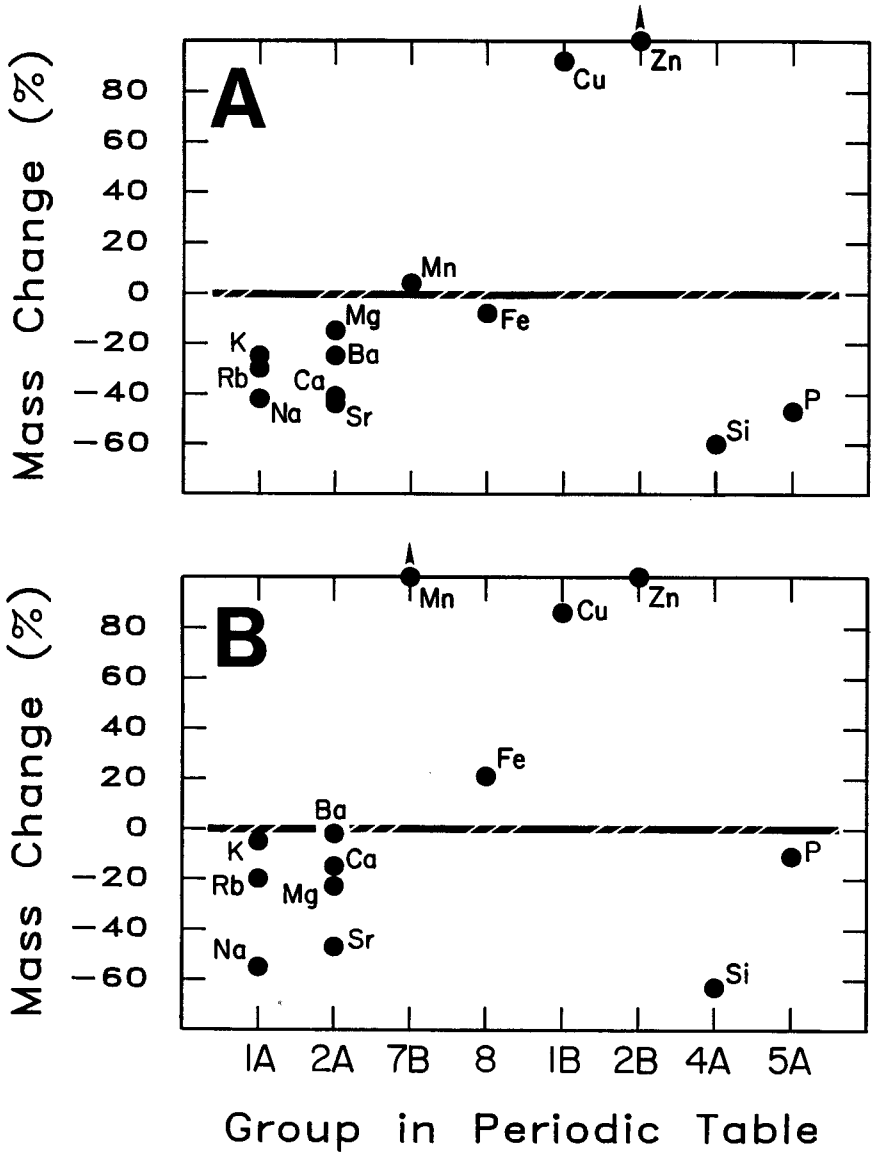


Fig. 17. Calculated mass changes versus Group in the periodic table for wallrock alteration examples I and II. Positive and negative values of mass change indicate mass gain and mass loss, respectively. Note overall similarity between the two alteration examples. Absolute values of percentage mass change greater than ~10 percent are indicative of significant mass transfer. Mass changes computed for the most silica-depleted selvage samples (JAW-137Bii and -125Aii) relative to their respective average protoliths (tables 10 and 12) using eq (2) in Ague (1994). (A) Example I. Zn mass change plots off-scale at +119 percent. (B) Example II. Mn mass change plots off-scale at +144 percent.

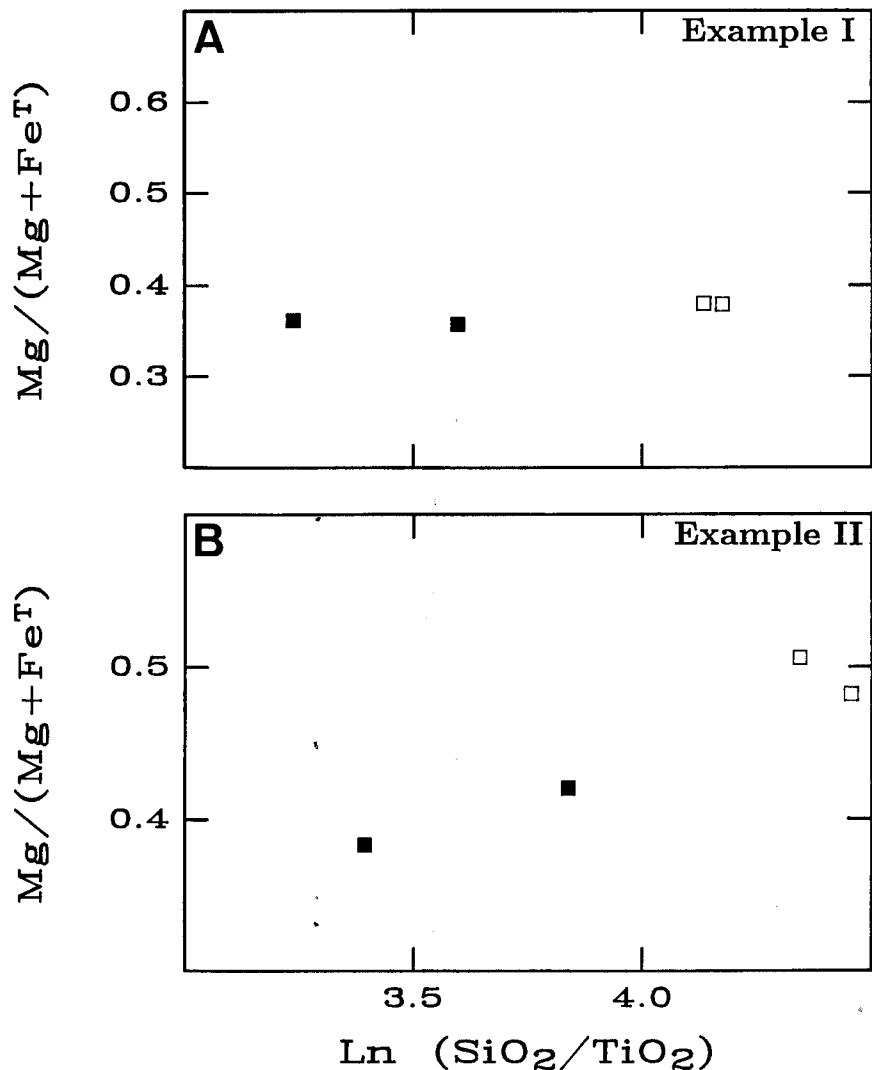


Fig. 18.  $\text{Mg}/(\text{Mg} + \text{Fe}^{\text{T}})$  (molar ratio) versus  $\ln(\text{SiO}_2/\text{TiO}_2)$  for wallrock alteration examples I and II.  $\text{Fe}^{\text{T}}$  denotes total iron. Open squares: inferred protolith; filled squares: selvages. (A) Example I:  $\text{Mg}/(\text{Mg} + \text{Fe}^{\text{T}})$  was apparently little changed during selvage formation. (B) Example II:  $\text{Mg}/(\text{Mg} + \text{Fe}^{\text{T}})$  dropped as a result of selvage formation.

pelite and the selvages. P was lost from kyanite zone rocks and the example I selvages, but there is no clear indication of major P transport in example II. The Mg/Fe of the most silica-depleted rock studied by Ague (1994) was probably decreased by metasomatism, similar to the

example II alteration. There is a suggestion of Ca and Sr loss from the average kyanite zone pelite, and both selvage examples lost Ca and Sr. The average kyanite zone rock is inferred to have *gained* Zn and Mn. Both selvage examples gained Zn, and Mn gain is evident in example II.

Chemical changes in the average kyanite zone rock also differ in several respects from the selvage metasomatism. Mass transfer of K, Rb, or Ba was not detected for the average kyanite zone rock (Ague, 1994), but the example I selvages lost K and Ba, and both examples lost Rb. The example I selvages have K/Ti and Rb/Ti ratios lower than those observed in the regional pelite study (Ague, 1994) and very low Ba/Ti. Therefore, example I probably represents an extreme case of alkali and alkaline earth element metasomatism in pelites. However, loss of K (and Na) appears to be relatively common during amphibolite facies metamorphism of metacarbonates (Orville, 1969; Hewitt, 1973; Ferry, 1982; Tracy and others, 1983).

The overall chemical changes preserved in the average kyanite zone rock and the selvages are similar. Regional bulk-chemical shifts in pelite chemistry (Ague, 1994), therefore, were probably genetically related to vein development and associated wallrock alteration.

#### *Overall Heterogeneous Reactions between Wallrocks and Infiltrating Fluids*

*Methods.*—Metasomatism typically leads to changes in rock mineral assemblages (Korzhinski, 1950; Ramberg, 1952; Thompson, 1959; Vidale and Hewitt, 1973). The overall heterogeneous reactions between aqueous species and minerals which proceeded as a result of fracture-controlled wallrock alteration provide a description of the metasomatic controls on mineralogic evolution during selvage formation. Determining the reactions requires consideration of the principles of irreversible thermodynamics and conservation of mass in open systems. On the basis of Prigogine's (1955) general treatment of irreversible thermodynamics, Brimhall (1979) showed that the stoichiometric reaction coefficient for a mineral phase  $\phi$  in an overall reaction is given by:

$$\nu_{\phi} = \frac{d\hat{n}_{\phi}}{d\xi}, \quad (3)$$

where  $\nu_{\phi}$  is the stoichiometric coefficient,  $\hat{n}_{\phi}$  is the number of moles of  $\phi$ , and  $\xi$  is the reaction progress variable for the overall reaction. Because  $\xi$  is an extensive variable, the mass changes accompanying the alteration must be accounted for explicitly when computing the  $\nu_{\phi}$ . Once the  $\nu_{\phi}$  are determined, the stoichiometric coefficients for aqueous species are calculated using conservation of mass and conservation of charge constraints (Brimhall, 1979). The procedure used to determine the overall reactions, which takes full account of metasomatic mass and volume changes, is discussed in detail in app. B.

*Results.*—The balanced heterogeneous reactions for the two examples are broadly similar in many respects but differ in detail (tables 13, 14). The primary mineralogical changes to the example I protolith

TABLE 13

*Example I overall reaction*

Reactants	Products
1.000 Quartz	0.039 Kyanite
0.054 Muscovite	0.009 Staurolite
0.035 Plagioclase	0.001 Rutile
0.013 Garnet	1.223 SiO <sub>2</sub> , <i>aq</i>
0.010 Biotite	0.048 *K <sup>+</sup>
0.176 *H <sup>+</sup>	0.041 *Na <sup>+</sup>
	0.017 *Fe <sup>+2</sup>
	0.014 *Mg <sup>+2</sup>
	0.011 *Ca <sup>+2</sup>
	0.001 *Mn <sup>+2</sup>
	0.143 H <sub>2</sub> O

TABLE 14

*Example II overall reaction*

Reactants	Products
1.000 Quartz	0.023 Garnet
0.078 Plagioclase	0.012 Muscovite
0.028 Biotite	0.009 Kyanite
0.086 *H <sup>+</sup>	0.003 Staurolite
0.029 *Fe <sup>+2</sup>	0.002 Rutile
0.003 *Mn <sup>+2</sup>	1.146 SiO <sub>2</sub> , <i>aq</i>
	0.054 *Na <sup>+</sup>
	0.030 *Mg <sup>+2</sup>
	0.016 *K <sup>+</sup>
	0.010 *Ca <sup>+2</sup>
	0.055 H <sub>2</sub> O

Notes: Asterisks indicate that speciation in the aqueous phase has not been determined. SiO<sub>2</sub>, *aq* denotes aqueous silica.

during selvage formation were the destruction of quartz, muscovite, and plagioclase and the growth of staurolite and kyanite (table 13; fig. 19A and B). Some protolith garnet and biotite were also destroyed. The destruction of plagioclase led to Na and Ca loss from the selvages, whereas mica destruction led to K loss. Furthermore, plagioclase and mica breakdown no doubt caused Rb, Sr, and Ba loss from the selvages. Because staurolite is the primary host for Zn, the pronounced Zn addition to the selvages was probably due in large part to the partitioning of Zn into staurolite during staurolite growth.

Example II selvage alteration is characterized by the growth of staurolite, kyanite, garnet, and muscovite at the expense of quartz, plagioclase, and biotite (table 14; fig. 19C and D). The calculation results indicate that plagioclase destruction was responsible for the Na, Ca (and probably Sr) loss from the protolith. Unlike example I, muscovite was a reaction product, and K loss was relatively small. Another difference between the two examples is that net garnet growth occurred apparently in the example II selvages, consistent with the garnet textural relations discussed above. The overall reaction indicates that the pronounced Mn enrichment in the selvages was primarily the result of garnet growth. As was the case for example I, the addition of Zn to the selvages was probably a consequence of staurolite growth. The decrease in bulk-rock Mg/(Mg + Fe) with increasing alteration intensity (fig. 18B) is reflected mineralogically in the crystallization of the Fe-rich phases garnet and staurolite.



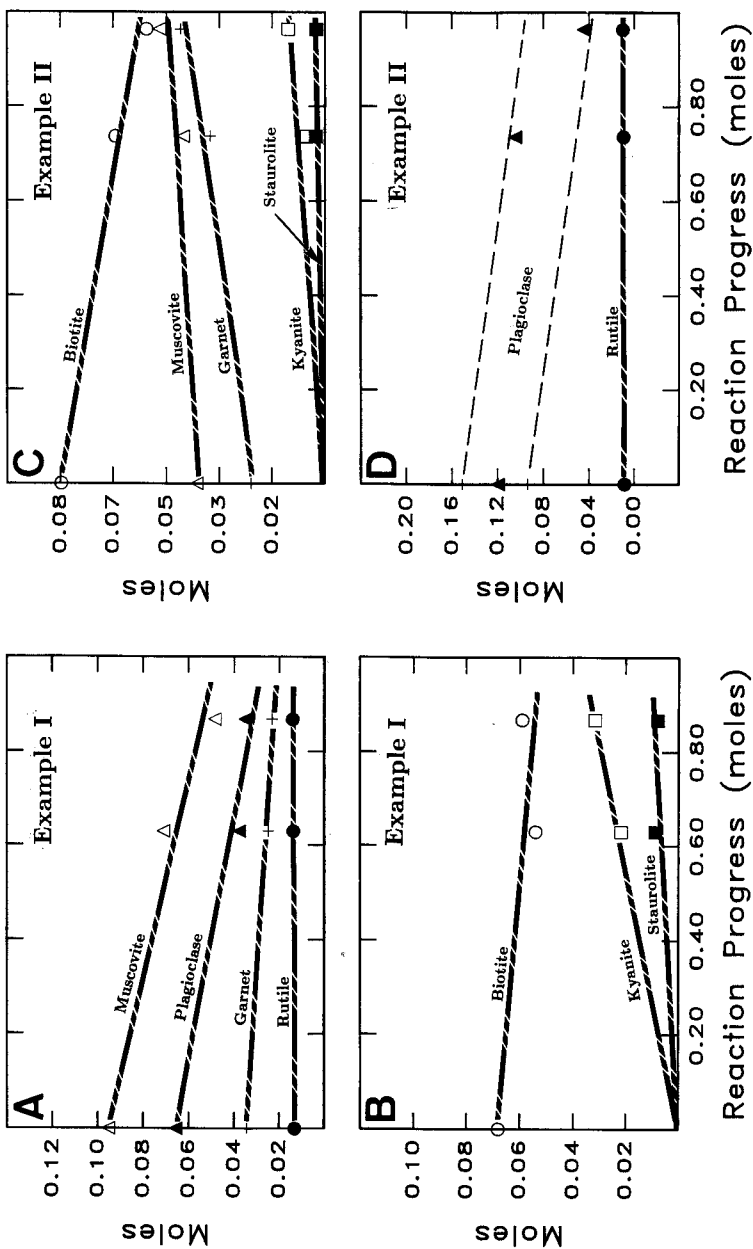


Fig. 19. Reaction progress analysis of overall selvage-forming reactions. Moles of a given mineral ( $n_{i0}$ ) are plotted as a function of the progress of the overall reaction ( $\xi$ , moles). The index mineral used to gauge the overall reaction progress is quartz. The unreacted protolith plots at a reaction progress value of 0 moles. When reaction progress is equal to 1, all quartz in the reacting system (the selvages) has been destroyed, and the stoichiometry of the overall reaction must change because quartz has been completely removed from the system. The graphs were constructed using the mineral abundances given in table 11 and the methods described in app. B.

(A), (B) Mineral moles as a function of reaction progress for example I. (C), (D) Mineral moles as a function of reaction progress for example II. The plagioclase content of the example II protolith is somewhat variable. The vertical distance between the dashed lines in (D) is equal to the observed variation in the protolith's plagioclase content. Although the variability adds uncertainty to the calculations, plagioclase content clearly varies as a function of reaction progress.

The overall reactions show that highly aluminous schists may be generated from "ordinary" quartzofeldspathic metasediments as a result of high-grade metamorphic mass transfer. The significant leaching of alkali and alkaline earth metals implies that the selvages were attacked by chemically reactive hydrothermal fluids. The calculation results suggest that "hydrogen metasomatism," involving the destruction of alkali-bearing minerals by  $H^+$  in infiltrating fluids, played a crucial role in the mineralogical transformations (Yardley, 1986; Ague and Brimhall, 1989). The overall reactions suggest that kyanite and staurolite grew simultaneously during alteration, a result consistent with the alteration textures observed along grain boundaries and cracks in plagioclase (fig. 11C). In summary, the critical point to emphasize is that the crystallization of aluminous index minerals and the positions of isograds in the field may be controlled by *metasomatic* reactions involving significant alteration of bulk-rock chemistry.

#### SOURCES OF VEIN SILICA

Determining the source(s) of the quartz deposited in the veins is essential for gaining a deeper understanding of silica transport processes and vein formation mechanisms and quantitatively assessing time-integrated fluid fluxes. Two primary sources of silica must be considered: (1) local wallrocks adjacent to veins and (2) externally-derived fluids moving through fractures.

#### *Vein-selvage Relations*

Mass balance analysis of vein-selvage relations in amphibolite facies pelites provides a means for estimating the amounts of both locally derived and "exotic" silica in the veins. If the silica lost from vein selvages were redeposited in the immediately adjacent veins, (total selvage width)/(vein width) ratios can be predicted based on observed total selvage widths. The predicted ratios may then be compared to the observed ones to determine if silica loss from the selvages can account for all the silica in the veins. If not, then silica was added to or lost from an external sink/source. The following calculations were done using appropriate mass balance expressions that describe mass change and volume strain in metasomatic systems (Brimhall and others, 1988; Ague, 1994).

The average protolith compositions and grain densities given in tables 10 and 12 were used in conjunction with a Ti reference frame in order to predict (total selvage width)/(vein width) ratios for alteration examples I and II. The predicted ratios for examples I and II are  $\sim 2.0$  and  $\sim 1.8$ , respectively. In contrast, the observed ratios are  $\sim 1.0$  (example I) and  $\sim 1.1$  (example II). Thus, the predicted ratios are about a factor of 1.6 to 2 greater than the observed ones. The analysis may be extended to all the selvage-vein width relations depicted in figure 8. As discussed previously, (total selvage width)/(vein width) ratios vary between 1 and 2, with an average of 1.3 (fig. 8). This average is significantly less than the ratio of  $\sim 2$  predicted by examples I and II.

The vein-selvage relations suggest that some proportion of the quartz in the veins was externally derived. For alteration examples I and II, a maximum of about 50 volume percent of the quartz could have been derived from the selvages. The remainder of the quartz is inferred to have been introduced from outside the local vein-wallrock system. Comparison of the mean predicted (total selvage width)/(vein width) ratios for examples I and II with the mean observed ratio computed for the data shown in figure 8 suggests that the amounts of internally- and externally-derived quartz in the average amphibolite facies vein are about 70 and 30 percent, respectively.

#### *Observed and Predicted Vein/Wallrock Ratios*

A second way to address the problem of silica sources is to consider the overall silica mass loss from pelitic wallrocks documented by Ague (1994), in relation to the proportion of quartz veins in the schists (fig. 20). The bulk chemical and grain density data for pelitic schists presented by Ague (1994) was used jointly with appropriate mass balance expressions to predict the volumetric vein/wallrock ratio in the garnet, staurolite, and kyanite zones, assuming that all the silica lost from wallrocks was redeposited in local veins. The predicted ratios were then compared to the observed ones in order to determine if more quartz was present in the form of veins than could be accounted for by silica depletion of pelitic wallrocks. The silica mass balance was computed relative to low-grade chlorite and biotite zone protolith rocks using a Ti reference frame (see Ague, 1994, for detailed discussion). Because the vein density measurements (fig. 5) include all the lithologies present at each measurement site, they must be corrected to account for the fact that nearly all the veins are restricted to the aluminous pelitic units. The corrections were done by assuming that 70 percent of the metasedimentary section is composed of aluminous pelite (Ague, 1994).

The average silica mass loss from pelitic wallrocks and the proportion of quartz veins in outcrop both increase systematically as metamorphic grade increases across the Wepawaug (fig. 20). The predicted mean vein/wallrock ratios for the garnet, staurolite, and kyanite zones are  $0.096_{-0.08}^{+0.41}$ ,  $0.249_{-0.09}^{+0.13}$ , and  $0.336_{-0.10}^{+0.15}$ , respectively ( $\pm 2\sigma$ ; geometric mean). On the other hand, the observed mean ratios are  $0.111_{-0.07}^{+0.22}$  (garnet zone),  $0.376_{-0.11}^{+0.16}$  (staurolite zone), and  $0.543_{-0.09}^{+0.11}$  (kyanite zone). Thus, the observed ratios for the staurolite and kyanite zones are noticeably higher than the predicted ones. Statistical tests appropriate for compositional data (Aitchison, 1986; Woronow and Love, 1990; Ague, 1994) indicate that the observed and predicted vein proportions for the kyanite zone are different at the 97.6 percent confidence level. Statistical analysis of the staurolite zone results is hampered, because the number of vein proportion measurements and bulk composition determinations are relatively small (fig. 20; Ague, 1994). Comparison of the observed and expected ratios for the staurolite and kyanite zones suggests that a maximum of about 70 volume percent of the quartz was derived from amphibolite

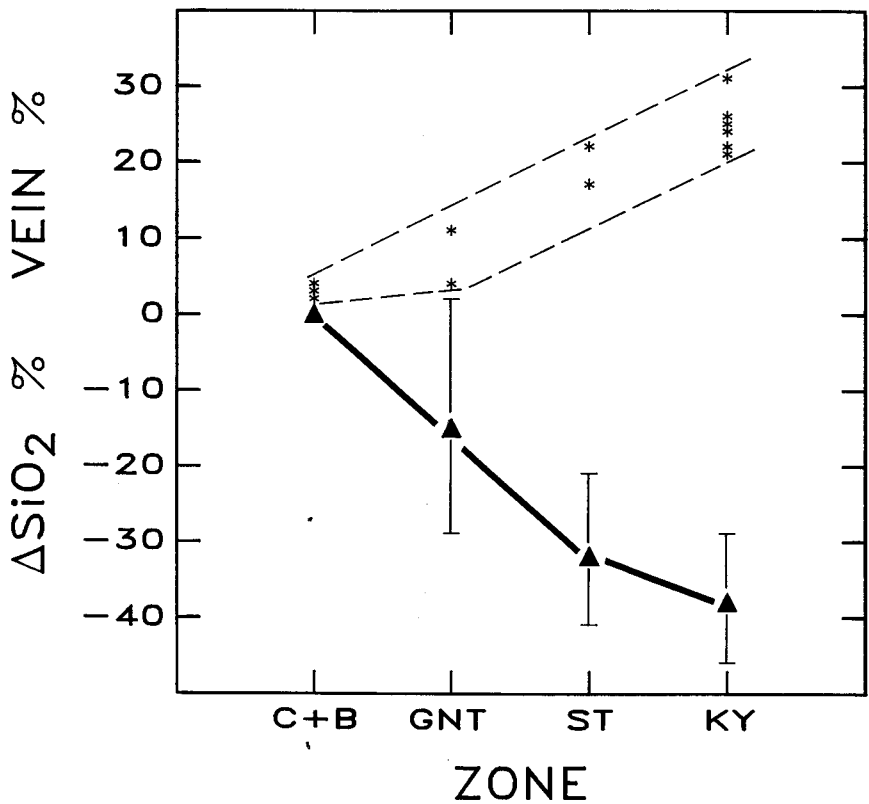


Fig. 20. Vein density and silica mass change ( $\Delta\text{SiO}_2$  percent) plotted as functions of metamorphic grade. Negative mass change values indicate mass loss (see text and Ague, 1994, for discussion of mass change computations). Metamorphic zones: C + B: chlorite and biotite; GNT: garnet; ST: staurolite; KY: kyanite.

facies wallrocks and that ~30 percent of the quartz was introduced from outside local vein-wallrock systems.

The vein/wallrock ratio analysis described in this section and the vein-selvage relations presented above both yield the same estimate for the proportions of internally- and externally-derived quartz in the average amphibolite facies vein. It is interesting to note that these proportions are identical to those inferred for the micron-scale alteration of plagioclase along grain boundaries and cracks (fig. 11C). The proportions of internally- and externally-derived quartz in greenschist facies veins are presently unknown and will be investigated in future studies.

#### *Review of Stable Isotopic Evidence for Fluid Infiltration in the Wepawaug*

Previous stable isotopic work in the Wepawaug (Tracy and others, 1983; Palin, ms; Palin and Rye, 1992) has shown that bulk quartz vein samples from the staurolite and kyanite zones may be grossly out of

oxygen isotopic equilibrium (by as much as 2.5 permil) with wallrock quartz. This observation suggests that some proportion of the vein quartz was deposited from externally-derived fluids.

The high-spatial resolution isotopic study of van Haren, Rye, and Ague (1992) revealed that oxygen isotopic ratios of quartz within a single kyanite zone vein are highly variable.  $\delta^{18}\text{O}$  ranges from values comparable to those measured in local wallrocks far-removed from veins to values as much as 1.5 permil lighter. Preliminary calculations indicate that the isotopic variations could not have resulted from net transfer reactions in a closed system (Chamberlain, Ferry, and Rumble, 1990). Van Haren, Rye, and Ague (1992) concluded that vein quartz was precipitated from fluids derived in part from outside the local wallrock.

#### REGIONAL FLUID FLOW AND AMPHIBOLITE FACIES VEIN FLUID FLUXES

##### *Evidences for Regional Fluid Flow*

Four critical lines of evidence suggest that the veins were zones of significant fluid infiltration during metamorphism. The discussion is focused on the amphibolite facies veins, because they preserve the most complete petrologic and isotopic record of fluid flow. First, the chemical alteration of wallrock adjacent to veins involving transport of a broad spectrum of rock-forming and trace elements (fig. 17) could only have occurred if the veins were conduits for significant volumes of fluid (Ferry and Dipple, 1991; Yardley and Botrell, 1992). Second, the increase in estimated  $f_{\text{HCl}}/f_{\text{H}_2\text{O}}$  adjacent to veins (fig. 15) is evidence that fluids with elevated  $f_{\text{HCl}}$  were introduced into the Wepawaug by advection through fractures. Third, the silica mass balance indicates that about 30 volume percent of the quartz in the average amphibolite facies vein was externally-derived. The only reasonable way to introduce silica on the regional scale is through widespread fluid infiltration. Finally, the observation of isotopic disequilibrium between vein and matrix quartz (Tracy and others, 1983; Palin, ms; van Haren, Rye, and Ague, 1992) suggests that some proportion of the vein fluids were externally-derived. On the basis of the above evidence, it is concluded that the veins were conduits for the regional scale transport of large volumes of fluid during metamorphism. In order to precipitate vein quartz, the fluids were almost certainly moving down temperature and pressure gradients. Stable isotope systematics and metacarbonate phase relations suggest that fluid flow was in a direction of decreasing temperature throughout the Wepawaug (Palin, ms; Palin and Rye, 1992).

##### *Fracture Flow and Quartz Precipitation*

Using the model of Ferry and Dipple (1991), the time-integrated fluid fluxes involved in vein formation can be estimated, if it is assumed that the fluids were always in local chemical equilibrium with respect to quartz along the flow path, and that the effects of diffusion and hydrodynamic dispersion can be neglected. The calculations were done for representative amphibolite facies conditions of 600°C and 0.8 GPa, using regional temperature and pressure gradients of  $-0.025^\circ\text{C m}^{-1}$  and

$-2.75 \times 10^4 \text{ Pa m}^{-1}$ , respectively. The temperature gradient is discussed further in the context of advective heat transport in the following section. Aqueous silica solubility gradients were computed with the model of Fournier and Potter (1982). Based on the foregoing mass balance analysis, it was assumed that 30 percent (by volume) of the vein quartz was deposited from through-going fluids.

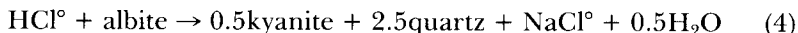
The time-integrated fluid flux necessary to produce the average amphibolite facies vein is estimated to have been  $\sim 2.8 \times 10^5 \text{ m}^3 \text{ m}^{-2}$ . As pointed out by Ferry and Dipple (1991), fluxes of this magnitude are sufficient to cause significant major and trace element metasomatism. Using the vein proportion measurements of figure 5, the best estimate of the time-integrated fluid flux due to flow through veins in the amphibolite facies is  $\sim 6 \times 10^4 \text{ m}^3 \text{ m}^{-2}$ . Similar flux estimates have been made by Ferry (1992) and Skelton, Graham, and Bickle (1993) for regional fluid outflow zones in Vermont and the Scottish Dalradian, respectively. It should be noted that if regional gradients in the activity of water existed during flow, then the flux estimates may be in error owing to the effect of water activity on silica solubility (Crerar and Anderson, 1971; Walther and Orville, 1983). However, the nature and magnitude of such gradients are not known at this time.

#### *Hydrogen Metasomatism*

The heterogeneous reaction analysis (tables 13 and 14) suggests that wallrock alteration involved significant H metasomatism and alkali transport. The nature and extent of the metasomatism can be used potentially to estimate fluid fluxes. However, theoretical analysis is severely hampered for a number of reasons. For example: (1) thermodynamic data for aqueous species are considered to be reliable only at pressures below about 0.5 GPa (Johnson, Oelkers, and Helgeson 1992), (2) the kinetics of the heterogeneous reactions are not tightly constrained, (3) thermodynamic data and activity models for key phases such as staurolite are highly uncertain, and (4) considerable controversy surrounds the speciation of high P-T electrolyte solutions (Oelkers and Helgeson, 1993). In the light of these complications, only a highly simplified model of H metasomatism has been considered here. The calculations were done using the thermodynamic data for minerals derived by Berman (1988), as modified by Sverjensky, Hemley, and D'Angelo (1991), in conjunction with the SUPCRT92 software package of Johnson, Oelkers, and Helgeson (1992). The thermodynamic properties of  $\text{HCl}^\circ$  were taken from Sverjensky, Hemley, and D'Angelo (1991), whereas the default SUPCRT92 data base (Johnson, Oelkers, and Helgeson, 1992) was used for all other aqueous species and water. The activity coefficients of uncharged aqueous species were taken to be unity (Sverjensky, 1987; Sverjensky, Hemley, and D'Angelo, 1991).

One of the key aspects of the alteration is the destruction of plagioclase and the consequent loss of Na and growth of aluminous index minerals (fig. 11C; tables 13, 14; Ague, 1994). A simple hydrolysis

reaction that describes this alteration is:



The reaction is written in terms of  $\text{HCl}^\circ$  and  $\text{NaCl}^\circ$ , because available thermodynamic data (Johnson, Oelkers, and Helgeson, 1992) indicate that these will be the dominant H and Na species in a broad spectrum of Cl-bearing metamorphic fluids in the amphibolite facies (Ferry and Dipple, 1991; Ferry, 1992). As shown in figure 21, if local equilibrium is maintained, then down-temperature fluid flow will promote the crystallization of aluminosilicate at the expense of plagioclase.

An *order-of-magnitude* estimate of the time-integrated fluid fluxes involved can be made if it is assumed that local equilibrium between aluminosilicate, quartz, albite, and fluid is maintained along the flow path

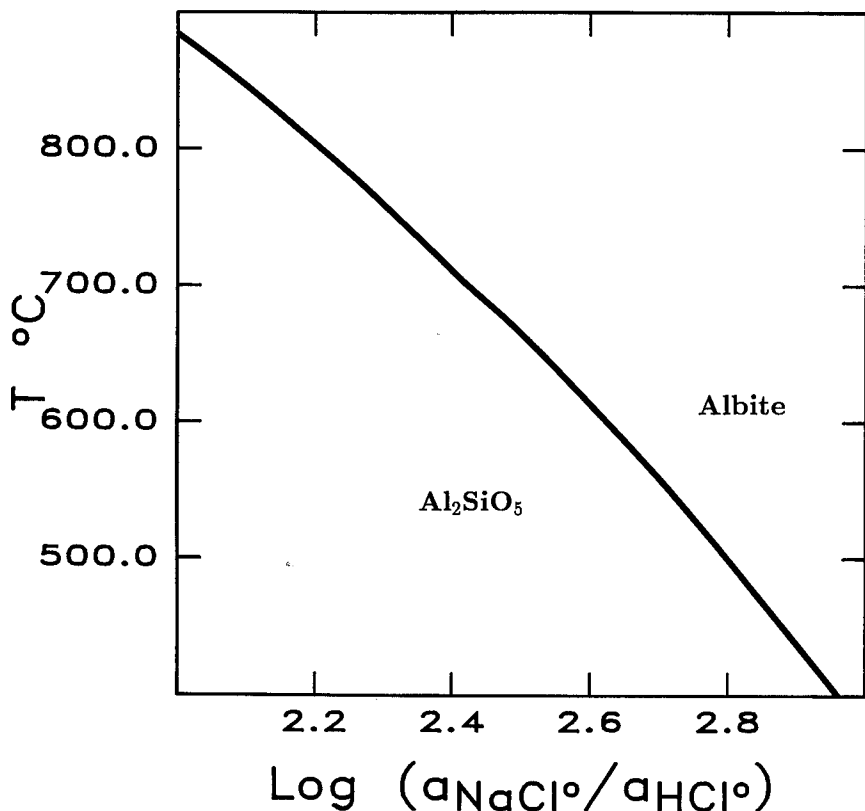


Fig. 21. T versus  $\log (a_{\text{NaCl}^\circ}/a_{\text{HCl}^\circ})$  (base 10 logarithms). Total P is 0.8 GPa.  $\text{H}_2\text{O}$  activity = 1. Using the method of Zhu and Sverjensky (1992), the  $a_{\text{HCl}^\circ}$  adjacent to kyanite zone veins is estimated to have been  $\sim 10^{-3}$ . At 600°C, the corresponding  $\text{NaCl}^\circ$  concentration is  $\sim 0.5$  molal. See text for additional discussion.

and that the effects of diffusion and hydrodynamic dispersion are negligible. With these assumptions, the metasomatic model of Ferry and Dipple (1991) can be extended to trivariant hydrolysis reactions such as eq (4), as discussed in detail by Steefel (ms). Using the methodology of Baumgartner and Ferry (1991) and Steefel (ms), the time-integrated fluid flux ( $q_{TI}$ ) is related to fluid composition and the progress of the albite  $\rightarrow$  kyanite reaction in a 1-dimensional system by:

$$q_{TI} = - \frac{\xi_{Albite}}{\frac{[NaCl^{\circ}]^2}{([NaCl^{\circ}] + [HCl^{\circ}])} \left( \frac{\partial([HCl^{\circ}]/[NaCl^{\circ}])}{\partial T} \frac{\partial T}{\partial x} \right)} \quad (5)$$

where  $\xi_{Albite}$  is the reaction progress variable, and the square brackets indicate concentrations of aqueous species (moles volume<sup>-1</sup>). The change in  $[HCl^{\circ}]/[NaCl^{\circ}]$  with pressure is very small and therefore may be neglected. As emphasized by Steefel (ms), calculation of fluid fluxes using trivariant reactions requires that temperature and pressure gradients, reaction progress, and fluid composition in the reacting system be known. This fact places severe restrictions on the usefulness of eq (5). However, for a representative set of input variables, some constraints on the fluid fluxes can be made in the local equilibrium case.

For example, consider a representative electrolyte solution with an  $NaCl^{\circ}$  concentration of 0.5 molal (fig. 21) which coexists with quartz, aluminosilicate, and albite at 600°C and 0.5 GPa. The value of  $\partial([HCl^{\circ}]/[NaCl^{\circ}])/\partial T$  is  $1.3 \times 10^{-5} \text{ } ^{\circ}\text{C}^{-1}$ . The temperature gradient was taken to be  $-0.025 \text{ } ^{\circ}\text{C m}^{-1}$ . The initial rock contains 50 volume percent of both quartz and albite. Under these conditions, production of 2 volume percent kyanite (comparable to the modal abundance of kyanite in the Wepawaug pelites) from albite would require a time-integrated fluid flux on the order of  $10^6$ – $10^7 \text{ m}^3 \text{ m}^{-2}$ . Although the uncertainties on the estimated flux are probably at least  $\pm$ one order of magnitude, the calculations suggest that hydrogen metasomatism is feasible under amphibolite facies conditions if fluid fluxes are large. This result is consistent with the observation that aluminous index minerals are concentrated in selvages adjacent to fracture flow conduits (veins).

Hydrogen metasomatism will be enhanced if the infiltrating fluids have values of  $a_{HCl^{\circ}}/a_j$  ( $j =$  a given mobile species, such as  $NaCl^{\circ}$ ) significantly higher than those in equilibrium with pelitic mineral assemblages. Tonalitic-granitic magmas are a potential source of such fluids. Syn-metamorphic intrusions are locally abundant in the amphibolite facies of the Wepawaug, but the role of magmatic fluids in the metasomatism remains to be resolved.

#### FLUID FLOW AND HEAT TRANSPORT

Focusing of fluid flow into regional fracture systems can significantly affect the thermal regime of metamorphism (Bickle and McKenzie, 1987; Brady, 1988; Chamberlain and Rumble, 1988; Hoisch, 1991; Ferry,



1992). Following Ferry (1992), the impact of channelized fluid flow on heat transport can be evaluated using the Peclet number ( $B$  parameter) formulation of Brady (1988):

$$B = \frac{QL\rho_f c_{p,f}}{K_r} \quad (6)$$

where  $Q$  is the average Darcy velocity,  $L$  is the length scale of the system,  $\rho_f$  is the fluid density,  $c_{p,f}$  is the fluid heat capacity, and  $K_r$  is the thermal conductivity of the rock. When  $B > 1$ , fluid advection will play a significant role in heat transport. The Darcy velocity is related to the time-integrated fluid flux,  $q_{TI}$ , by:

$$Q = \frac{q_{TI}}{\Delta t}, \quad (7)$$

where  $\Delta t$  is the time span over which the flow occurs. If we take the length scale of transport to be 10 km (comparable to the presently exposed dimensions of the amphibolite facies of the Wepawaug),  $q_{TI} = 6 \times 10^4 \text{ m}^3 \text{ m}^{-2}$ ,  $\rho_f \cdot c_{p,f} = 3.5 \times 10^6 \text{ J m}^{-3} \text{ K}$  (Brady, 1988), and  $K_r = 2.5 \text{ J m}^{-1} \text{ s}^{-1} \text{ K}$ , then  $B$  can be estimated for a range of time scales and corresponding Darcy velocities. The calculations suggest that fluid advection would have played an important role in heat transport if the time scale of flow was  $\sim 10^7$  yr or less. For example, if  $\Delta t = 10^7$  yr, then  $B = 2.7$ . Because the length of the entire Acadian orogeny was on the order of  $10^7$  yr (Osberg and others, 1989), fluid flow associated with vein development may have transported significant heat.

The calculated  $B$  values depend on the  $q_{TI}$  estimate which, in turn, depends on the estimate of the thermal gradient in the direction of flow. As discussed above,  $q_{TI}$  was computed using a representative regional gradient of  $-25^\circ\text{C km}^{-1}$ . However, if the fluids transported heat, then the thermal gradient could have been considerably different from this. The thermal modeling of Brady (1988) indicates that in the deeper parts of the crust, advective heat transport will tend to decrease the thermal gradients in the direction of flow. As a result, the  $q_{TI}$  and  $B$  estimates may both be *minimum* estimates. Even if regional temperature gradients were as high as  $-50^\circ\text{C km}^{-1}$ ,  $B$  would still be in excess of 1.5 for  $\Delta t \leq 10^7$  yr.

It is tempting to speculate that the steep metamorphic field temperature gradient leading to the amphibolite facies schists (fig. 13A) was the result of fluid-driven heat transport during amphibolite facies metamorphism (Brady, 1988; Hoisch, 1991). In this case, the amphibolite facies of the Wepawaug would constitute a metamorphic "hot-spot," analogous in many ways to the Bristol, New Hampshire, hot spot described by Chamberlain and Rumble (1988).

#### REGIONAL FLUID FLOW PATHS

Fluid sources and regional fluid flow paths remain unresolved. The most obvious potential fluid source is dehydration of underlying crust.

The present-day depth to the Moho in New England ( $\sim 40$  km; Ando and others, 1984) provides an estimate of the vertical length scale over which crustal fluids could have been derived. For convenience, consider a cylindrical region of dehydrating crust. The radius,  $r$ , of the cylindrical volume that must be dehydrated to produce a given volume of fluid is:

$$r = \left( \frac{q_{TI}A}{\pi L f_v} \right)^{0.5}, \quad (8)$$

where  $q_{TI}$  is the time-integrated fluid flux,  $A$  is the total area over which the flux is measured,  $L$  is the length of the cylinder (40 km), and  $f_v$  is the volume of fluid evolved per unit volume of rock undergoing dehydration. For the amphibolite facies of the Wepawaug,  $q_{TI} \sim 6 \times 10^4 \text{ m}^3 \text{ m}^{-2}$ . The average kyanite zone pelite contains about 3 wt percent volatiles (Ague, 1994). Complete dehydration of similar rocks would yield  $f_v = 0.09 \text{ m}^3 \text{ fluid} (\text{m}^3 \text{ rock})^{-1}$  (assuming fluid and rock densities of 1.0 and  $2.85 \text{ g cm}^{-3}$ , respectively). For  $A = 1 \text{ m}^2$ , the radius of the cylinder is estimated to be  $\sim 2.3 \text{ m}$ . Because the cross sectional area of the cylinder is about 17 times greater than  $A$ , some focusing of flow into the amphibolite facies would have been required if fluids were derived solely from dehydration of underlying crust (or devolatilization of underlying magma).

Ferry (1992, 1994) has advanced the far-reaching hypothesis that metamorphism of the Waits River Formation, Vermont, was largely driven by *horizontal*, up-temperature fluid flow over length scales of 10 to 100 km. Ferry (1992) concluded that quartz veins in the amphibolite facies of the Waits River Formation represented the outflow conduits for the fluids. The regional time-integrated fluid flux for the outflow zones in Vermont estimated by Ferry (1992) ( $\sim 10^5 \text{ m}^3 \text{ m}^{-2}$ ) is very similar to that estimated for the amphibolite facies of the Wepawaug ( $\sim 6 \times 10^4 \text{ m}^3 \text{ m}^{-2}$ ). On this basis, it could be proposed that the amphibolite facies of the Wepawaug represents an outflow region for fluids that migrated horizontally up regional temperature gradients. However, the petrologic and stable isotopic studies of Palin (ms) and Palin and Rye (1992) suggest that fluid flow was in a direction of decreasing temperature throughout the greenschist and amphibolite facies of the Wepawaug.

The main conclusion to be drawn for the Wepawaug is that regardless of whether fluids were derived from underlying or adjacent crust, focusing of fluid into the amphibolite facies was probably required to produce the observed network of syn-metamorphic quartz veins.

#### QUARTZ VEIN DEVELOPMENT AND ROCK VOLUME CHANGE

The derivation of vein quartz from both wallrocks and infiltrating fluids has important implications for the interpretation of rock volume strain. Ague (1994) concluded that the average garnet, staurolite, and kyanite zone pelites lost approx 12, 22, and 28 percent of their volume, respectively, relative to their inferred protoliths (low-grade chlorite + biotite zone rocks). The bulk of the volume change was due to silica loss.\*

As discussed by Ague (1994), these estimates are only relevant for the hand sample scale because quartz veins were not considered in the analysis. If all the quartz lost from the pelites was redeposited in local veins, then small amounts (several percent) of volume loss would have occurred at the outcrop and regional scales due to the volatile loss and small increases in rock density that attend prograde metamorphism (Ague, 1991, 1994). However, the situation is more complicated than this because quartz was also introduced into the veins by infiltrating fluids. As a result, the pelitic units may have *gained* a small amount of volume during metamorphic mass transfer and vein growth. Comparison of the observed and predicted volumetric vein/wallrock ratios for the amphibolite facies pelites suggests that bulk volume increases were, at most, ~10 percent.

#### DISCUSSION: METASOMATISM AND THE GROWTH OF ALUMINOUS INDEX MINERALS

##### *K/Al—Na/Al Relations*

The classical studies of Hoschek (1967) and Thompson, Lyttle, and Thompson (1977) demonstrated that the mineralogical evolution of pelites is strongly influenced by their bulk-rock molar Na/Al, K/Al, and Na/K ratios. For example, crystallization of aluminous index minerals such as staurolite and kyanite will be favored in those rocks that contain significantly more Al than is required to combine with Na and K in the course of mica and feldspar formation. The amphibolite facies pelites of the Wepawaug are an example of the relationships between mineralogy and Na–K–Al systematics. The bulk-rock K/Al and Na/Al ratios (molecular basis) for the rocks studied by Ague (1994) and the average protolith and selvage compositions studied here (tables 10, 12) are shown in figure 22. The rocks containing staurolite  $\pm$  kyanite (St  $\pm$  Ky) plot within a compositional field distinct from the one defined by the rocks that lack the aluminous index minerals (fig. 22A). Thus, bulk-rock Na/Al and K/Al ratios were fundamental controls on the development of staurolite and kyanite during metamorphism. It follows that any metasomatic processes that operated to alter these ratios could have had a profound impact on mineralogic evolution. As demonstrated in the analysis of selvage metasomatism presented above and in the regional geochemical study of Ague (1994), significant shifts in Na/Al and, in some cases, K/Al were almost certainly an integral part of the amphibolite facies metamorphism of the Wepawaug.

A clearer picture of the probable impact of metasomatism on index mineral growth can be obtained by extending the analysis of Na–K–Al relations to the inferred low-grade (chlorite and biotite zone) protoliths of the amphibolite facies schists (Ague, 1994). The protolith rocks form a compositional array with a negative slope on the  $\ln(\text{Na}/\text{Al})$  versus  $\ln(\text{K}/\text{Al})$  diagram (fig. 22B). The negative slope reflects the mineralogy of the pelites. Those rocks with the highest modal mica/plagioclase ratios have the highest K/Al and lowest Na/Al, whereas plagioclase-rich, mica-

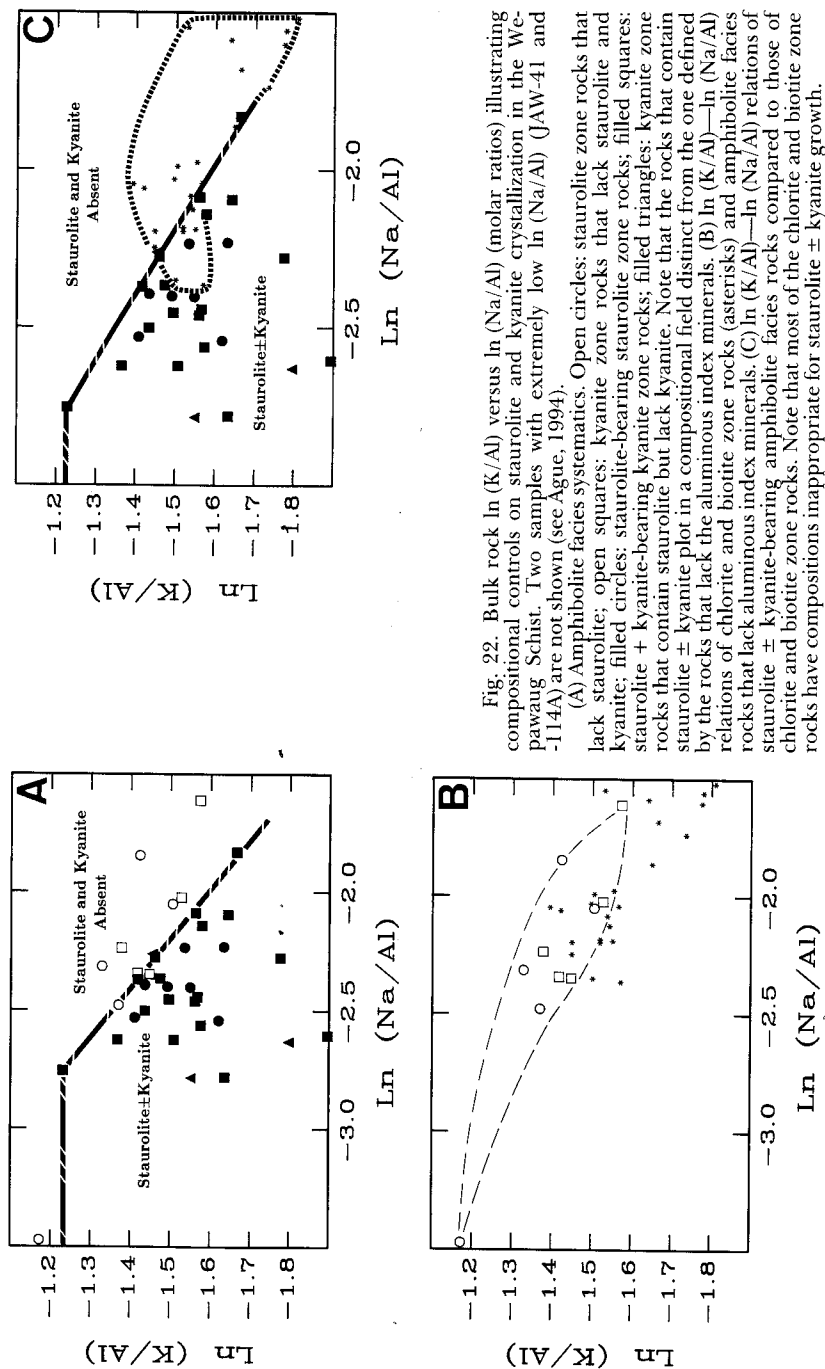


Fig. 22. Bulk rock  $\ln(K/Al)$  versus  $\ln(Na/Al)$  (molar ratios) illustrating compositional controls on staurolite and kyanite crystallization in the We-pawaug Schist. Two samples with extremely low  $\ln(Na/Al)$  (JAW-41 and -114A) are not shown (see Ague, 1994).

(A) Amphibolite facies systematics. Open circles: staurolite zone rocks that lack staurolite; open squares: kyanite zone rocks that lack staurolite and kyanite; filled circles: staurolite-bearing staurolite zone rocks; filled squares: staurolite + kyanite-bearing kyanite zone rocks; filled triangles: kyanite zone rocks that contain staurolite but lack kyanite. Note that the rocks that contain staurolite  $\pm$  kyanite plot in a compositional field distinct from the one defined by the rocks that lack the aluminous index minerals. (B)  $\ln(K/Al)$ — $\ln(Na/Al)$  relations of chlorite and biotite zone rocks (asterisks) and amphibolite facies rocks that lack aluminous index minerals. (C)  $\ln(K/Al)$ — $\ln(Na/Al)$  relations of staurolite  $\pm$  kyanite-bearing amphibolite facies rocks compared to those of chlorite and biotite zone rocks. Note that most of the chlorite and biotite zone rocks have compositions inappropriate for staurolite  $\pm$  kyanite growth.

poor rocks have high Na/Al and low K/Al. These variations are almost certainly a consequence of chemical heterogeneity in the original sediments.

The amphibolite facies rocks that lack  $St \pm Ky$  also form a compositional array with a negative slope on the  $\ln(K/Al)$  versus  $\ln(Na/Al)$  diagram (fig. 22B). However, this array extends to significantly higher K/Al and lower Na/Al ratios than does the protolith array. Rocks with the highest K/Al and the lowest Na/Al are found in the staurolite zone (fig. 22B). The trend toward high K/Al and low Na/Al defined by the amphibolite facies rocks is suggestive of coupled Na loss and K gain during metamorphism. This could reflect the growth of muscovite at the expense of plagioclase (Orville, 1962; Dipple and Ferry, 1992), for example, by:



The  $St \pm Ky$ -bearing rocks and their inferred protoliths define compositional fields that overlap only slightly on the  $\ln(K/Al)$  versus  $\ln(Na/Al)$  diagram (fig. 22C). The  $St \pm Ky$ -bearing rocks have significantly lower Na/Al than their protoliths. In fact, only about 20 percent of the protolith rocks have  $\ln(K/Al)$ - $\ln(Na/Al)$  values that extend well into the  $St \pm Ky$  field. Furthermore, no clear correlation between  $\ln(K/Al)$  and  $\ln(Na/Al)$  is evident for the  $St \pm Ky$ -bearing rocks (fig. 22C). The difference in Na/Al between the  $St \pm Ky$ -bearing rocks and their inferred protoliths is believed to result largely from  $\sim 30$  to 40 percent loss of Na during prograde metamorphism (Agué, 1994). In addition, mass transfer resulted in decreases in K/Al in some cases (fig. 17A). Because most of the protoliths have bulk-rock K/Al and Na/Al ratios that are *inappropriate* for the growth of staurolite and kyanite, it is concluded that *metasomatism involving major Na loss played a crucial role in stabilizing aluminous index minerals during amphibolite facies metamorphism.*

#### *Vein Plagioclase*

The occurrence of plagioclase feldspar at some vein-wallrock contacts (fig. 4) is problematic. The necessary Na, Ca, Al, and Si may have been derived from local wallrocks by diffusion-controlled processes acting to fill cracks formed by hydrofracturing (for example, pressure solution; Yardley, 1975) or from externally-derived hydrothermal fluids moving through fractures (Anderson and Burnham, 1983). Evidence for hydrothermal transport of feldspar out of alteration zones adjacent to veins in Wepawaug marbles was presented by Tracy and others (1983).

If pressure solution of plagioclase occurred, then the mineralogic evolution of the selvages could have been affected. Congruent dissolution of plagioclase from wallrocks (Yardley, 1975) will result in decreases in bulk-rock Na/Al (fig. 23). In fact, if a rock that initially has K/Al and Na/Al ratios inappropriate for staurolite and kyanite growth undergoes extreme plagioclase removal, the lowering of its Na/Al may result in a bulk composition that falls within the staurolite  $\pm$  kyanite field (fig. 23).

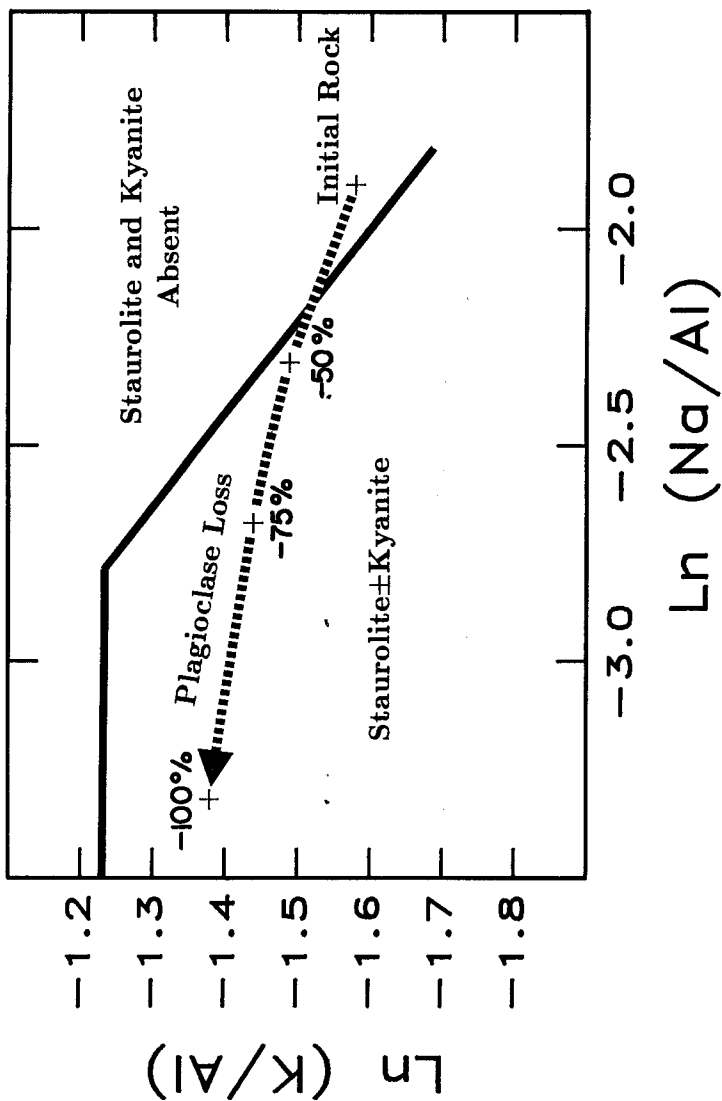


Fig. 23. Effect of congruent removal of plagioclase on rock composition. The initial rock contains quartz, plagioclase, muscovite, biotite, and garnet. The calculations were done using a representative set of mineral proportions and compositions (see below). If plagioclase was removed from the rock, then the rock's bulk composition would evolve in the direction of the arrow. Percentage values indicate amount of plagioclase mass change (on a molar basis); -100 percent corresponds to complete plagioclase removal. Note that plagioclase loss causes Na/Al to drop which, in turn, makes the rock's composition suitable for staurolite ± kyanite crystallization (fig. 22). Plagioclase, muscovite, biotite, and garnet are initially present in the molar proportions 1.00:1.00:0.75:0.75. Biotite Al, Na, and K atoms per formula unit (apfu) are 1.65, 0.01, and 0.85, respectively. Muscovite Al, Na, and K apfu are 2.80, 0.20, and 0.75, respectively. The plagioclase is  $An_{20}$ .

Thus, subsequent mineral reaction during continued metamorphism of the rock could cause staurolite  $\pm$  kyanite crystallization.

It is unclear if local plagioclase mass transfer was important in altering bulk-rock chemistry in the Wepawaug. For example, no indication of Al loss from pelites has been found in this study or by Ague (1994), which suggests that the feldspars were not locally derived. In addition, the evidence for significant mass transfer of a wide variety of major and trace elements adjacent to veins (fig. 17) cannot be accounted for by pressure solution of plagioclase. Moreover, many veins with well developed aluminous selvages do not contain plagioclase. Petrologic and stable isotopic work is currently underway in order to constrain better the source(s) of accessory vein plagioclase.

#### *Fluid Flow and Wallrock Alteration Processes*

Fracture-controlled fluid flow caused widespread chemical alteration of the Wepawaug Schist during amphibolite facies metamorphism. Deformation probably resulted from extensional hydraulic fracturing or shear failure associated with fluid pressure buildup during prograde devolatilization (Yardley, 1986). A given devolatilization reaction may generate enough fluid to cause hydrofracturing every  $\sim 10$  to  $10^2$  yr (Nishiyama, 1989). Hydrofracturing produces rapid fluid release and an immediate drop in pore fluid pressure (Nur and Walder, 1990). Fractures increase the permeability of the rock mass and serve to channelize fluid flow. In the Wepawaug, flow was probably focused into pelitic layers, because they are significantly less competent than quartz- and feldspar-rich psammitic rocks (compare Tullis and Yund, 1992).

The major conduits for advective fluid escape are now represented by quartz veins. In addition, fluid advection probably occurred in the selvages because they commonly contain networks of fine scale quartz veinlets. The transport of critical rock-forming metals such as Na almost certainly resulted from diffusion and hydrodynamic dispersion of solutes in selvages adjacent to major fracture conduits and from advection through the selvages. The incipient effects of the alteration are inferred to be the growth of muscovite at the expense of plagioclase resulting in bulk Na loss and K and Ba gain. This type of alteration is best preserved in the staurolite zone (Ague, 1994). More intense alteration, monitored continuously by the reaction progress variable, involved alkali depletion and the growth of staurolite  $\pm$  kyanite at the expense of plagioclase and micas (tables 13 and 14). Bulk Mn or Zn enrichment is inferred to have taken place if the infiltration was synchronous with garnet or staurolite growth, respectively. Because the selvages contain both reactant and product phases, the metasomatic reactions did not go to completion, a phenomenon commonly observed adjacent to veins in ore deposits (Brimhall, 1977, 1979). The nature and degree of alteration were undoubtedly a function of a large number of geologic variables, including P, T, vein density, fluid fluxes, timing of infiltration, and the extent of

chemical disequilibrium between wallrocks and infiltrating fluids (Lasaga and Rye, 1993).

Following fluid release episodes, diffusional mass transport of silica from the wallrock to the fractures probably acted to seal the fractures (Ramberg, 1952; Yardley, 1975; Smith and Evans, 1984). The dominant mode of diffusive mass transfer is inferred to have been pressure solution of quartz (Elliot, 1973; Yardley, 1975; Paterson, 1973; Rutter, 1983; Elias and Hajash, 1992). In addition, hydrogen metasomatism could have made silica available for deposition in veins (eq 4; tables 13 and 14). Once the fractures were sealed, the permeability of the rock mass decreased to low levels, and pore pressure buildup resumed as devolatilization reactions proceeded. The widespread crack-seal textures (Ramsay, 1980) in the Wepawaug veins (fig. 3) suggest that the cycle of fracturing, fluid flow, and crack healing was repeated many times during vein growth. Thus, the rock permeability was almost certainly a dynamic function of the fluid flux, as discussed by Nur and Walder (1990) and Walther (1990). A critical point to emphasize is that the local mass transfer of silica was probably linked directly to regional scale fluid flow through fractures. Thus, in all likelihood, the veins are not simple "segregations" of quartz, even though most of the vein quartz was derived from local wallrocks.

The chemical alteration of the Wepawaug Schist appears to have been the result of coupled mass transfer processes that operated over an immense range of length scales. At the regional scale, fluids flowed down temperature and pressure gradients through fracture conduits. Mass exchange between infiltrating fluids and adjacent pelitic wallrocks occurred on 1 to 10 cm length scales perpendicular to fractures and at the regional scale along the flow path. Asymmetric selvages (for example, fig. 7A) probably resulted when fracturing, fluid flow, and wallrock alteration occurred preferentially on one side of a vein. Ultimately, the avenues of both local and regional mass transport were micron-scale fractures, grain boundaries, and pores (fig. 11C). Transport of the bulk of the alkalis and alkaline earths documented here and in Ague (1994) is inferred to have been regional in scope, because local source-sink relationships have not been identified. Silica deposition in veins resulted from both the regional scale movement of fluids and local scale, diffusion-controlled mass transfer from wallrocks to fractures.

#### CONCLUDING REMARKS

The progression of Barrovian index mineral zones from chlorite to sillimanite is thought to be primarily the result of systematic increases in the temperatures and pressures of regional metamorphism. The results presented here and in Ague (1994) strongly suggest that significant chemical alteration of pelites may also occur during Barrovian metamorphism as a result of regional scale, down-temperature fluid flow through fractures. One of the primary consequences of the chemical alteration is



that pelitic wallrocks adjacent to quartz veins become depleted in alkali metals, relative to more residual elements such as Al and Ti. The alkali metal loss can stabilize the key aluminous index minerals staurolite and kyanite. For the case of the Wepawaug Schist, it is concluded that the widespread growth of staurolite and kyanite was largely the result of regional scale fluid flow and metasomatism under amphibolite facies conditions. If this conclusion is correct, then the position of the staurolite and kyanite isograds in Barrovian terranes can reflect P, T, fluid composition, protolith lithology, and metasomatic shifts in bulk chemistry caused by fluid infiltration. Widespread syn-amphibolite facies quartz vein development and associated staurolite and kyanite growth may mark zones of major fluid outflow and advective heat transport in orogenic belts.

#### ACKNOWLEDGMENTS

I would like to thank D. M. Rye, M. T. Brandon, A. C. Lasaga, B. J. Skinner, P. Ihinger, and P. R. Bartholomew for many stimulating discussions on the topic of regional metamorphism and J. L. M. van Haren and M. Breault for laboratory and field assistance. J. M. Ferry and R. B. Hanson provided thorough and insightful reviews which substantially improved the clarity of the presentation. E. J. Essene, S. N. Olsen, and R. P. Wintsch made many helpful comments on an earlier version of the manuscript. D. A. Sverjensky kindly provided a version of SUPCRT92 (Johnson, Oelkers, and Helgeson, 1992) suitable for use with the thermodynamic data base of Berman (1988, 1991). W. C. Phelps provided valuable assistance with sample preparation, and W. Sacco carefully prepared the photographic prints. Support from National Science Foundation grant EAR-918006 and Yale University is gratefully acknowledged.

#### APPENDIX A

##### *Values of intensive variables during metamorphism*

The pressure (P) and temperature (T) of equilibration were estimated in most samples using the multi-equilibrium methods described by Berman (1991). The calculations were done with the TWEEQU software package (Berman, 1991), which incorporates the internally consistent thermodynamic data of Berman (1988, 1990), Mäder and Berman (1991), and McMullin, Berman, and Greenwood (1991). To avoid uncertainties associated with the activity-composition relations of fluids, only equilibria that do not involve fluid species were used for P-T estimation. Activity-composition relations for garnet, muscovite-paragonite, biotite, and plagioclase were calculated using the models of Berman (1990), Chatterjee and Froese (1975), McMullin, Berman, and Greenwood (1991), and Fuhman and Lindsley (1988), respectively. The biotite activity model of McMullin, Berman, and Greenwood (1991) was modified slightly by assuming that  $X_K^{Bi} = K/1.0$  (structural formula on an 11 oxygen basis; R. G. Berman, personal communication, 1992). Ideal mixing was assumed for ilmenite. Quartz and rutile were taken to be pure. Reconnaissance microprobe analyses indicate that kyanite contains a small amount of Fe substituting for Al. Therefore, based on an ideal mixing model, the activity of kyanite was set to 0.99 in the calculations.

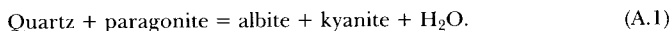
With Berman's (1991) multi-equilibrium approach, average pressures and temperatures are calculated using all equilibria, both stable and metastable, implied by a given

assemblage of phases. For example, for the mineral assemblage biotite–muscovite–ilmenite–rutile–plagioclase–garnet–kyanite–quartz, 21 equilibria may be calculated and plotted in P–T space (see table 4 in Berman, 1991). Four of these equilibria are linearly independent. If all the phases equilibrated at the same time and if the thermodynamic data and activity models are sound, then all the equilibria should intersect at a point on a P–T diagram. In natural samples, the equilibria will not intersect at a point, owing to “disequilibrium” between phases and errors in the thermodynamic data, activity models, and microprobe analyses. The average P–T estimates computed using TWEEQU are weighted toward: (1) those equilibria that are the best-constrained thermodynamically, and (2) those pairs of equilibria that intersect at the highest angles on a P–T diagram (Berman, 1991). The ranges in P and T over which the equilibria intersect provide a measure of uncertainty for the P–T estimate. Berman (1991) suggested that TWEEQU uncertainties ( $\pm 1\sigma$ ) of about 40°C and 0.05 GPa or less are consistent with the assumption that “equilibrium” compositions are preserved in a given mineral assemblage.

Temperatures of equilibration were also estimated for three carbonate samples using the calcite–dolomite thermometer calibration of Anovitz and Essene (1987).

The fugacity ratios  $f_{\text{HCl}}/f_{\text{H}_2\text{O}}$  and  $f_{\text{HF}}/f_{\text{H}_2\text{O}}$  were computed from measured biotite compositions using the approach of Zhu and Sverjensky (1992) and Munoz (1984, 1992) (see eqs 23 and 24 in Zhu and Sverjensky, 1992). The thermodynamic data for the biotite endmembers, HCl(g), HF(g), and H<sub>2</sub>O(g) used in the calculations are from Zhu and Sverjensky (1992), Robie, Hemingway, and Fisher (1978), Stull and Prophet (1971), and Johnson, Oelkers, and Helgeson (1992), respectively. For each sample, the T and P derived from the multi-equilibrium calculations described above were used for computing the fugacity ratios. Cl and F atoms per formula unit were calculated assuming 2 hydroxyl sites per mole of biotite.

The activity of H<sub>2</sub>O was estimated using the multi-equilibrium approach in conjunction with reactions involving the paragonite component of muscovite and the albite component of plagioclase (Chatterjee and Froese, 1975; Cheney and Guidotti, 1979). One such reaction is:



These calculations are subject to sizable uncertainties, because the mole fraction of paragonite in the muscovites is small, and the corresponding paragonite activity coefficient is large (~5–6; Chatterjee and Froese, 1975). The calculations were done using the liquid standard state for water (unit activity of the pure phase at any T and P).

#### APPENDIX B

##### *Overall heterogeneous reaction analysis*

Changes in the moles of a species  $j$  (such as a mineral species) in an open system may be divided conceptually into two parts (Prigogine, 1955; Brimhall, 1979): (1) an external part due to mass exchange with the surroundings ( $dn_{j,\text{Ext}}$ ), and (2) an internal part resulting from chemical reactions proceeding within the system ( $dn_{j,\text{Int}}$ ). The total change in the moles of  $j$ ,  $dn_{j,\text{Tot}}$ , is given by (Prigogine, 1955; Brimhall, 1979):

$$dn_{j,\text{Tot}} = dn_{j,\text{Ext}} + \sum_{\rho=1}^{\hat{p}} (dn_{j,\text{Int}})_{\rho}, \quad (\text{B.1})$$

where the internal mass changes are summed over all chemical reactions  $\rho$  proceeding simultaneously during the alteration. If we introduce the reaction progress variable,  $\xi$

(Prigogine, 1955; Brimhall, 1979; Ferry, 1983), then the internal mole changes can be expressed as:

$$\sum_{\rho=1}^{\hat{\rho}} (dn_{j,Int})_{\rho} = \sum_{\rho=1}^{\hat{\rho}} v_{j,\rho} d\xi_{\rho}, \quad (\text{B.2})$$

where the  $v_{j,\rho}$  are stoichiometric reaction coefficients. We will simplify the problem by considering only the overall heterogeneous reaction rather than attempting to determine each of the simultaneous reactions  $\rho$  separately. Thus,

$$dn_{j,Total} = dn_{j,Ext} + v_j d\hat{\xi}, \quad (\text{B.3})$$

where  $\hat{\xi}$  denotes the reaction progress variable for the overall reaction. As shown by Brimhall (1979), it is convenient to choose an index mineral to gauge the progress of the overall reaction. Quartz has been chosen as the index mineral here, in view of the pronounced silica loss that accompanied selvage formation.

It is critical to point out that because  $\xi$  is an extensive variable, the stoichiometric reaction coefficients in eq (B.3) can be quantified *only* if the overall mass change attending alteration is known. As shown by Ague (1991, 1994), the mass change is given by:

$$\frac{\text{Altered rock mass}}{\text{Initial rock mass}} = \frac{C_i^{\circ}}{C_i'}, \quad (\text{B.4})$$

where  $C_i^{\circ}$  and  $C_i'$  are the concentrations of a reference component in the protolith and the altered states, respectively. For example,  $\hat{\xi}$  monitors the number of moles of quartz destroyed as the overall reaction proceeds. Taking into account the rock mass changes that accompany the alteration yields:

$$\hat{\xi} = M_r \left[ \frac{n_{Qtz}^{\circ}}{M_r} - \left( \frac{C_i^{\circ}}{C_i'} \right) \frac{n'_{Qtz}}{M_r} \right], \quad (\text{B.5})$$

where  $n_{Qtz}^{\circ}/M_r$  and  $n'_{Qtz}/M_r$  are the number of moles of quartz per a given mass,  $M_r$ , of protolith and altered rock, respectively. Similarly, the number of moles of a given mineral phase  $\phi$  in an altered rock relative to the initial mass  $M_r$  of protolith,  $\hat{n}_{\phi}$ , is given by:

$$\hat{n}_{\phi} = M_r \left[ \left( \frac{C_i^{\circ}}{C_i'} \right) \frac{n'_{\phi}}{M_r} \right], \quad (\text{B.6})$$

where  $n'_{\phi}/M_r$  denotes the number of moles of  $\phi$  per  $M_r$  g of altered rock. If we substitute eqs (B.5) and (B.6) into eq (B.3), and note that  $dn_{j,Ext}$  is zero for a mineral phase  $\phi$  (minerals do not move physically into or out of the system), then the stoichiometric reaction coefficient for  $\phi$  in the overall reaction is given by:

$$v_{\phi} = \frac{d\hat{n}_{\phi}}{d\hat{\xi}}. \quad (\text{B.7})$$

Eq (B.7) demonstrates that to determine successfully stoichiometric reaction coefficients using reaction progress methods, a mass balance study of rock alteration must be done in order to identify a reference component and the overall mass changes in the system. This is in contrast to the traditional reaction progress approach, in which metasomatic mass (and volume) changes are assumed to be small or negligible. For convenience, the size of the reacting system is defined as the mass of protolith that contains 1 mole of the index mineral. Thus,  $\xi$  is 0 at the start of the reaction and 1 when the index mineral has been completely destroyed. For JAW-137B and -125A, the appropriate protolith  $M_r$  values are 0.1646 and 0.1580 kg, respectively. As discussed above, a Ti reference frame is appropriate for assessing the mass changes associated with selvage formation.

Mineral abundances (moles  $\text{kg}^{-1}$ ; table 11) were determined using least-squares methods in conjunction with electron microprobe analyses of minerals (tables 1-7) and bulk-rock analyses (tables 10 and 12) (compare Villas and Norton, 1977; Brimhall, Cunningham, and Stoffregen, 1984; Böhlke, 1989). Quartz, rutile, and kyanite were assumed to be pure. The least-squares problems for all the protoliths and selvages studied here were overdetermined and solved using the singular value decomposition method (Lawson and Hanson, 1974). Because staurolite and kyanite have very similar molar Al/Si ratios, the least squares analysis does not provide a highly accurate estimate of their respective abundances. Therefore, modal analyses of staurolite and kyanite were incorporated into the least-squares problems using linear equality constraints (Lawson and Hanson, 1974). The molar volume data used in the calculations were taken from Helgeson and others (1978) and Berman (1988, 1991). The best-fit solutions are given in table 11. Multiple correlation coefficients for the best-fit solutions are all  $> 0.9999$ .

The derived  $\hat{n}_\phi$  values were plotted against  $\hat{\xi}$  in order to determine if mineral stoichiometric coefficients vary as a function of reaction progress (fig. 19). To a first order approximation,  $d\hat{n}_\phi/d\hat{\xi}$  appears to be constant for all minerals involved in the overall reactions that took place in examples I and II. For simplicity, therefore, the vector of stoichiometric coefficients for minerals participating in each overall reaction,  $\Delta$ , was computed using:

$$\Delta = \frac{M_r}{\hat{\xi}} \left[ \left( \frac{C_i^o}{C_i'} \right) \mathbf{x}' - \mathbf{x}^o \right], \quad (\text{B.8})$$

where  $\mathbf{x}^o$  and  $\mathbf{x}'$  are the mineral abundance vectors determined for the protolith and the selvages, respectively, using the least-squares method. The reaction coefficients are positive for products and negative for reactants. Eq (B.8) was solved separately for examples I and II, because the overall reactions that operated in them are different. The most silica-depleted selvage samples (JAW-125Aii and -137Bii) and the average protolith compositions were used for the calculations (tables 10 and 12). Once the net mole transfer among the solids had been determined using eq (B.8), stoichiometric coefficients for the aqueous species were derived using conservation of mass and conservation of charge constraints. This balancing approach does not account for the precise speciation in the aqueous phase, but it does accurately express fluid-driven mole transfer (the external mass changes) in the heterogeneous system. Very slight adjustments were made to the reaction coefficients determined using eq (B.8) so as to conserve Al in the solid phases.

The determination of metasomatic mineralogical changes involves a number of important assumptions and simplifications which can lead to uncertainties in the derived overall reaction. First, the balancing approach assumes that at the time selvage formation began, the presently observed protolith mineralogy had already been established in the rocks. The reaction history of chlorite poses the most serious problem in this regard. For example, if chlorite were still present during the early stages of selvage formation, then the overall reactions would be in error since prograde chlorite is no longer present in the rocks, and, therefore, it has not been accounted for in the calculations. However, because selvage formation appears largely to post-date garnet growth (most chlorite is destroyed by garnet-producing reactions), the errors introduced by this assumption are probably minor. Second, chemical zoning in garnet has not been explicitly accounted for in the calculations. This simplification primarily affects the Mn mass balance, owing to the pronounced bell-shaped Mn growth zoning evident in the Wepawaug garnets (fig. 10). Third, small differences in the average composition of a given mineral between the protolith and the selvages have been ignored. Fourth, sulfides, graphite, apatite, tourmaline, F, Cl,  $\text{Fe}^{2+}$ / $\text{Fe}^{3+}$ , and trace elements have not been explicitly considered in the calculations, because

our focus is on the major metasomatic changes in silicate mineralogy. Finally, the small amounts of retrograde phases that occur in the rocks (for example, chlorite, sericite) have not been considered in the analysis. Although the above assumptions and simplifications will have an impact on the calculation results, a general picture of the overall mineralogical transformations can be easily obtained owing to the extreme bulk-chemical changes that accompanied selvage formation.

## REFERENCES

- Ague, J. J., 1991, Evidence for major mass transfer and volume strain during regional metamorphism of pelites: *Geology*, v. 19, p. 855–858.
- 1992, Hydrochemical differentiation during metamorphism of pelites: Fracture flow-controlled major element mass transfer and the growth of Barrovian zone index minerals: *Geological Society of America Abstracts with Programs*, v. 24, p. A264.
- 1994, Mass transfer during Barrovian metamorphism of pelites, south-central Connecticut, I: Evidence for changes in composition and volume: *American Journal of Science*, v. 294, p. 989–1057.
- Ague, J. J., and Brimhall, G. H., 1989, Geochemical modelling of steady-state fluid flow and chemical reaction during supergene enrichment of porphyry copper deposits: *Economic Geology*, v. 84, p. 506–528.
- Aitchison, J., 1986, *The statistical analysis of compositional data*: London, Chapman and Hall, 416 p.
- 1989, Measures of location of compositional data sets: *Mathematical Geology*, v. 21, p. 787–790.
- Anderson, G. M., and Burnham, C. W., 1983, Feldspar solubility and the transport of aluminum under metamorphic conditions: *American Journal of Science*, v. 283-A, p. 283–297.
- Ando, C. J., Czuchra, B. L., Klemperer, S. L., Brown, L. D., Cheadle, F. J., Cook, F. A., Oliver, J. E., Kaufman, S., Walsh, T., Thompson, J. B., Jr., Lyons, J. B., and Rosenfeld, J. L., 1984, Crustal profile of mountain belt: COCORP deep seismic reflection profiling in New England Appalachians and implications for the architecture of convergent mountain chains: *American Association of Petroleum Geologists Bulletin*, v. 68, p. 819–837.
- Anovitz, L. M., and Essene, E. J., 1987, Phase equilibria in the system  $\text{CaCO}_3\text{-MgCO}_3\text{-FeCO}_3$ : *Journal of Petrology*, v. 28, p. 389–414.
- Armstrong, T. R., Tracy, R. J., and Hames, W. E., 1992, Contrasting styles of Taconian, eastern Acadian and western Acadian Metamorphism, central and western New England: *Journal of Metamorphic Geology*, v. 10, p. 415–426.
- Ayers, J. C., and Watson, E. B., 1993, Rutile solubility and mobility in supercritical aqueous fluids: *Contributions to Mineralogy and Petrology*, v. 114, p. 321–330.
- Bahr, J. M., ms, 1976, Structure and petrology of the Woodbridge granite: B.S. thesis, Yale University, New Haven, 38 p.
- Baumgartner, L. P., and Ferry, J. M., 1991, A model for coupled fluid flow and mixed-volatile mineral reactions with applications to regional metamorphism: *Contributions to Mineralogy and Petrology*, v. 106, p. 273–285.
- Bebout, G. E., and Barton, M. D., 1989, Fluid flow and metasomatism in a subduction zone hydrothermal system: Catalina schist terrane, California: *Geology*, v. 17, p. 976–980.
- Berman, R. G., 1988, Internally-consistent thermodynamic data for minerals in the system  $\text{Na}_2\text{O-K}_2\text{O-CaO-MgO-FeO-Fe}_2\text{O}_3\text{-Al}_2\text{O}_3\text{-SiO}_2\text{-TiO}_2\text{-H}_2\text{O-CO}_2$ : *Journal of Petrology*, v. 29, p. 445–522.
- 1990, Mixing properties of Ca-Mg-Fe-Mn garnets: *American Mineralogist*, v. 75, p. 328–344.
- 1991, Thermobarometry using multi-equilibrium calculations: A new technique, with petrological applications: *Canadian Mineralogist*, v. 29, p. 833–855.
- Bickle, M. J., and McKenzie, D., 1987, The transport of heat and matter by fluids during metamorphism: *Contributions to Mineralogy and Petrology*, v. 95, p. 384–392.
- Böhlke, J. K., 1989, Comparison of metasomatic reactions between a common  $\text{CO}_2$ -rock vein fluid and diverse wall rocks: Intensive variables, mass transfers, and Au mineralization at Alleghany, California: *Economic Geology*, v. 84, p. 291–327.
- Brady, J. B., 1988, The role of volatiles in the thermal history of metamorphic terranes: *Journal of Petrology*, v. 29, p. 1187–1213.
- Brantley, S. L., 1992, The effect of fluid chemistry on quartz microcrack lifetimes: *Earth and Planetary Science Letters*, v. 113, p. 145–156.

- Breault, M., ms, 1992, Relative timing of metamorphic mineral growth and veining in kyanite zone pelites of the Wepawaug Schist, Connecticut: B.S. thesis, Yale University, New Haven, 33 p.
- Brimhall, G. H., Jr., 1977, Early fracture-controlled disseminated mineralization at Butte, Montana: *Economic Geology*, v. 72, p. 37–59.
- 1979, Lithologic determination of mass transfer mechanisms of multiple-stage porphyry copper mineralization at Butte, Montana: Vein formation by hypogene leaching and enrichment of potassium silicate protore: *Economic Geology*, v. 74, p. 556–589.
- Brimhall, G. H., Cunningham, A. B., and Stoffregen, R., 1984, Zoning in precious metal distribution within base metal sulfides: A new lithologic approach using generalized inverse methods: *Economic Geology*, v. 79, p. 209–226.
- Brimhall, G. H., Lewis, C. J., Ague, J. J., Dietrich, W. E., Hampel, J., Teague, T., and Rix, Peter, 1988, Metal enrichment in bauxites by deposition of chemically mature aeolian dust: *Nature*, v. 333, p. 819–824.
- Burger, H. R., Hewitt, D. A., and Vidale, R. J., 1968, Progressive metamorphism of pelitic, carbonate, and basic rocks in south-central Connecticut, in Orville, P. M., editor, *Guidebook for Fieldtrips in Connecticut*: New Haven, CT, New England Intercollegiate Geological Conference Guidebook, trip D-1, 19 p.
- Chamberlain, C. P., Ferry, J. M., and Rumble, D., 1990, The effect of net-transfer reactions on the isotopic composition of minerals: *Contributions to Mineralogy and Petrology*, v. 105, p. 322–336.
- Chamberlain, C. P., and Rumble, D., 1988, Thermal anomalies in a regional metamorphic terrane: An isotopic study of the role of fluids: *Journal of Petrology*, v. 29, p. 1215–1232.
- Chapman, C. A., 1950, Quartz veins formed by metamorphic differentiation of aluminous schists: *American Mineralogist*, v. 35, p. 693–710.
- Chatterjee, N. D., and Froese, E., 1975, A thermodynamic study of the pseudobinary join muscovite-paragonite in the system  $KAlSi_3O_8$ - $NaAlSi_3O_8$ - $Al_2O_3$ - $SiO_2$ - $H_2O$ : *American Mineralogist*, v. 60, p. 985–993.
- Cheney, J. T., and Guidotti, C. V., 1979, Muscovite-plagioclase equilibrium in sillimanite + quartz bearing metapelites, Puzzle Mountain area, N. W. Maine: *American Journal of Science*, v. 279, p. 411–434.
- Clark, G. S., ms, 1966, Isotopic age study of metamorphism and intrusion in Western Connecticut and southeastern New York: Ph.D. thesis, Columbia University, New York.
- Crerar, D. A., and Anderson, G. M., 1971, Solubility and solvation reactions of quartz in dilute hydrothermal solutions: *Chemical Geology*, v. 8, p. 107–122.
- Dieterich, J. H., ms, 1968, Sequence and mechanics of folding in the area of New Haven, Naugatuck, and Westport, Connecticut: Ph.D. thesis, Yale University, New Haven, 153 p.
- Dipple, G. M., and Ferry, J. M., 1992, Metasomatism and fluid flow in ductile fault zones: *Contributions to Mineralogy and Petrology*, v. 112, p. 149–164.
- Elias, B. P., and Hajash, A., Jr., 1992, Changes in quartz solubility and porosity due to effective stress: An experimental investigation of pressure solution: *Geology*, v. 20, p. 451–454.
- Elliot, D., 1973, Diffusion flow laws in metamorphic rocks: *Geological Society of America Bulletin*, v. 84, p. 2645–2664.
- Etheridge, M. A., Wall, V. J., and Vernon, R. H., 1983, The role of the fluid phase during regional metamorphism and deformation: *Journal of Metamorphic Geology*, v. 1, p. 205–226.
- Ferry, J. M., 1982, A comparative geochemical study of pelitic schists and metamorphosed carbonate rocks from south-central Maine, USA: *Contributions to Mineralogy and Petrology*, v. 80, p. 59–72.
- 1983, On the control of temperature, fluid composition, and reaction progress during metamorphism: *American Journal of Science*, v. 283-A, p. 201–232.
- 1992, Regional Metamorphism of the Waits River Formation, eastern Vermont, Delineation of a new type of giant metamorphic hydrothermal system: *Journal of Petrology*, v. 33, p. 45–94.
- 1994, Overview of the petrologic record of fluid flow during regional metamorphism in northern New England: *American Journal of Science*, v. 294, p. 905–988.
- Ferry, J. M., and Dipple, G. M., 1991, Fluid flow, mineral reactions, and metasomatism: *Geology*, v. 19, p. 211–214.
- Fisher, D. M., and Brantley, S. L., 1992, Models of quartz overgrowth and vein formation: Deformation and episodic fluid flow in an ancient subduction zone: *Journal of Geophysical Research*, v. 97, p. 20,043–20,061.

- Fournier, R. O., and Potter, R. W., II, 1982, An equation correlating the solubility of quartz in water from 25° to 900°C at pressures up to 10,000 bars: *Geochimica et Cosmochimica Acta*, v. 46, p. 1969–1973.
- Fritts, C. E., 1962a, Bedrock geology of the Mount Carmel and Southington quadrangles, Connecticut: U.S. Geological Survey Open-file Report 644, 213 p.
- 1962b, Age and sequence of metasedimentary and metavolcanic formations northwest of New Haven, Connecticut: U.S. Geological Survey Professional Paper 450-D, p. 32–36.
- 1963, Bedrock geology of the Mount Carmel quadrangle, Connecticut: U.S. Geological Survey Quadrangle Map GQ-199.
- 1965a, Bedrock geologic map of the Ansonia quadrangle, Fairfield and New Haven Counties, Connecticut: U.S. Geological Survey Quadrangle Map GQ-426.
- 1965b, Bedrock geologic map of the Milford quadrangle, Fairfield and New Haven Counties, Connecticut: U.S. Geological Survey Quadrangle Map GQ-427.
- Frost, B. R., 1979, Mineral equilibria involving mixed-volatiles in a C-O-H fluid phase: The stabilities of graphite and siderite: *American Journal of Science*, v. 279, p. 1033–1059.
- Fuhrman, M. L., and Lindsley, D. H., 1988: Ternary feldspar modelling and thermometry: *American Mineralogist*, v. 73, p. 201–215.
- Fyfe, W. S., Price, N. J., and Thompson, A. B., 1978, *Fluids in the Earth's crust*: Amsterdam, Elsevier, 383 p.
- Gates, O., 1975, Geologic map and cross-section of the Eastport Quadrangle, Washington County, Maine: Augusta, Maine Geological Survey, Geology Map Series 3, scale 1:62,500.
- Hames, W. E., and Menard, T., 1993, Fluid-assisted modification of garnet composition along rims, cracks, and mineral inclusion boundaries in samples of amphibolite facies schists: *American Mineralogist*, v. 78, p. 338–344.
- Hames, W. E., Tracy, R. J., and Bodnar, R. J., 1989, Postmetamorphic unroofing history deduced from petrology, fluid inclusions, thermochronometry, and thermal modeling: An example from southwestern New England: *Geology*, v. 17, p. 727–730.
- Hanson, R. B., Sorenson, S. S., Barton, M. D., and Fiske, R. S., 1993, Long-term evolution of fluid-rock interactions in magmatic arcs: Evidence from the Ritter Range pendant, Sierra Nevada, California, and numerical modeling: *Journal of Petrology*, v. 34, p. 23–62.
- Helgeson, H. C., Delany, J. M., Nesbitt, H. W., and Bird, D. K., 1978, Summary and critique of the thermodynamic properties of rock-forming minerals: *American Journal of Science*, v. 278-A, 229 p.
- Hewitt, D. A., 1973, The metamorphism of micaceous limestones from south-central Connecticut: *American Journal of Science*, v. 273-A, p. 444–469.
- Hodges, K. V., and Royden, 1984, Geologic thermobarometry of retrograded metamorphic rocks: An indication of the uplift trajectory of a portion of the northern Scandinavian Caledonides: *Journal of Geophysical Research*, v. 89, p. 7077–7090.
- Hoisch, T. D., 1991, The thermal effects of pervasive and channelized fluid flow in the deep crust: *Journal of Geology*, v. 99, p. 69–80.
- Hoschek, G., 1967, Untersuchungen zum Stabilitätsbereich von chloritoid und staurolith: *Contributions to Mineralogy and Petrology*, v. 14, p. 123–162.
- Hueber, F. M., Bothner, W. A., Hatch, N. L., Jr., Finney, S. C., and Aleinikoff, J. N., 1990, Devonian plants from southern Quebec and northern New England and the age of the Connecticut Valley trough: *American Journal of Science*, v. 290, p. 360–395.
- Johnson, J. W., Oelkers, E. H., and Helgeson, H. C., 1992, SUPCRT92: A software package for calculating the standard molal thermodynamic properties of minerals, gases, aqueous species, and reactions from 1 to 5000 bars and 0° to 1000°C: *Computers and Geosciences*, v. 18, p. 899–947.
- Kerrick, D. M., 1988, Al<sub>2</sub>SiO<sub>5</sub>-bearing segregations in the Lepontine Alps, Switzerland: Aluminum mobility in metapelites: *Geology*, v. 16, p. 636–640.
- Korzhinsky, D. S., 1950, Differential mobility of components and metasomatic zoning in metamorphism: International Geological Congress, 18th, London, Report part II, p. 50–65.
- Lanzilotto, A., and Hanson, G. N., 1992, Multiple generations of monazite growth in the Wepawaug Schist, southern Connecticut: *Geological Society of America Abstracts with Programs*, v. 24, no. 7, p. A219.
- Lasaga, A. C., and Rye, D. M., 1993, Fluid flow and chemical reaction kinetics in metamorphic systems: *American Journal of Science*, v. 293, p. 361–404.
- Lawson, C. L., and Hanson, R. J., 1974, *Solving least squares problems*: Englewood Cliffs, New Jersey, Prentice-Hall, 340 p.

- Mäder, U. K., and Berman, R. G., 1991, A high pressure equation of state for carbon dioxide consistent with phase equilibrium and P-V-T data: *American Mineralogist*, v. 76, p. 1547–1559.
- Manning, C. E., and Bird, D. K., 1991, Porosity evolution and fluid flow in the basalts of the Skaergaard magma-hydrothermal system, east Greenland: *American Journal of Science*, v. 291, p. 201–257.
- McMullin, D. W. A., Berman, R. G., and Greenwood, H. J., 1991, Calibration of the SGAM thermobarometer for pelitic rocks using data from phase-equilibrium experiments and natural assemblages: *Canadian Mineralogist*, v. 29, p. 889–908.
- Miller, S. J., and Tracy, R. J., 1991, High pressure metamorphism of the Straits schist, northwestern Connecticut: *Geological Society of America Abstracts with Programs*, v. 23, no. 1, p. 105.
- Moecher, D. P., and Cosca, M. A., 1992,  $^{40}\text{Ar}/^{39}\text{Ar}$  evidence for delayed post-Acadian cooling in the southernmost Connecticut Valley Synclinorium: *Geological Society of America Abstracts with Programs*, v. 24, no. 7, p. A187.
- Munoz, J. L., 1984, F-OH and Cl-OH exchange in micas with applications to hydrothermal ore deposits, in Bailey, S. W., editors, *Micas: Reviews in Mineralogy*, v. 13, p. 469–494.
- 1992, Calculation of HF and HCl fugacities from biotite compositions: Revised equations: *Geological Society of America Abstracts with Programs*, v. 24, p. A221.
- Nishiyama, T., 1989, Kinetics of hydrofracturing and metamorphic veining: *Geology*, v. 17, p. 1068–1071.
- Nur, A., and Walder, J., 1990, Time-dependent hydraulics of the Earth's crust, in Bredehoeft, J. D., and Norton, D. L., editors, *The role of fluids in crustal processes: Washington, D.C., National Academy Press, Studies in Geophysics*, p. 113–127.
- Oelkers, E. H., and Helgeson, H. C., 1993, Calculation of dissociation constants and the relative stabilities of polynuclear clusters of 1:1 electrolytes in hydrothermal solutions at supercritical pressures and temperatures: *Geochimica et Cosmochimica Acta*, v. 57, p. 2673–2697.
- Oliver, N. H. S., Valenta, R. K., and Wall, V. J., 1990, The effect of heterogeneous stress and strain on metamorphic fluid flow, Mary Kathleen, Australia, and a model for large scale fluid circulation: *Journal of Metamorphic Geology*, v. 8, p. 311–332.
- Orville, P. M., 1962, Alkali metasomatism and the feldspars: *Norsk Geologisk Tidsskrift*, v. 42, p. 283–316.
- 1969, A model for metamorphic differentiation origin of thin-layered amphibolites: *American Journal of Science*, v. 267, p. 64–86.
- Osberg, P. H., Tull, J. F., Robinson, P., Hon, R., and Butler, J. R., 1989, The Acadian Orogen, in Hatcher, R. D., Jr., Thomas, W. A., and Viele, G. W., editors, *The Appalachian-Ouachita Orogen in the United States: Boulder, Colorado, Geological Society of America, The Geology of North America*, v. F-2, p. 179–232.
- Palin, J. M., ms, 1992, Stable isotope studies of regional metamorphism in the Wepawaug Schist, Connecticut: Ph.D. thesis, Yale University, New Haven, 170 p.
- Palin, J. M., and Rye, D. M., 1992, Direct comparison of mineralogic and stable isotopic records of metamorphic fluid flow: *Geological Society of America Abstracts with Programs*, v. 24, no. 7, p. A172.
- Palin, J. M., and Seidemann, D. E., 1990, Intergranular control of argon and oxygen isotope transport in metamorphic rocks: Implications for cooling-rate studies [abstract]: V. M. Goldschmidt Conference, 2nd, Program and Abstracts, Baltimore, Maryland, p. 71.
- Paterson, M. S., 1973, Nonhydrostatic thermodynamics and its geologic application: *Reviews in Geophysics and Space Physics*, v. 11, p. 355–389.
- Philippot, P., and Selverstone, J., 1991, Trace-element-rich brines in eclogitic veins: Implications for fluid composition and transport during subduction: *Contributions to Mineralogy and Petrology*, v. 106, p. 417–430.
- Prigogine, I., 1955, *Introduction to thermodynamics of irreversible processes*: New York, John Wiley & Sons, 119 p.
- Ramberg, H., 1952, *The origin of metamorphic and metasomatic rocks*: Chicago, The University of Chicago Press, 317 p.
- Ramsay, J. G., 1980, The crack-seal mechanism of rock deformation: *Nature*, v. 284, p. 135–139.
- Read, H. H., 1932, On quartz-kyanite rocks in Unst, Shetland Islands, and their bearing on metamorphic differentiation: *Mineralogical Magazine*, v. 23, p. 317–328.
- Robie, R. A., Hemingway, B. S., and Fisher, J. R., 1978, Thermodynamic properties of minerals and related substances at 298.15 K and 1 bar ( $10^5$  Pascals) pressure and at higher temperatures: *U.S. Geological Survey Bulletin* 1452, 456 p.



- Rodgers, John, 1985, Bedrock Geological Map of Connecticut: Hartford, Connecticut Geological and Natural History Survey, Department of Environmental Protection, scale 1:125,000.
- Rumble, D., and Hoering, T. C., 1986, Carbon isotope geochemistry of graphite vein deposits from New Hampshire, U.S.A.: *Geochimica et Cosmochimica Acta*, v. 50, p. 1239–1247.
- Rutter, E. H., 1983, Pressure solution in nature, theory and experiment: *Geological Society of London Journal*, v. 140, p. 725–740.
- Rye, D. M., and Bradbury, H. J., 1988, Fluid flow in the crust: An example from a Pyrenean thrust ramp: *American Journal of Science*, v. 288, p. 197–235.
- Rye, R. O., Schuiling, R. D., Rye, D. M., and Jansen, J. B. H., 1976, Carbon, hydrogen and oxygen isotope studies of the regional metamorphic complex at Naxos, Greece: *Geochimica et Cosmochimica Acta*, v. 40, p. 1031–1049.
- Schandl, E. S., Davis, D. W., and Krogh, T. E., 1990, Are the alteration halos of massive sulfide deposits syngenetic? Evidence from U-Pb dating of hydrothermal rutile at the Kidd volcanic center, Abitibi subprovince, Canada: *Geology*, v. 18, p. 505–508.
- Sibson, R. H., Robert, F., and Poulsen, K. H., 1988, High-angle reverse faults, fluid pressure cycling, and mesothermal gold quartz deposits: *Geology*, v. 16, p. 551–555.
- Silverman, S. G., ms, 1976, Microstructures and fluid inclusion compositions found in quartz veins in the Wepawaug Schist, western Connecticut: B. S. thesis, Yale University, New Haven.
- Skelton, A. D. L., Graham, C. M., and Bickle, M. J., 1993, Devolatilisation of the Earth's crust during greenschist facies regional metamorphism of the Dalradian of the SW Scottish Highlands: *Geological Society of America Abstracts with Programs*, v. 25, p. A-323.
- Smith, D. L., and Evans, B., 1984, Diffusional crack healing in quartz: *Journal of Geophysical Research*, v. 89, p. 4125–4135.
- Spry, A., 1969, *Metamorphic Textures*: New York, Pergamon Press, 350 p.
- Steeffel, C. I., ms, 1992, Coupled fluid flow and chemical reaction: Model development and application to water-rock interaction: Ph.D. thesis, Yale University, New Haven, 234 p.
- Stull, D. R., and Prophet, H., 1971, JANAF thermochemical tables: U.S. National Bureau of Standards, Standard Reference Data Series, v. 37, 1141 p.
- Sverjensky, D. A., 1987, Calculation of the thermodynamic properties of aqueous species and the solubilities of minerals in supercritical electrolyte solutions, in Carmichael, I. S. E., and Eugster, H. P., editors, *Thermodynamic modeling of geological materials: Minerals, fluids, and melts*: Mineralogical Society of America Reviews in Mineralogy, v. 17, p. 177–209.
- Sverjensky, D. A., Hemley, J. J., and D'Angelo, W. M., 1991, Thermodynamic assessment of hydrothermal alkali feldspar-mica-aluminosilicate equilibria: *Geochimica et Cosmochimica Acta*, v. 55, p. 989–1004.
- Thompson, A. B., Lyttle, P. T., and Thompson, J. B., Jr., 1977, Mineral reactions and A-Na-K and A-F-M facies types in the Gassetts Schist, Vermont: *American Journal of Science*, v. 277, p. 1152–1167.
- Thompson, J. B., Jr., 1959, Local equilibrium in metasomatic processes, in Abelson, P. H., editor, *Researches in Geochemistry*: New York, John Wiley & Sons, p. 427–457.
- Tracy, R. J., Rye, D. M., Hewitt, D. A., and Schiffries, C. M., 1983, Petrologic and stable-isotopic studies of fluid-rock interactions, south-central Connecticut: I. The role of infiltration in producing reaction assemblages in impure marbles: *American Journal of Science*, v. 283-A, p. 589–616.
- Tullis, J., and Yund, R. A., 1992, The brittle-ductile transition in feldspar aggregates: An experimental study, in Evans, B., and Wong, T., editors, *Fault mechanics and transport properties of rocks*: London, Academic Press, p. 89–117.
- Turekian, K. K., and Wedepohl, K. H., 1961, Distribution of the elements in some major units of the Earth's crust: *Geological Society of America Bulletin*, v. 72, p. 175–192.
- van Haren, J. L. M., Rye, D. M., and Ague, J. J., 1992, Fluid flow history determined from a petrographic and oxygen isotope study of a metamorphic quartz vein: EOS (Transactions of the American Geophysical Union), v. 73, p. 147.
- Vidale, R. J., 1974, Vein assemblages and metamorphism in Dutchess County, New York: *Geological Society of America Bulletin*, v. 85, p. 303–306.
- Vidale, R. J., and Hewitt, D. A., 1973, "Mobile" components in the formation of calc-silicate bands: *American Mineralogist*, v. 58, p. 991–997.
- Villas, R. N. V., and Norton, D. L., 1977, Irreversible mass transfer between circulating hydrothermal fluids and the Mayflower stock: *Economic Geology*, v. 72, p. 1471–1504.

- Vrolijk, P., 1987, Tectonically driven fluid flow in the Kodiak accretionary complex, Alaska: *Geology*, v. 15, p. 466-469.
- Walther, J. V., 1990, Fluid dynamics during progressive regional metamorphism, in Bredehoeft, J. D., and Norton, D. L., editors, *The role of fluids in crustal processes*: Washington, D. C., National Academy Press, *Studies in Geophysics*, p. 64-70.
- Walther, J. V., and Orville, P. M., 1982, Volatile production and transport in regional metamorphism: *Contributions to Mineralogy and Petrology*, v. 79, p. 252-257.
- 1983, The extraction-quench technique for determination of the thermodynamic properties of solute complexes: Application to quartz solubility in fluid mixtures: *American Mineralogist*, v. 68, p. 731-741.
- Woronow, A., and Love, K. M., 1990, Quantifying and testing differences among means of compositional data suites: *Mathematical Geology*, v. 22, p. 837-852.
- Yardley, B. W. D., 1975, On some quartz-plagioclase veins in the Connemara schists, Ireland: *Geological Magazine*, v. 112, p. 183-190.
- 1986, Fluid migration and veining in the Connemara schists, Ireland, in Walther, J. V., and Wood, B. J., editors, *Fluid-rock interactions during metamorphism*: New York, Springer-Verlag, p. 109-131.
- Yardley, B. W. D., and Bottrell, S. H., 1992, Silica mobility and fluid movement during metamorphism of the Connemara schists, Ireland: *Journal of Metamorphic Geology*, v. 10, p. 453-464.
- Zen, E-an, 1991, Phanerozoic denudation history of the southern New England Appalachians deduced from pressure data: *American Journal of Science*, v. 291, p. 401-424.
- Zhu, C., and Sverjensky, D. A., 1992, F—Cl—OH partitioning between biotite and apatite: *Geochimica et Cosmochimica Acta*, v. 56, p. 3435-3467.